# CHAPTER 2
# Perylene Based Conductors

**M. Almeida and R. T. Henriques**
*Departamento de Química, Instituto Tecnológico e Nuclear, P-2686 Sacavém Codex, Portugal*



## 1 INTRODUCTION

Perylene is one of the oldest donors used in the preparation of highly conducting organic solids, and its use dates back at least to the 1954 report, by Akamatu *et al.* [1], of the conducting perylene–bromine complexes. As in the case of many other molecular conductors that have been subsequently studied, the high electrical conductivity of the perylene based conductors is a consequence of the extended interaction in the solid of the HOMO $\pi$-electrons of the planar perylene molecules, that in the crystal structure are closely packed face to face. If the packing of the molecules in the solid is in regular stacks, a partial oxidation of the perylene (Per) molecules can lead to partially filled bands with metallic properties. On many occasions, either because of an integer degree of oxidation or due to the irregular stacking formation, the solids are poorer semiconductors or insulators.

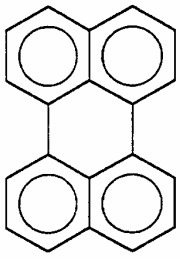

(Perylene)

Although far from presenting the lowest oxidation potential among many other known $\pi$-donors, the perylene molecule can be oxidised in several organic solvents, either by the direct action of chemical oxidants such as iodine or bromine, or electrochemically. In dichloromethane solutions, at a potential of $\sim 0.9$ V versus SCE (saturated calomel electrode), it

Handbook of Organic Conductive Molecules and Polymers. Volume 1 Charge-Transfer Salts, Fullerenes and Photoconductors.
Edited by H.S. Nalwa. 

undergoes a quasi-reversible oxidation [2,3]. The perylene cation is however relatively unstable and in this solvent it undergoes a fast rearrangement as $Per_2^+$ [3].

When compared with other donors more recently used to prepare conducting molecular crystals such as tetrathiafulvalene (TTF), tetramethyltetraselenafulvalene (TMTSF) or bis(ethylenedithio)tetrathiafulvalene (BEDT-TTF), a few important differences, with strong implications in the crystal preparation and in the electronic properties of these solids, should be kept in mind. First, and as discussed in more detail in Section 5.1.1 for the $Per_nM(mnt)_2$ compounds, the relative instability of the perylene cation and the low solubility of perylene in most common organic solvents, greatly limits the size and quality of the crystals that can be prepared, which usually are much smaller and of poorer quality than the TMTSF or BEDT-TTF salts. Second, in the absence of any chalcogen atoms in the perylene molecule, the hydrogen atoms on its periphery, completely shield the $\pi$-HOMO from any possible in-plane neighbour interactions and only allow a good interaction between face to face next neighbour molecules in a stack. As a consequence, a strong one-dimensional character of the bands is expected, at variance with conductors based on other donors, where the chalcogen atoms in the molecular periphery allow stronger interstack interactions and, as a result, an increased dimensionality of the electronic structure is observed.

Almost all known charge-transfer solids based on perylene or its derivatives are full charge-transfer complexes. Their transport properties are essentially determined by the packing pattern of the perylene molecules in the solid and their degree of partial oxidation. In full charge-transfer complexes the average degree of oxidation of the perylene molecules is entirely governed by the number of counterions. The packing pattern of the perylene molecules is strongly dependent on the geometry and volume of the counterions. In the different conductors described in this chapter, many types of molecular overlap are observed between perylene or perylene derivative molecules in their crystal structure. However and as will become clear, the high electrical conductivity and strong metallic properties, as observed in $Per_2X_{1.1}\cdot 0.8CH_2Cl_2$ with $X = PF_6$ or $AsF_6$, $Per_2M(mnt)_2$, $PerCo(mnt)_2\cdot 0.5(CH_2Cl_2)$, CPP–Iodine (CPP = 1,2,7,8-tetrahydrodicyclopenta[*cd*:*lm*]perylene), $CPP_2PF_6\cdot CH_2Cl_2$, or TTP–iodine (TTP = 3,4,9,10-tetrathioperylene), are always associated with the graphite-like overlap mode depicted in Figure 2.1b which maximises the HOMO interaction between neighbouring molecules (see Figure 2.1a). A strong effect of the counterion on the magnetic properties can take place if it is paramagnetic. In a few such cases interesting effects derived from the interaction of conduction electrons in the perylene stacks and the localised magnetic moment of the counterions are also observed. In this chapter a discussion of the different perylene based compounds is organised in groups according to the type of counterions: halides, simple inorganic anions, organic anions, and metallocomplex anions. Finally some conductors based on closely related perylene derivatives will be also considered. A listing of these compounds appears in Table 2.9.

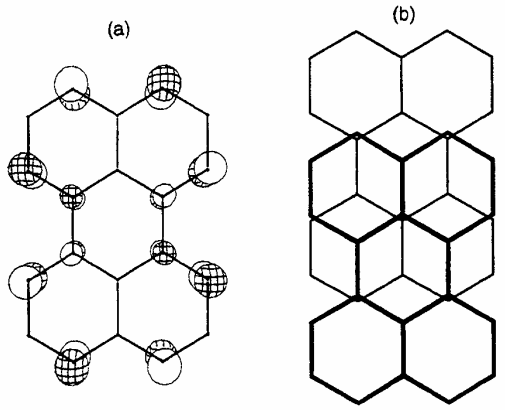


**Figure 2.1.** Schematic representation of the HOMO of the perylene molecule (a) and graphite-like overlap mode typical of the highly conducting perylene based conductors (b)

## 2 PERYLENE–HALOGEN COMPLEXES

This class of complex merits the honour of being the first of the vast field of organic conductors. The first report by Akamatu, Inokuchi and Matsunaga about a high conducting perylene–bromine complex was published in *Nature* in 1954 [1]. It was found, however, that the bromine content of the complex does not remain constant, and this fact reflects on the electrical resistivity, which was *ca.* 8 $\Omega$ cm in freshly prepared samples and increased to $10^3$ $\Omega$ cm after several weeks [4]. The authors attributed such evolution to the substitution of the additively linked bromine for hydrogen in the perylene molecule, resulting in dibromoperylene, which in turn can also have bromine additively linked. The formal composition '$PerBr_4$'

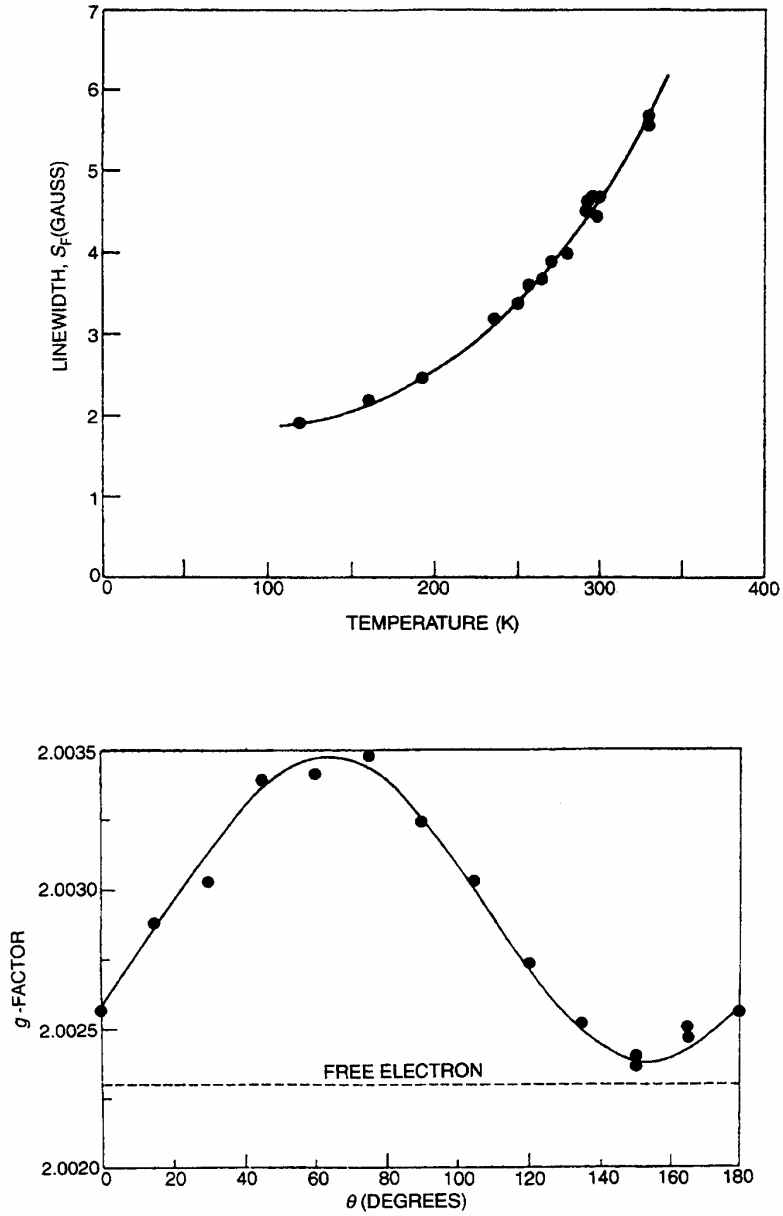


**Figure 2.2.** Temperature dependence of the EPR linewidth of $Per_2(I_2)_3$ (upper) and anisotropy of the EPR g-factor at 77 K temperature (lower). (Reproduced by permission of American Institute of Physics, from ref. 8.)

was in fact a mixture of 80% dibromoperylene and 20% perylene tetrabromide. For that formal composition, in freshly prepared samples, an energy gap of 0.13 eV was estimated from the thermal dependence of the electrical conductivity. To our knowledge no single crystals of these complexes were obtained.

For iodine, the situation is even more complicated. Although complexes with iodine were known for a long time [5], the electrical conductivity was only studied after the bromine complex was reported, independently by Kommandeur and Hall [6] and by Uchida and Akamatu [7]. Both found crystals with the (Per):$I_2$ ratio of 2:3 but the Japanese group, based on X-ray diffraction patterns and magnetic susceptibility measurements, claimed also the existence of a different complex with stoichiometry $Per(I_2)_3$. Room temperature values of conductivity agree quite well in the two publications, (1–1.25) $\times$ $10^{-1}$ S/cm for the 2:3 complex but disagreement appears about the energy gap, 0.038 eV from Kommandeur and Hall but 0.06 eV from Uchida Akamatu. The latter authors obtained the same energy gap and room temperature conductivity for the 1:3 complex and suggested hole conduction by the observation of a positive thermoelectric power. Discrepancies may arise from several sources, such as the use of four-probe [6] or two-probe contacts [7], or the performance of electrical measurements in compressed pellets, in which intergrain activation energies are present. Kommandeur and Hall concluded also that the perylene–iodine complex is only stable when kept under its own vapour pressure. EPR studies were made in the complex, formulated by Singer and Kommandeur as $Per_2(I_2)_3$ [8]. The linewidth is *ca.* 5.5 G at 300 K, decreasing upon cooling (Figure 2.2). The *g*-value is 2.0033(1) at room temperature. However it is anisotropic and at 77 K the usual $\cos^2\theta$ dependence is found with extreme values of 2.0035 and 2.0024. The spin concentration is 4.6 $\times$ $10^{19}$ spins/g at 300 K and its temperature dependence correlates well with the predicted activated behaviour found in the electrical

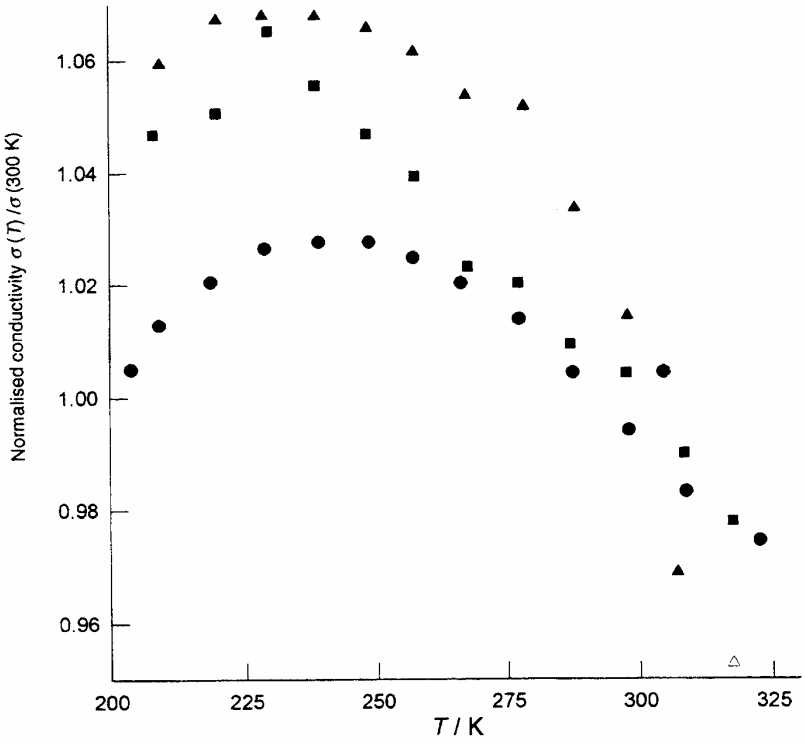


**Figure 2.3.** The normalised conductivity of several samples of $Per(I_2)_4$ showing the metallic regime ($d\sigma/dT < 0$) above the broad maximum. (Reproduced by permission of Royal Society of Chemistry, from ref. 10.)

conductivity measurements with an activation energy of 0.019 eV in the range 77–300 K. The electronic spin–lattice relaxation time, $T_1$, derived from EPR is $2 \times 10^{-7}$ s (77 K) increasing to $8 \times 10^{-6}$ s at 4.2 K. Measurements of the static magnetic susceptibility in the range 77–296 K give a very small and almost temperature-independent paramagnetic value, $\chi_P = 62 \times 10^{-6}$ emu/mol [9].

The first report of a perylene–iodine complex with metallic conductivity was $Per(I_2)_4$ by Kao *et al.* [10], with values as high as 51.9 S/cm at 300 K. A broad maximum of conductivity exists at *ca.* 235 K (Figure 2.3). In a few samples that did not crack at lower temperatures, a gap of 0.1 eV was measured. The EPR linewidth at room temperature is 10.9 G, clearly distinguishable from the $Per_2(I_2)_3$ complex. The authors indicate that spin density from EPR exhibits an activated behaviour with $E_a = 0.02$ eV in the range 100–300 K, consistent with a model of a narrow band-gap semiconductor. The determination of the crystalline structure was not accomplished, but from X-ray oscillation photographs, an incommensurate structure was proposed.

The lack of agreement between compositions of complexes prepared from different authors led to several studies aiming at clarifying this problem. Cobb and Wallis [11], through measurements of the absorption of iodine by perylene at various temperatures and iodine pressures, concluded that complexes of the following compositions can exist: $Per_3(I_2)_4$, $Per_7(I_2)_{10}$, $Per_2(I_2)_3$, $Per_2(I_2)_2$ and $Per_7(I_2)_{20}$. The above-described formulation $Per(I_2)_3$ [7] would in fact be $Per_7(I_2)_{20}$. In a different study, using an electrochemical technique, Aronson *et al.* [12] found threshold pressures for formation and decomposition of this compound, formulated by the authors as $Per(I_2)_{2.9}$. Other clarification came from the combined use of resonance Raman and $^{129}I$ Mössbauer spectroscopy, usually employed for ascertaining which iodine species are present ($I_2$, $I^-$, $I_3^-$, etc.). When applied to '$Per_2(I_2)_3$' [6], Teitelbaum *et al.* [13] concluded that such complex (formulated as $PerI_{2.92}$ by the authors) is a partially oxidised material with a charge distribution of $Per^{+0.4}(I_3^- 2I_2)_{0.4}$. In spite of several attempts [7,14], the crystal structure of these compounds has remained unsolved. Coppens [15] used a generalised ternary phase diagram of compounds containing aromatic hydrocarbons and iodine, previously established from known structures, in order to predict the type of structure of three of the perylene–iodine complexes. According to this method, he predicts that perylene molecules are perpendicular to sheets of $I_3^-$ and $I_2$ in $Per_2(I_2)_3$ and parallel to the corresponding iodine sheets in $Per_7(I_2)_{20}$ (the $Per(I_2)_3$ complex of ref. 9) and $Per(I_2)_4$ [8].

# 3 PERYLENE COMPLEXES WITH ORGANIC ANIONS

## 3.1 TCNQ complexes

Two different complexes of perylene with 7,7′,8,8′-tetracyanoquinodimethane (TCNQ), Per–TCNQ and $Per_3TCNQ$, have been synthesised, the first by slow evaporation of a mixed solution of the donor and acceptor [16] and the second by a diffusion procedure [17]. Although these compounds are poor semiconductors, some details about the structure and oxidation states will be briefly discussed as they appear in other complexes for which more than one stoichiometry was found.

The crystalline structure of Per–TCNQ consists of an alternated stacking of perylene and TCNQ molecules almost parallel to each other (the angle between the mean planes is 4.1°) at a distance of 3.44 Å (Figure 2.4) [18]. (The overlap mode of the two organic molecules is displayed in Figure 2.6a.) $Per_3TCNQ$ has a TCNQ sandwiched between two perylene species flanked by another perylene in an almost perpendicular configuration [19] (Figure 2.5).

Infrared spectroscopy of the 3 : 1 compound showed two types of perylene molecules, one pair of molecules associated with TCNQ and one free molecule [17]. The charge distribution was clarified by UV and near infrared spectroscopy [20]. For both perylene–TCNQ compounds a charge-transfer band was identified and also the monomer $TCNQ^-$ spectrum. The typical bands of $(TCNQ)_2^-$ are not observed. For $Per_3TCNQ$ the UV spectrum clearly shows the existence of neutral perylene. Thus the suggestion from the crystalline structure that the flanking perylene molecules are neutral seems confirmed. Therefore, given the existence of the anion $TCNQ^-$, each of the two other perylene species share one positive charge. EPR lines are narrow for both compounds: 0.61 G and 0.97 G for the 3 : 1 and 1 : 1 compounds respectively at room temperature, and 0.67 G and 0.84 G at 77 K [17].

## 3.2 Other organic acceptors

All other perylene complexes with organic counterparts present the 1 : 1 stoichiometry and alternate stacking, being consequently poor conductors. Structural data are

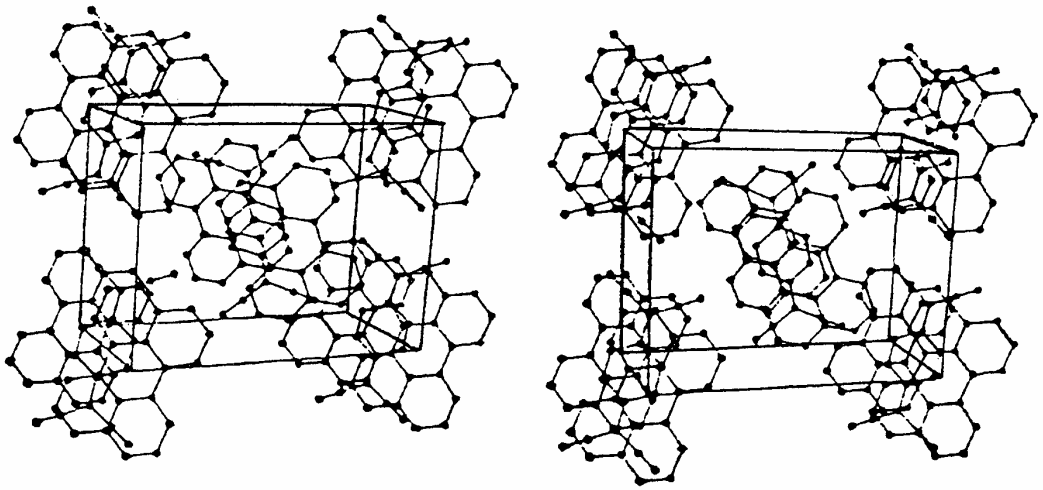

**Figure 2.4.** Stereoview of the crystalline structure of Per(TCNQ). (Reproduced by permission of Royal Society of Chemistry, from ref. 18.)

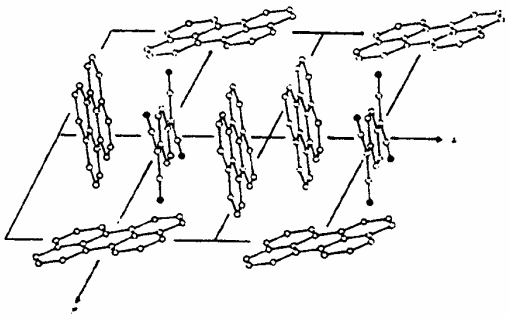

**Figure 2.5.** View along **a** of the crystal structure of $Per_3(TCNQ)$, showing the stacking with the repetition motive: one TCNQ sandwiched between two perylene species. This stack is flanked by extra perylene molecules. (Reproduced by permission of International Union of Crystallography, from ref. 19.)

summarised in Table 2.1. The values of room temperature conductivity obtained by different authors may differ by more than one order of magnitude, reflecting the importance of impurity and defect concentrations. For instance, single crystals of Per–fluoranil, in which fluoranil = 2,3,5,6-tetrafluoro-*p*-benzoquinone, have reported values of $3.5 \times 10^{-12}$ S/cm and a gap of 1.44 eV [21], or $1.5 \times 10^{-14}$ S/cm and a gap of 1.46 eV [22]. The latter authors found an anisotropic conductivity ratio of 3, the above value being along the *c* direction. Besides it is photoconductive with a photoconduction activation energy of 0.12 eV and a room temperature value of $3.0 \times 10^{-12}$ S/cm [22]. It is interesting to note that the overlap mode of the fluoranil face to perylene [2[3] is very similar to the 1 : 1 compound with TCNQ (see Figure 2.6b). A different overlap is found for the

**Table 2.1.** Summary of crystallographic data for complexes of perylene (Per), with organic acceptors

| Complex | Space group | *a* (Å) | *b* (Å) | *c* (Å) | $\alpha$ (°) | $\beta$ (°) | $\gamma$ (°) | *Z* | $d_{D-A}$ (Å) | Ref. |
|---|---|---|---|---|---|---|---|---|---|---|
| Per(TCNQ) | $P2_1/b$ | 7.32(2) | 14.55(3) | 10.88(2) | 90 | 90.4 | 90 | 2 | 3.44 | 18 |
| $Per_3TCNQ$ | $\bar{P}1$ | 10.8750(3) | 12.6993(4) | 10.4217(3) | 114.905(2) | 90.797(2) | 112.615(2)1 | 1 | 3.29 | 19 |
| Per–fluoranil | $P2_1/n$ | 17.13(1) | 7.49(1) | 6.97(1) | 90 | 90.4 | 90 | 2 | 3.23 | 23 |
| Per(pmda) | $P2_1/n$ | 14.613(3) | 7.16(1) | 10.1309(4) | 90 | 94.67(3) | 90 | 2 | 3.33 | 24 |
| Per(TCNE) | $P2_1/a$ | 15.763(12) | 8.234(6) | 7.346(5) | 90 | 96.4(1) | 90 | 2 | 3.186 | 25 |
| Per(HCBD) | $P2_1/a$ | 16.251(1) | 8.3811(5) | 7.8109(4) | 90 | 91.583 | 90 | 2 | | 26 |

TCNQ = 7,7′,8,8′-tetracyanoquinodimethane, fluoranil = 2,3,5,6-tetrafluoro-*p*-benzoquinone, TCNE = tetracyanoethylene, HCBD = hexacyanobutadiene, pmda = pyromellitic dianhydride, $d_{D-A}$ = donor–acceptor interplanar distance.

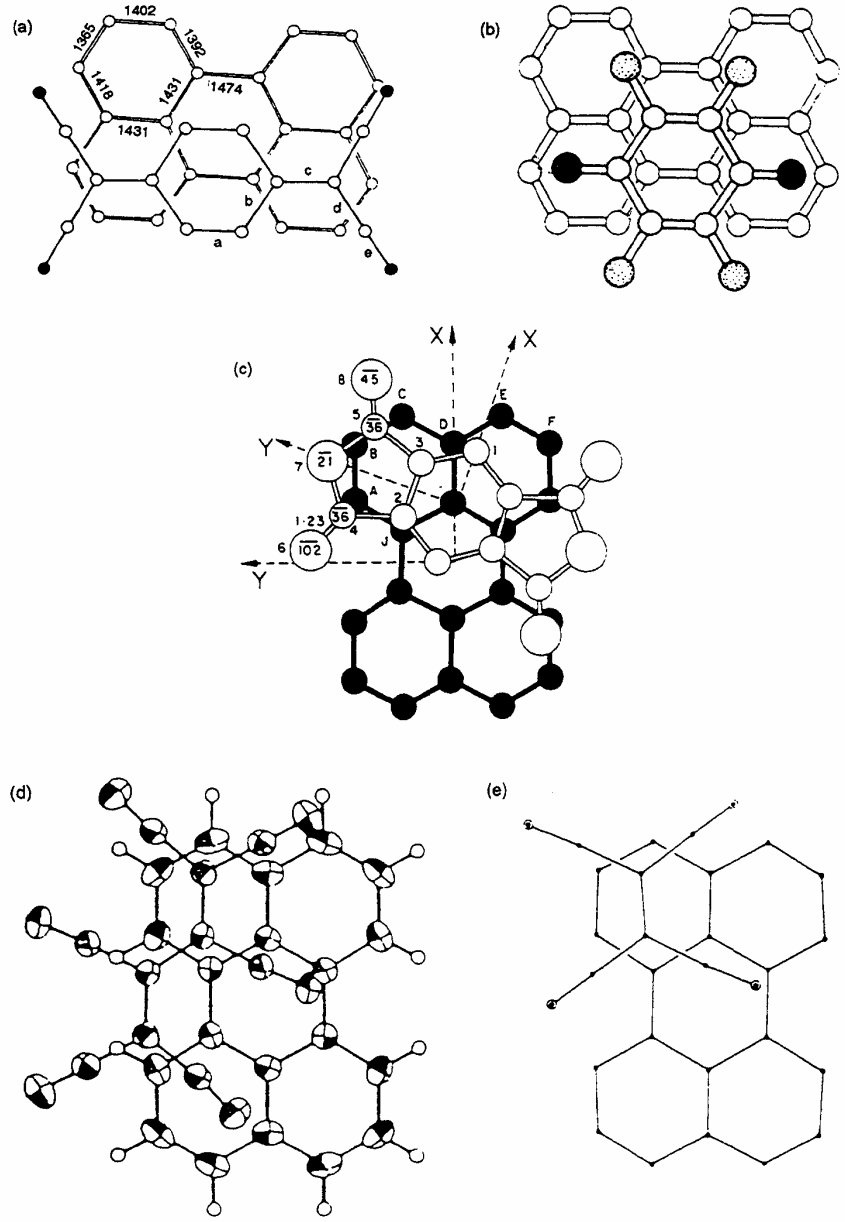


**Figure 2.6.** Overlap of donor and acceptor molecules for several perylene complexes with organic molecules. (a) TCNQ (tetracyanoquinodimethane) in $Per_3(TCNQ)$. (Reproduced by permission of International Union of Crystallography, from ref. 19); in the 1 : 1 complex the overlap is slightly twisted relative to this one. (b) Fluoranil. (Reproduced by permission of International Union of Crystallography, from ref. 23). (c) PMDA (pyromellitic dianhydride). (Reproduced by permission of The American Chemical Society, from ref. 24); (d) HCBD (hexacyanobutadiene). (Reproduced by permission of Elsevier Science, from ref. 26). (e) TCNE (tetracyanoethylene). (Reproduced by permission of International Union of Crystallography, from ref. 25.)

complex with pyromellitic dianhydride (PMDA) [24]. In this complex the centroid of the acceptor molecule is placed above one of the carbon atoms which belongs to three rings of the perylene molecule, and the longer symmetry axis of PMDA is transversal to the corresponding axis of perylene (Figure 2.6c). The overlap for complexes of tetracyanoethylene (TCNE) [25] and hexacyanobutadiene (HCBD) [26] is different from the preceding ones but similar to one another (see Figures 2.6d–e), although the surroundings in the direction perpendicular to the stacking become different for the two compounds: unimolecular sheets for HCBD with short N–N contacts (homo sheet), and equimolar donor and acceptor occupancy for TCNE (hetero sheet). The relevance of this type of transversal arrangement was discussed in the context of the possibility of neutral-to-ionic transition in HCBD, as the $\Delta E_{redox} = 0.29$ V situates this complex as neutral, but not far from the critical value for the neutral-to-ionic transition of $\Delta E_{redox} = 0.2$ V [26].

# 4 PERYLENE COMPLEXES WITH SIMPLE INORGANIC ANIONS

The first known examples of this class of compound with simple inorganic anions, $Per_mX$, were those with $X = ClO_4^-$ and $SbCl_5$ [27,28]. A great deal of interest in this class of compound was generated after the report of metallic conductivity over a wide range of temperature both in the Bechgaard salts [29] and in $Per_2Pt(mnt)_2$ [30]. Cation radical salts of perylene with the anions $AsF_6^-$, $PF_6^-$, $SbF_6^-$ and $BF_4^-$ were synthesised by two German groups [31–33] and soon later $ClO_4^-$ was revisited [34]. In the following we will devote special attention to the different stoichiometries of perchlorate salts and the modes of packing of the perylene species therein and then refer in more detail to the $AsF_6^-$ and $PF_6^-$ salts which were the most widely studied members of this family. At the end, new perylene charge-transfer salts with haloiron anions will also be described [35]. In Table 2.2 the structural data for this class of compounds are summarised.

## 4.1 Perchlorate salts

The first report on a perylene–perchlorate charge-transfer solid was made by Sato *et al.* [27] who isolated the product of a perylene oxidation reaction in dichloromethane–acetonitrile solutions containing $AgClO_4$. The solid obtained by this procedure was poorly characterised and the authors considered it a mixture of $PerClO_4$ and AgI in equal amounts. The paramagnetic susceptibility, after correction for diamagnetism and removal of the AgI contribution, was interpreted according to the singlet–triplet model with the exchange coupling constants $J = 0.085$ eV. In the same publication the magnetic susceptibility of $PerSbCl_5$, obtained by a similar procedure, was also measured and found to follow the Curie–Weiss law with a Curie constant $\theta = -44$ K. A different stoichiometry, $Per_2ClO_4$, was pointed out by Chiang *et al.* [28] for a solid obtained by electrochemical oxidation of perylene in tetrahydrofuran solutions with tetrabutylammonium perchlorate. Electrical conductivity was not measured in this system, but an EPR study was reported. No anisotropy was found both in $g$-values and linewidth. The spin susceptibility, only given in relative arbitrary units, was found to increase with temperature for $T > 250$ K, whereas at lower temperatures it followed $1/T$ behaviour. This behaviour was interpreted as the contribution both from a doublet following the Curie law and a triplet exciton with an activation energy $\Delta E = 0.27$ eV, following the expression:

$$\chi(T) = A/T + (B/T)[3 + \exp(\Delta E/k_B T)]^{-1} \quad (2.1)$$

As in the case of the iodine complexes, the composition of the perylene–perchlorate salts was subjected to some criticism. Ristagno and Shine [36] made electrochemical preparations obtaining "small crystals containing both perylene and its cation radical perchlorate, but in varying proportions". Several years later Rosseinsky and Kathirgamanathan [3], reported the existence of both covalent and ionic compounds as products of the electrochemical reaction of perylene and perchlorate (perchloratoperylene = $C_{20}H_{11}ClO_4$) and perylenium perchlorate ($C_{20}H_{12}^+ClO_4^-$) respectively, besides the 2 : 1 compound bisperylene perchlorate whose positive charge could be $Per^0Per^+$ or $Per_2^+$,

**Table 2.2.** Summary of structural data for complexes of perylene (Per), with simple inorganic anions

| Compound | Space group | $a$(Å) | $b$ (Å) | $c$ (Å) | $\alpha$ (°) | $\beta$ (°) | $\gamma$ (°) | $Z$ | Vol. (Å$^3$) | Ref. |
|---|---|---|---|---|---|---|---|---|---|---|
| $Per_6ClO_4$ | $\bar{P}1$ | 12.571(7) | 13.699(5) | 13.835(11) | 110.43(4) | 107.13(7) | 107.09(4) | 1 | 1913 | 34 |
| $Per_3ClO_4$ | $\bar{P}1$ | 13.009(8) | 13.821(10) | 13.850(15) | 66.05(7) | 83.36(8) | 63.51(6) | 2 | 2030 | 34 |
| $Per_6PF_6$ | $\bar{P}1$ | 12.412(4) | 13.766(5) | 13.855(5) | 110.63(3) | 106.86(3) | 106.94(3) | 1 | 1904.6 | 39 |
| $Per_2(PF_6)_{1.1}$0.8·DCM | *Pnmn* | 4.285 | 12.915 | 14.033 | 90 | 90 | 90 | 1 | 776.56 | 31 |
| $Per_2(AsF_6)_{1.1}$·0.8DCM | *Pnmn* | 4.294 | 13.077 | 14.132 | 90 | 90 | 90 | 1 | 793.55 | 31 |
| $Per_2PF_6$·2/3THF | *P2/m* | 13.04(1) | 8.234(6) | 7.346(5) | 90 | 110.80(2) | 90 | 3 | 2367 | 34 |
| $Per_2(PF_6)_{1.5}$·1/2THF[a] | *Pnmn* | 4.26 | 12.79 | 13.89 | 90 | 90 | 90 | 1 | 756.80 | 31 |
| $Per_3FeCl_4$ | $\bar{P}1$ | 12.839(1) | 14.133(1) | 14.840(2) | 91.680(7) | 113.11(1) | 115.12(1) | 2 | 2179.4 | 35 |

[a] In the original reference $Per_2(PF_6)_{1.4}$·(0.6THF) [31]. This composition was taken from ref. 37.
THF = tetrahydrofuran, DCM = dichloromethane.

obtained under conditions very similar to those used in ref. 28. Perchloratoperylene was obtained by a photochemical process: equal moles of perylene and tetrabutylammonium dissolved in $CCl_4$ were irradiated during 8 h under a 100 W Hanovia medium pressure lamp [3]. The synthesis of both 2 : 1 or 1 : 1 cation radical salts was performed in electrochemical cells, by a potentiostatic method, but under different conditions: $Per_2ClO_4$ was obtained in dichloromethane at 1.026 V versus SCE and $PerClO_4$ in nitrobenzene at 1.235 V versus SCE. The main reason for the different stoichiometry obtained may lie in the stability of the $Per^+$ ion in nitrobenzene whereas in dichloromethane it is unstable. Quite surprisingly the highest conductivity is for the 1 : 1 compound with 0.1 S/cm$^{-1}$ with a semiconducting behaviour (see Table 2.3). Unfortunately the crystal structures of these compounds remain unsolved. However, for two different stoichiometries, 6 : 1 and 3 : 1, the crystalline structure has been solved [34]. Apparently the species obtained depend basically on the perylene concentration.

The structure of the 6 : 1 compound has three perylene species at general positions in the asymmetric unit and disordered $ClO_4^-$ (Figure 2.7). Each perylene species belongs to a $\pi$-dimer whose counterpart is generated by the nearest inversion centre. The interplanar distances within the dimers are 3.38(2), 3.44(2) and 3.46(3) Å, with similar overlap patterns. The dimers do not stack, as they are isolated in the crystal and tilted towards each other with dihedral angles of 102°, 84° and 103°.

In the 3 : 1 salt, the perylene species form tetramers, in which they are almost parallel, running along the [001] direction, flanked by other perylene molecules making interplanar angles of 88°, 73° and 78° (see Figure 2.8). Within the tetramer there are two independent interplanar distances of 3.39(8) and 3.36(5) Å.

**Table 2.3.** Electrical conductivity of perylene–perchlorate salts

| Compound | $\sigma$ (S/cm) | Sample config.[a] | Reference |
|---|---|---|---|
| $PerClO_4$ | 0.1–0.8 | s.c., 2-probe | 3 |
| $Per_2ClO_4$ | (1–1.6) × 10$^{-7}$ | s.c., needle axis, 2-probe | 3 |
| $Per_2ClO_4$ | 5 × 10$^{-5}$ | s.c., transverse, 2-probe | 3 |
| $Per_3ClO_4$ | 0.5–2 | s.c., needle axis, 4-probe | 37 |
| $Per_6ClO_4$ | 10$^{-2}$ | s.c., needle axis, 4-probe | 37 |
| Perchlorateperylene | 1.6 × 10$^{-4}$ | c.p., 2-probe | 3 |

[a] s.c. = single crystal; c.p. = polycrystalline compressed pellet.

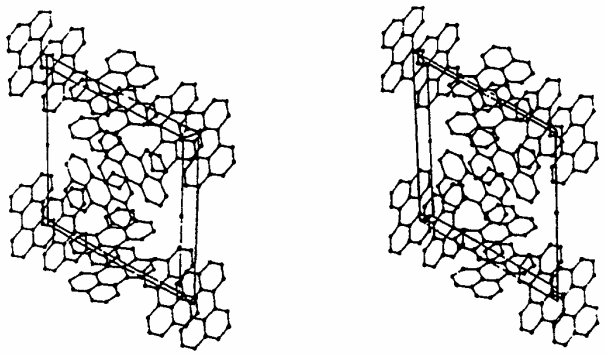

**Figure 2.7.** Stereoview of the crystal structure of $Per_6ClO_4$ along **a**, where the disordered $ClO_4^-$ groups are omitted for clarity. (Reproduced by permission of International Union of Crystallography, from ref. 34.)

## 4.2 Hexafluoro-arsenate, -phosphate and -antimonate salts

These are undoubtedly the most widely studied compounds of perylene with simple anions, mainly $AsF_6^-$ and $PF_6^-$ and their solid solutions, and for some stoichiometries the most conductive at room temperature. Besides the several stoichiometries they present, as in the perchlorate salts [3,36], an additional problem comes from the incorporation of solvent in the crystal structure. In the following we will divide into sections the discussion of the different aspects of the chemistry and physics of these compounds and their solid solutions.

### *4.2.1 Preparative aspects*

All crystals were obtained on the platinum anode of an electrochemical cell by a galvanostatic technique, using typically current densities of 2–5 $\mu A/cm^2$ during $\sim 3$ days and in the absence of light, from solutions of perylene and the corresponding tetrabutylammonium salts of $PF_6^-$, $AsF_6^-$ or $SbF_6^-$.

The composition of the crystals obtained depends on the solvent employed. With tetrahydrofuran (THF), five compositions were detected, apparently both for $X = PF_6$ and $AsF_6$: $Per_6X_1$, $Per_3X_1$, $Per_2X_1 \cdot 2/3THF$, $Per_2X_{1.5} \cdot 1/2THF$ and $Per_1X_1$ [36]. If saturated solutions of dichloromethane (DCM) are used, where perylene is

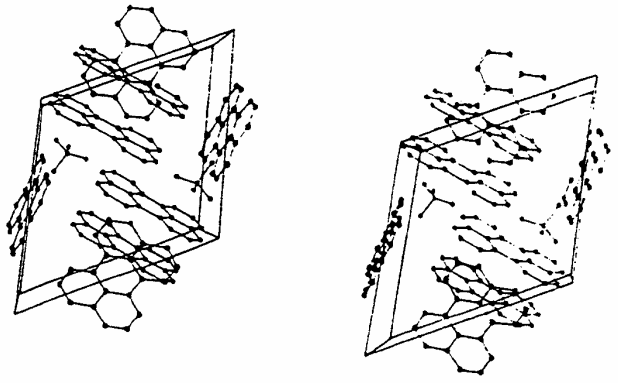

**Figure 2.8.** Stereoview of the crystal structure of $Per_3ClO_4$ along **c**, showing two perylene species of adjacent tetramers. (Reproduced by permission of International Union of Crystallography, from ref. 34.)

about ten times less soluble than in THF, only one type of crystal is obtained, with the stoichiometry $Per_2X_{1.1}$·0.8DCM [36] (different solvent contents for $PF_6$ and $AsF_6$, 0.8 and 0.7 respectively, were reported in early publications [31]). Two different crystalline habits were found in the same preparation, called 'thin' and 'thick' crystals. The first are needles with very small cross-section of rectangular or trapezoid form (smallest dimension 5–10 $\mu$m) and 10 to 50 times as broad. The 'thick' crystals have preferably hexagonal cross-section although they may also be rectangular or square, having for a minimum dimension at least 50 $\mu$m but are only 2 or 3 times as broad. These two types of 'thin' and 'thick' crystals were obtained in preparations from DCM solutions with a Per : ($PF_6$, $AsF_6$) ratio, either pure or mixed, of 2 : 1.1 [31,37]. For the other compositions, the so called 'thin' crystals were the only ones obtained, and for $Per_2X_{1.5}$·1/2THF they were found to be isostructural with 'thick' crystals of $Per_2X_{1.1}$·0.8DCM X = $PF_6$, $AsF_6$). Differences in the conductivity behaviour and EPR linewidth were found and they will be discussed in the appropriate sections.

In 1,1,2-trichloroethane (TCE), with larger molecules than DCM, the composition obtained was $Per_2X_{1.4}$ with no reference made to the inclusion of solvent [37]. A stoichiometry of 3 : 2 was reported for X = $SbF_6$, both in DCM and in THF, $Per_3(SbF_6)_2$·3/4DCM and $Per_3(SbF_6)_2$·THF [31].

Metallic conductivity is observed in crystals with a Per : X ratio of $2:(1+x)$ with $x = 0$ and 0.5 for THF, 0.1 for DCM and 0.4 for TCE.

### 4.4.2 *Crystalline structures*

The compounds with stoichiometry 6 : 1 and 3 : 1 are isostructural with the corresponding $ClO_4$ salts already described [33], and a detailed structure determination was also made for $Per_6PF_6$ [38]. It was found that the $PF_6^-$ anion has strong librations and/or positional disorder but is not freely rotating. The perylene species form dimers and by symmetry ($P\bar{1}$) there are three symmetrically independent perylene species (see Figure 2.9). The distances of perylenes intradimer/interdimer are the following (in Å): $d$(I–I′) = 3.23/4.36, $d$(II–II′) = 3.36/4.64 and $d$(III–III′) = 3.33/3.85.

The $Per_2PF_6$·2/3THF structure was solved by Endres *et al.* [34]. It is monoclinic, space group $P_2/m$, with cell parameters $a = 13.04(1)$ Å, $b = 14.12(1)$ Å, $c = 13.75(1)$ Å, $\beta = 110.80(2)°$. In this structure the

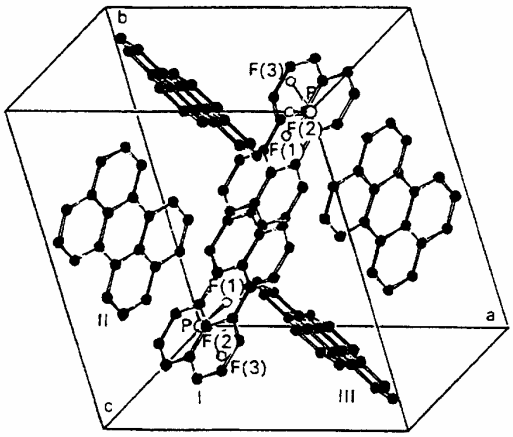


**Figure 2.9.** Crystal structure of $Per_6PF_6$ showing the six mutually perpendicular perylene species. (Reproduced by permission of International Union of Crystallography, from ref. 39.)

solvent molecules are disordered as well as one of the perylene species. In fact, three perylene species lie in special positions, two of them perpendicular to the mirror plane $y = 0$, the third on the mirror plane $y = 1/2$ with its centroid at the inversion centre (1/2,1/2,1/2). The fourth and disordered perylene species centred at (0,0,1) is over two symmetry related positions as indicated in Figure 2.10. The first two perylene molecules and their symmetry related counterparts

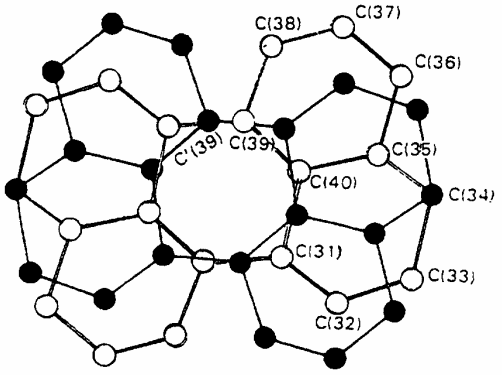


**Figure 2.10.** The two positions of the disordered perylene species of $Per_2PF_6$·2/3THF. A mirror plane bisects the line C(30–C′(39). (Reproduced by permission of International Union of Crystallography, from ref. 34.)

form stacks along the **c** direction, surrounded by the anions. The perylene species are slipped, resulting in a tetramerised arrangement along the slipping direction. The third and fourth perylene molecules have their molecular planes perpendicular, or near perpendicular, to the stacking direction (90° by symmetry for I–III and 73° for I–IV) and by symmetry are perpendicular to each to other (see Figure 2.11).

Crystals of $Per_2X_{1.1}$·0.8DCM (X = $PF_6$ and $AsF_6$) belong to the orthorhombic system, space group *Pnmn* [31]. The perylene species occupy a special position (0,1/2,0) and form regular stacks along the *a*-axis, leaving channels between them which are occupied by the anions and solvent molecules. The angle between the perylene and the **b**,**c** plane is 37.7° and the intermolecular distance is 3.40 Å with the overlap mode shown in Figure 2.1. The period for the anion in a channel is close to 2*a*, i.e., in the same channel there is an anion every second cell. However as the ratio is 2 : 1.1, some anions have to occupy the same channel in adjacent cells, implying a shift of their positions along the *a* direction. The remaining space within a channel is occupied by solvent molecules. This type of disorder is seen on rotation photographs as diffuse sheets between the layers perpendicular to **a**, meaning that the distribution in the channels has a translational period of 2*a*, but no correlation exists between different channels in the **b**, **c** plane. For the $AsF_6$ compound two different orientations of the octahedra are observed, whereas for $PF_6$ no special orientation is found, which may be attributed to the smaller volume of the latter, allowing free rotation within the channel. The projection onto the **a**,**c** plane is shown in Figure 2.12.

The structures of the compounds with other stoichiometries have not been solved.

### 4.2.3 *Electrical transport properties*

This section starts with a brief description of the systems with semiconducting behaviour at room temperature and then discusses in detail the compositions for which the metallic behaviour of electrical conductivity is found, which are in the range of Per : X ratios of 2 : 1 and 2 : 1.5. The ground state for these systems is insulating and the transition to the metallic state is always above 100 K.

The 6 : 1 salt, $Per_6PF_6$ is the poorer conductor from this series with a room temperature conductivity of $\sigma_{RT} \approx 10^{-4}$ S/cm. The $\sigma(1/T)$ curve may be described as the superposition of two thermally activated processes, at high and low temperatures, with activation energies $E_{aH} = 334$ meV and $E_{aL} = 149$ meV respectively [39]. The 3 : 1 salts are moderate conductors with a room temperature conductivity of 0.5 S/cm, reflecting the structure, where tetradic stacking of perylene is found but with weak overlap between the tetrades [37].

Crystals of $Per_2X_{1.1}$·0.8DCM (X = $PF_6$ and $AsF_6$) show electrical conductivity at room temperature ranging from 100 to 1200 S/cm, with typical values in the range 600–700 S/cm [31,40]. The electrical conductivity appears to have different behaviours according to the habit of the crystals [31]. D.c. measurements made on 'thick' crystals show a rounded maximum of conductivity at ~180 K followed at ~120 K by a large and sudden drop, of about two orders of magnitude, and at lower temperature the semiconducting regime takes place. The 'thin' crystals show only a rounded maximum centred at ~200 K (see Figure 2.13). Probably the jumps in conductivity are not intimately correlated to the habit. In fact in the mixed salt $Per_2(AsF_6)_{0.75}(PF_6)_{0.35}$·0.85DCM, this 'anomalous' behaviour is displayed by the 'thin' crystals [38]. An extremely sharp peak was observed in the $\sigma(T)$ curve of this compound, followed by a sudden decrease during cooldown (Figure 2.14). This sharp peak disappears after thermal cycling and the huge $\sigma_{max}/\sigma_{RT}$ exceeding 70, becomes only 3. For the pure $PF_6$ salt, Brütting and Riess [40] found recently only one behaviour: $\sigma$ increases with decreasing temperature, passing through a broad maximum between 200 and 150 K, without a sharp metal-to-insulator transition, and below the maximum no simple activated behaviour was found even for the lower temperature part. This profile was also found for the mixed composition referred to above in contactless microwave conductivity measurements made at 9.3 and 23.5 GHz, without sharp peaks or jumps, the only difference being the higher room temperature conductivity (750 S/cm) for a 'thin' crystal, in the upper limit of the scattered values of the observation made in different crystals at room temperature ($\sigma_{mw}$ = 20–750 S/cm) [39].

Metallic behaviour is also observed in thermoelectric power, from which a bandwidth W = 1.2 eV was derived, taking the slope of the linear part of $S(T)$ at high temperature [41], according to the tight-binding model [42]

$$S = (2\pi^2 k_B T/3eW)[\cos(\pi\rho/2)/\sin^2(\pi\rho/2)] \quad (2.2)$$

and taking as the density of charge carriers, $\rho = 0.55$ holes per site, as imposed by the stoichiometry. This corresponds to a degree of hole bandfilling slightly

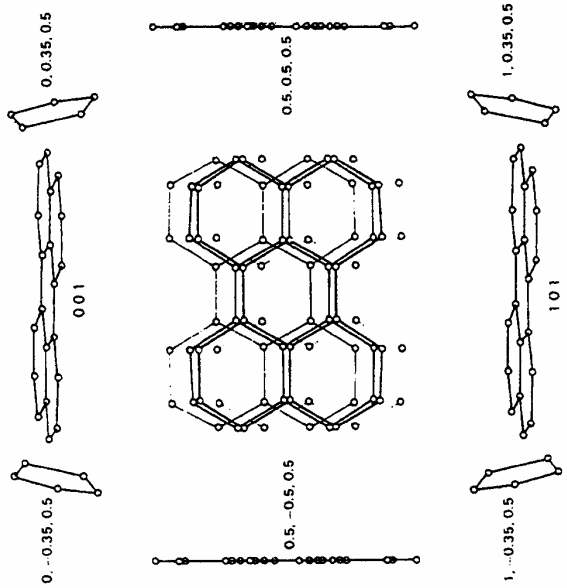


(Right) view along **c** omitting the anions, showing the perylene III and IV species. (Reproduced by permission of International Union of Crystallography, from ref. 34.)

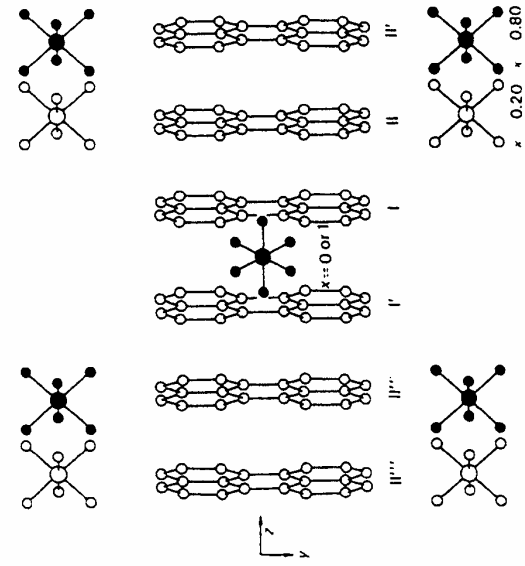


**Figure 2.11.** (Left) stack of perylene in $Per_2PF_6.2/3THF$, with the surrounding $PF_6^-$ anions, viewed along **a**.

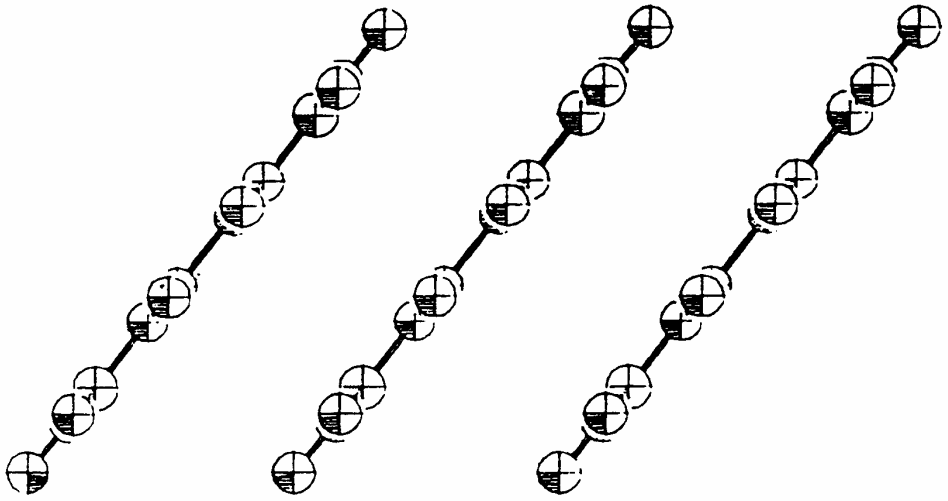

**Figure 2.12.** Projection of the perylene stacks of $Per_2(AsF_6)_{1.1}\cdot 0.8DCM$ along the **a**,**c** plane. (Reproduced by permission of Gordon & Breach, from ref. 31.)

above a quarter-filled: 0.275. Similar values of the bandwidth were obtained for the mixed anion-type compound $Per_2(AsF_6)_{0.75}(PF_6)_{0.35}\cdot 0.85DCM$ [37].

This value for the bandwidth is confirmed by polarised reflectance measurements [43–45]. With light polarised parallel to the needle axis, a plasma edge is observed, whereas for the direction of polarisation perpendicular to the axis, the behaviour is that of an insulator (Fig. 2.15). From the plasma frequency, an extremely low value of the effective mass was estimated, $m^* = 0.9m_0$ and the value obtained for the bandwidth was 1.1 eV, one of the largest among one-dimensional organic conductors. The one-dimensional character is also confirmed by the high anisotropy of the electrical conductivity. At room temperature the ratio $\sigma_{\parallel}/\sigma_{\perp}$, measured by the Montgomery method in crystals of $Per_2(AsF_6)_{0.75}(PF_6)_{0.35}\cdot 0.85DCM$, is about 640, decreasing with lowering temperature down to 130 at 35 K [38].

The isomorphous compound $Per_2X_{1.5}\cdot 1/2THF$ has an electrical conductivity as high as the 2 : 1.1 compound with DCM. The thermopower is linear with temperature in the range 100–300 K with a room temperature value $S = 10\ \mu V/K$, but it does not extrapolate to the origin at zero temperature [37].

$Per_2X_1\cdot 2/3THF$ is another system for which metallic behaviour of the conductivity was found, although not so high as in the previous compounds: 10–100 S/cm. In the $X = PF_6$ compound, besides the metal–insulator transition ($T_c = 120$ K), two first-order phase transitions are detected at 155 K and 220 K (Figure 2.16). The latter is attributed to an ordering process of the solvent molecules and the former to a small rotation of adjacent perylene species in the stack. These transitions are clearly detectable in d.c. electrical conductivity measurements. From the low temperature semiconducting regime, an energy gap $2\Delta(0) = 70$ meV was obtained [40].

Some crystals of this stoichiometry, but with a solid solution of the anions, i.e. $X = (AsF_6)_{0.45}(PF_6)_{0.55}$, present a sharp peak in the conductivity which is also observed as a minimum in the thermopower [37]. Typical metallic behaviour is observed in the thermopower above 220 K and a semiconducting behaviour below 120 K with an enhanced (negative) peak at 155 K (see Figure 2.6). The negative sign of the thermopower points out that in this case the degree of bandfilling cannot be simply derived from the stoichiometry. In fact, for a 2 : 1 compound, a 3/4 filled band would be expected and consequently a positive thermopower. However from the structure only 2/3 of the perylene species are in the *c* direction stacking. For a final assignment, the knowledge of the charge distribution is needed. In this compound an additional problem comes from the disordered perylene which introduces a step every four perylene species.

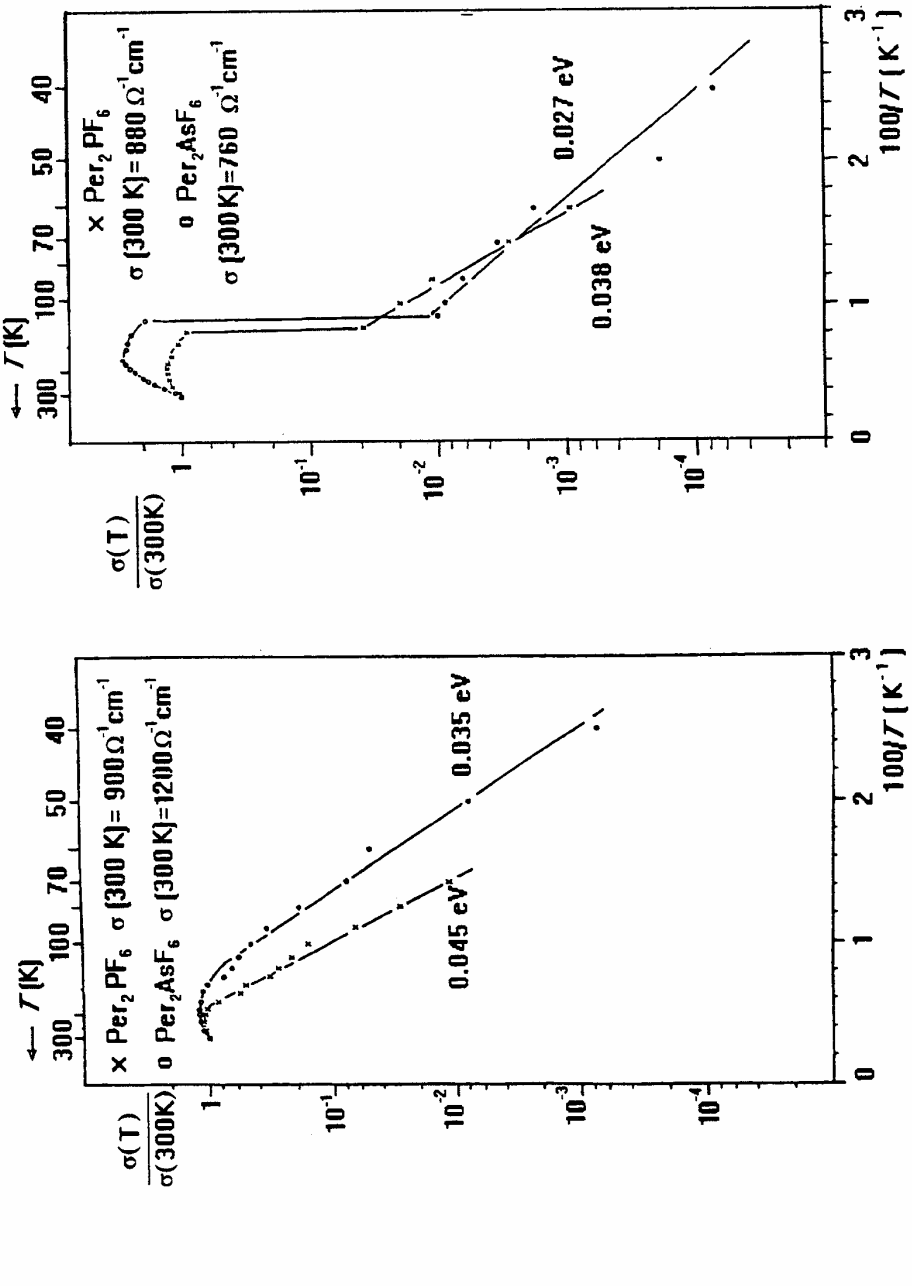


**Figure 2.13.** Normalised conductivity as a function of reciprocal temperature for 'thin' (left) and 'thick' (right) crystals of $Per_2(PF_6)_{1.1}$·0.8DCM and $Per_2(AsF_6)_{1.1}$·0.8DCM. (Reproduced by permission of Gordon & Breach, from ref. 31.)

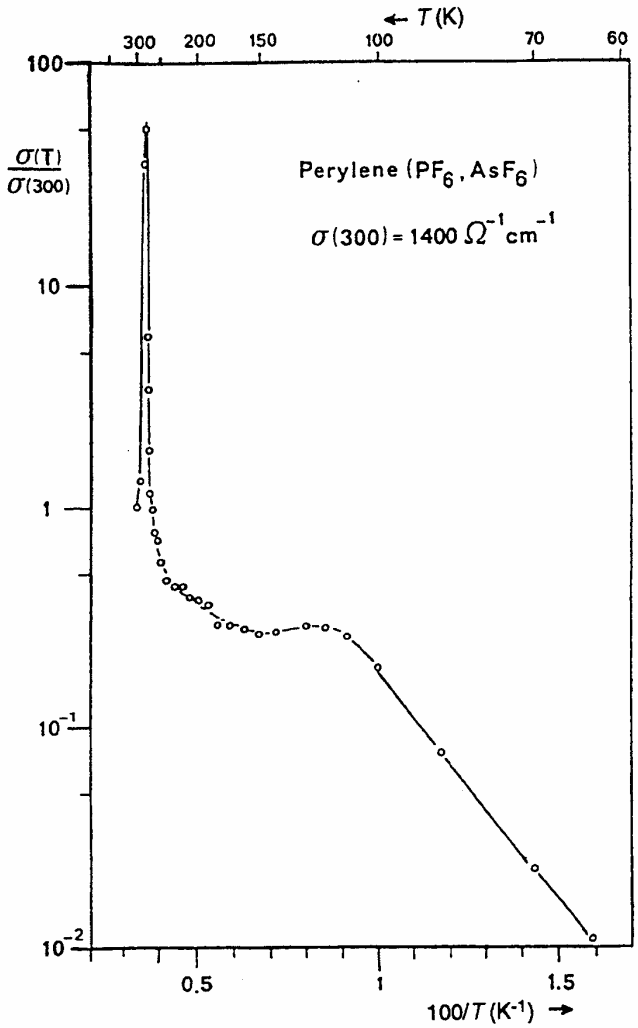


**Figure 2.14.** Normalised conductivity as a function of reciprocal temperature for a 'thin' crystal of the mixed salt $Per_2(AsF_6)_{0.75}(PF_6)_{0.35}\cdot 0.85DCM$. Note the anomalous narrow peak. (Reproduced by permission of Gordon & Breach, from ref. 38.)

The nature of the metal–insulator phase transition cannot be simply investigated through the usual diffuse X-ray scattering as the disorder of the anions and solvent molecules in the channels of the structure cause the appearance of diffuse scattering sheets. Recent work of Brütting and Riess [40] showed non-linear transport in $Per_2(PF_6)_{1.1}\cdot 0.8DCM$ and $Per_2(PF_6)\cdot 2/3THF$ similar to that previously found in $(fluoranthene)_2PF_6$, leading to the assignment of a Peierls ground state for the three compounds. The threshold field is lower for the THF compound ($\sim 0.1$ V/cm), intermediate for the fluoranthene compound and higher and not very well defined for the 2 : 1.1 DCM. These authors concluded that the strong non-linearity for $Per_2PF_6\cdot 2/3THF$, which shows an increase in conductivity of one order of magnitude for $E = 10$ V/cm, is due to an incommen-

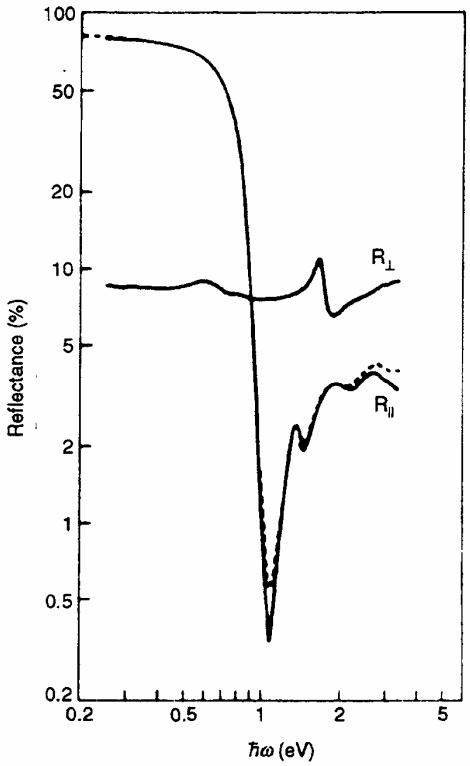


**Figure 2.15.** Reflectance with polarised light of $Per_2(PF_6)_{1.1}$·0.8DCM, showing a plasma edge for the polarisation parallel to the stacking axis and its absence for the perpendicular polarisation. (Reproduced by permission of Gordon & Breach, from ref. 44.)

surate charge density wave. On the other hand the weak non-linearity and high threshold field for $Per_2(PF_6)_{1.1\text{-}0.8}$DCM is attributed to the role of disorder, but this is a subject still under investigation.

### *4.2.4 Magnetic properties*

Static magnetic susceptibility measurements were reported only in some of these compounds. In $Per_6PF_6$ the susceptibility obeys the Curie–Weiss law with small $\theta$ above 40 K, with deviations showing weak antiferromagnetic interactions between 10 and 40 K (Figure 2.17) [39]. The number of spins involved is 98% of the total estimated for the concentration of free radicals according to 6 : 1 stoichiometry.

For the 2 : 1.1 salts, detailed measurements were carried out on $Per_2(AsF_6)_{0.75}(PF_6)_{0.35}$·0.85DCM [46], but as the compounds of this stoichiometry are isostructural and there is only the contribution of the conduction electrons to the susceptibility, the conclusions appear to be valid for the non-mixed salts. The value of the room temperature paramagnetic susceptibility $\chi = 9.2 \times 10^{-5}$ emu $mol^{-1}$, is enhanced by a factor of two relative to the theoretical Pauli susceptibility derived from the density of states at the Fermi level, taking the bandwidth $4t$ obtained by the reflectance measurements. At low temperature the paramagnetic susceptibility follows a $T^{-\alpha}$, with $\alpha < 1$, dependence that is characteristic of localised spins with random exchange coupling. The pressure dependence of $\chi_p$ was also measured, decreasing with applied pressure at a rate of $-3.4\%$ $kbar^{-1}$.

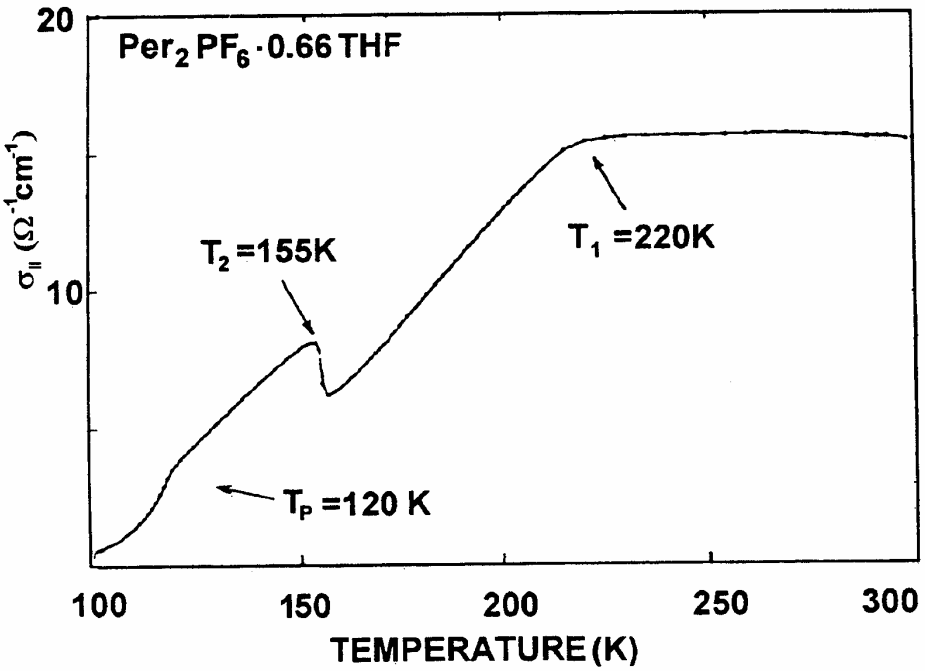


**Figure 2.16.** D.c. electric conductivity of $Per_2(PF_6)$·2/3THF as a function of temperature. The arrows point the two first-order phase transitions at 155 and 220 K and the Peierls transition at 120 K. (Reproduced by permission of Institute of Physics, Poland, from ref. 40.)

At variance with the static susceptibility measurements, is the dynamics of the electron spin, revealing some very interesting features. The conventional X-band EPR spectra for 'thick' crystals of $Per_2(PF_6)_{1.1}$·0.8DCM showed a single lorentzian line with the peak to peak linewidth, $\Delta H_{pp} = 0.6$ G, almost constant down to 190 K, then increasing very slightly and reaching 0.8 G at 100 K [31]. However, in the mixed salt $Per_2(AsF_6)_{0.75}(PF_6)_{0.35}$·0.85DCM, 'thin' crystals present lines as narrow as 95 mG, whereas 'thick' crystals have linewidths, depending on the sample, ranging from 0.5 to 1.2 G [38].

The linewidth is even smaller for $Per_2PF_6$·2/3THF, where $\Delta H_{pp} \approx 17$ mG [37]. In this system Overhauser effect experiments were performed [47] at room temperature in an apparatus combining the X-band EPR spectrometer with an NMR pulsed spectrometer where the enhancement of the fast induced decay of $^1H$ and $^{19}F$ nuclei under saturation conditions of the EPR absorption, were measured. The results showed that the interactions of electronic spins both with protons (in perylene) and fluorine nuclei (in the counterion) are scalar rather than dipolar. The enhancement is greater for protons than for fluorine, basically because the relaxation of protons comes mainly from the interaction with the unpaired electrons of conduction, while for the fluorine there are relaxation mechanisms connected with hindered rotation of the $PF_6^-$ species. The results are consistent with a metallic character for this compound at room temperature.

The electron spin dynamics of $Per_2PF_6$·2/3THF, of the $AsF_6$ analogue and of a mixed salt $(AsF_6)_{0.45}(PF_6)_{0.55}$ were also studied by electron spin echo (e.s.e.) experiments by Meenenga *et al.* [48]. Although they found some deviations of the e.s.e. decay function relative to the expected $\exp(-t^{3/2})$ dependence, they conclude that one-dimensional electron spin diffusion is the basic mechanism. The ratio of the in-stack to the out-of-stack diffusion rates $D_\parallel / D_\perp > 10^7$, with $D_\parallel = 1$ cm $s^{-1}$, a value comparable to the one found for $(fluoranthene)_2AsF_6$ [49]. Dobbert *et al.* [50] performed similar spin-echo experiments in the 2:1.1 mixed salt $Per_2(AsF_6)_{0.75}(PF_6)_{0.35}$·0.85DCM. They found that the relaxation properties can be

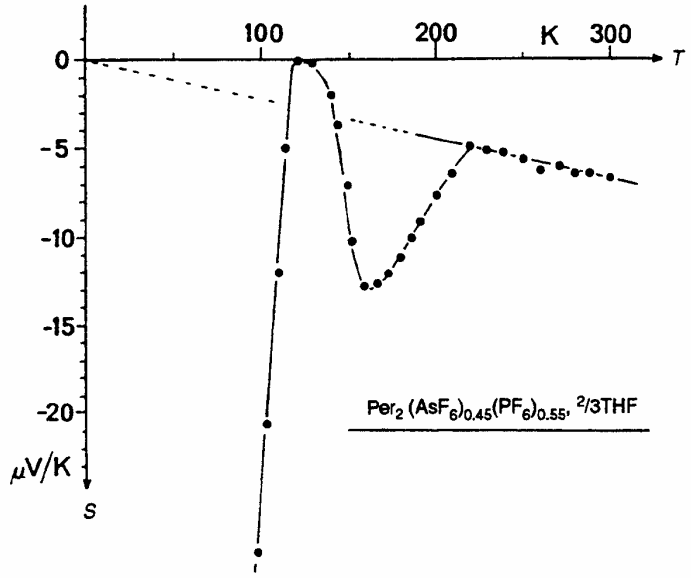


**Figure 2.17.** Thermopower of $Per_2(AsF_6)_{0.45}(PF_6)_{0.55}\cdot 2/3THF$ as a function of temperature. (Reproduced by permission of Gordon & Breach, from ref. 37.)

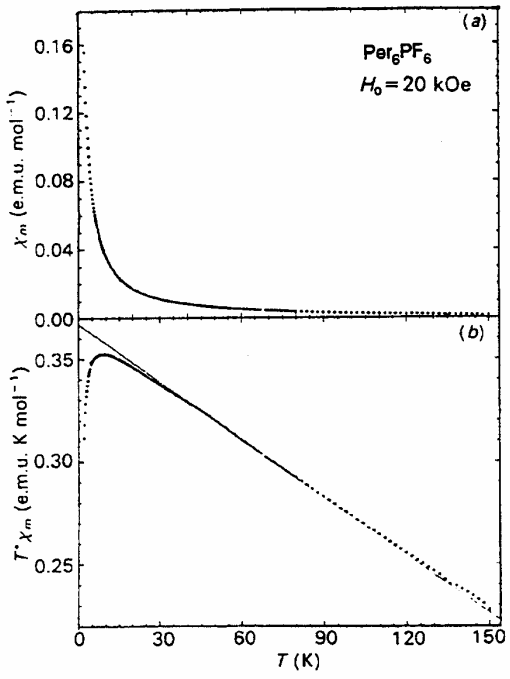


**Figure 2.18.** Magnetic susceptibility of $Per_6PF_6$, showing the deviations from the Curie–Weiss law below 40 K. (Reproduced by permission of International Union of Crystallography, from ref. 39.)

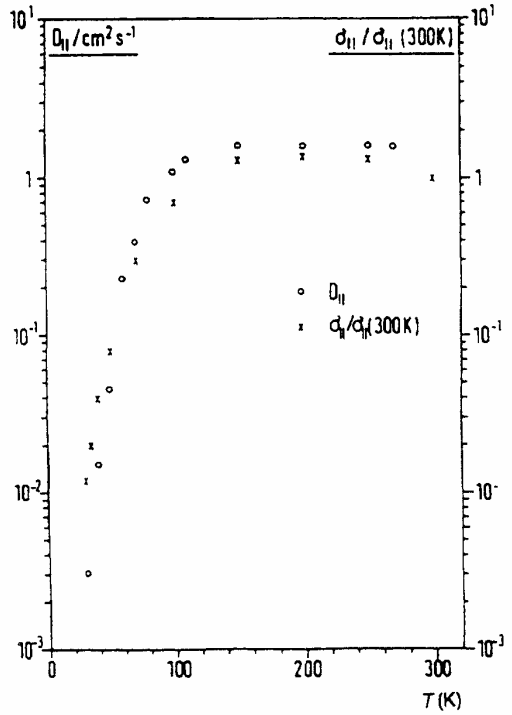


**Figure 2.19.** Thermal dependence of the spin diffusion constant ($D_{\parallel}$) and normalised d.c. conductivity ($\sigma_{\parallel}/\sigma_{\parallel}$(300 K)) data for $Per_2(AsF_6)_{0.75}(PF_6)_{0.35}$·0.85DCM. (Reproduced by permission of Elsevier Science, from ref. 50.)

modified if samples are annealed at 90°C for several hours, leading to a decrease of the EPR linewidth by a factor of 2.5 at room temperature and an increase of the longitudinal relaxation time, $T_{1e}$, at low temperature by the same factor. after annealing, both $T_{1e}$ and $T_{2e}$ are not further modified by thermal cycling. In the temperature range of the metallic regime and down to 100 K, $T_{1e}$ and $T_{2e}$ are equal within experimental error, having upwards and downwards deviations, respectively, at lower temperature. The spin diffusion rate is almost temperature-independent in the metallic regime, $D_{\parallel} = 1.8$ cm$^2$/s, but has a strong temperature-dependence in the semiconducting regime (see Figure 2.19), indicating that the most probable mechanism for electrical conductivity in that range is a thermally activated hopping process. Also in that low temperature range ($T < 100$ K), the relaxation rate $1/T_{2e}$ diverges (Figure 2.20). The interpretation is not yet clear but may be an indication of a fluctuating spin density wave.

The proton NMR spin–lattice relaxation rate, $1/T_1$, was studied in the mixed salt $Per_2(AsF_6)_{0.75}(PF_6)_{0.35}$·0.85DCM [51]. The results show that $1/T_1$ is proportional to the temperature above 180 K, the temperature at which the metal–insulator transition occurs. The range of temperature for the metallic regime is too narrow to notice deviations to the Korringa law observed in other quasi-one-dimensional conductors, e.g. in $Per_2Au(mnt)_2$ [52]. The frequency dependence of $1/T_1$ at room temperature follows the relation: $1/T_1 \propto \nu_L^{-1/2}$, where $\nu_L$ is the Larmor frequency, clearly showing the one-dimensional character of the motion of conduction electrons along the perylene stacks. An estimate of the residence time of a charge carrier in the perylene stack yields $\tau_{\perp} = 3.5 \times 10^{-10}$ s.

### *4.2.5 Final remarks*

From the above, it is clear that the apparent drawback for most of these conductors, i.e. the existence of disordered solvent and anion molecules, does not prevent high conductivity. The dimensionality of the

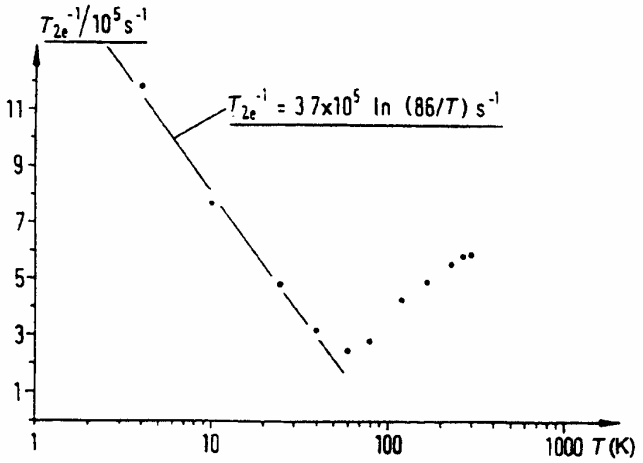


**Figure 2.20.** Temperature dependence of the electronic spin–spin relaxation rate, $1/T_{2e}$, for the mixed salt $Per_2(AsF_6)_{0.75}(PF_6)_{0.35}$·0.85DCM. (Reproduced by permission of Elsevier Science, from ref. 50.)

conductive systems, as inferred by magnetic resonance studies and by polarised reflectance measurements, is clearly one-dimensional. The observation of non-linear transport in some of the compositions is an indication of a Peierls ground state but more studies are needed to confirm this aspect.

The nature of the difference between 'thin' and 'thick' crystals remains unclear. From the available data, they probably do not correspond to drastically different phases, having the same mean structure, as defined by the perylene arrangement, and may differ only on the disposition of counterions and solvents along the channels, as in the case of $CPP_2(I_3)_{1-\delta}$ (see Section 6). Some of the anomalies in the transport properties, e.g. the 'phonon-drag like' peaks in conductivity and thermopower [37], have been tentatively explained evoking the role of the molecular librations, but the differences found in EPR linewidths, however, remain unexplained.

## 4.3 Haloiron salts

Recently two new perylene salts with tetrahedral iron(III) counterions, $Per_3FeCl_4$ and $Per_3FeBr_4$, were reported [35]. Although presenting modest semiconducting properties, these compounds are the first perylene based conductors with simple inorganic paramagnetic counterions. They were obtained on the anode of an electrochemical cell, under galvanostatic conditions, from a solution of perylene and tetraalkylammonium salts of $FeX_4$ in 1,1,2-trichloroethane or dichloromethane. The crystal structure of $Per_3FeCl_4$ was solved and consists of tetramerised stacks of perylene species along the *b*-axis, separated by the anions and two extra perylene molecules per unit cell (Figure 2.21). The perylene packing is very similar to that of $Per_2PF_6$·2/3THF, in spite of the different stoichiometry [34]. The tetramerisation is due to a transversal modulation of the chains, at variance with $Per_3ClO_4$, which is a compound of the same stoichiometry where the tetramerisation of the perylene stacks is due to a strong longitudinal modulation of the molecules [34]. There is evidence through the short Cl···H distances for interactions between $FeCl_4$ and the perylene species in the structure. These interactions may be responsible for the almost collinear Fe–Cl···Cl–Fe that otherwise would be unstable.

The electrical conductivity ($\sigma_{RT} = 0.17$ S/cm) of this compound shows that it is a semiconductor with an activation energy of 0.12 eV at room temperature, decreasing to 0.08 eV below 255 K. Thermopower ($S_{RT} = 275$ $\mu$V/K) indicates that transport is hole-dominated. The large paramagnetic susceptibility of both $Per_3FeCl_4$ and $Per_3FeBr_4$ is governed by the paramagnetic $Fe^{3+}$ ($S = 5/2$) ions, and its temperature dependence (Figure 2.22) was fitted by a model of interacting pairs of $S = 5/2$ spins [53].

The extended Hückel calculations performed for the perylene stacking show a one-dimensional dispersion of the electronic energy. Four bands are obtained from the HOMO with the Fermi level lying in the middle of the upper band gap, in agreement with the semiconductive properties found experimentally.

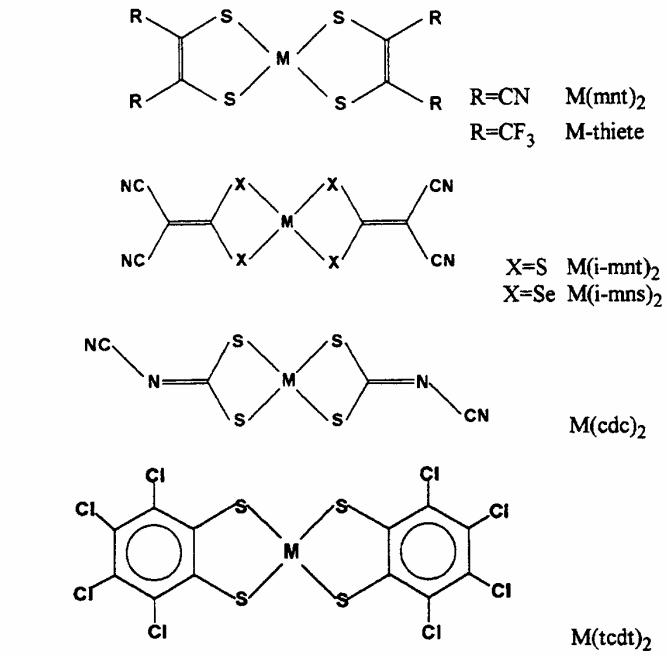


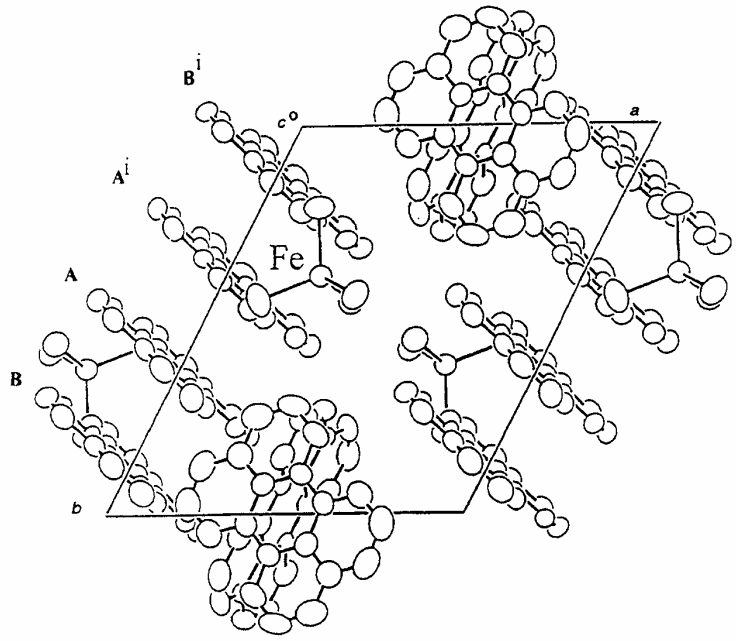


**Figure 2.21.** Projection along the **c**-axis of the $Per_3FeCl_4$ crystal structure, with the hydrogen atoms omitted for clarity. (Reproduced by permission of The Royal Society of Chemistry, from ref. 35.)

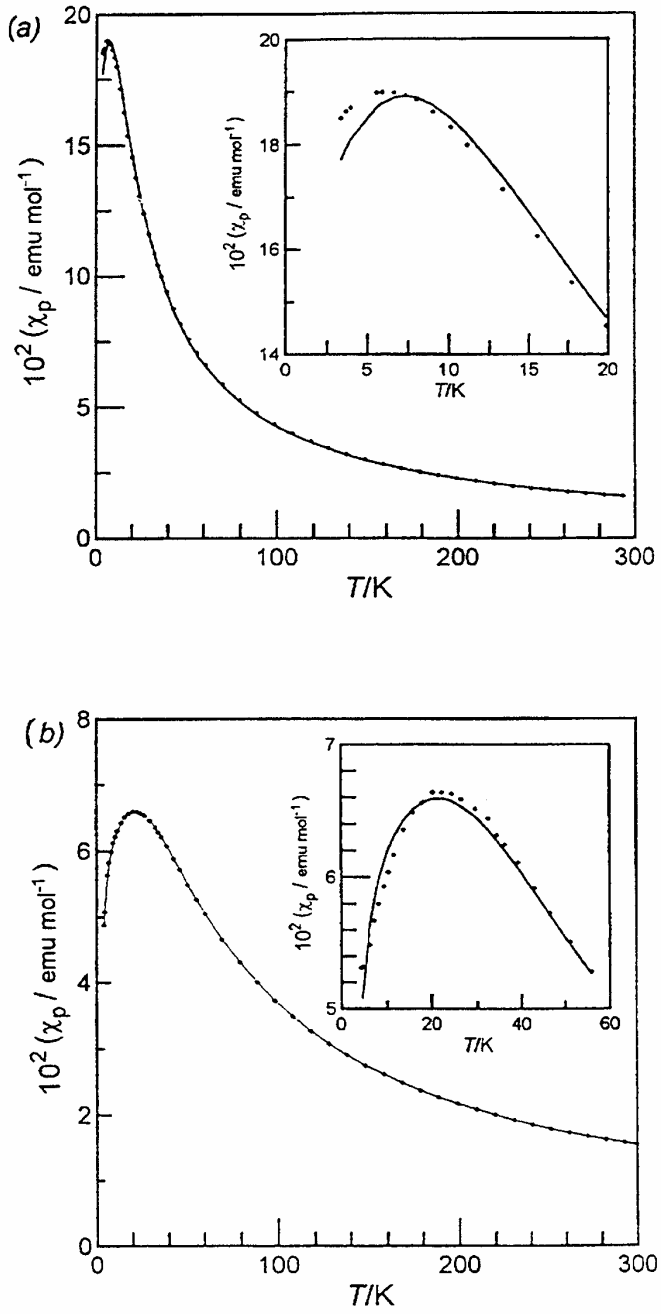


**Figure 2.22.** Magnetic susceptibility of $Per_3FeCl_4$ (a) and $Per_3FeBr_4$ (b) as a function of temperature. The solid line represents the fit of a model of interacting $S = 5/2$ spins. The insets display the low temperature behaviour around the maximum. (Reproduced by permission of The Royal Society of Chemistry, from ref. 35 .)

# 5 PERYLENE CONDUCTORS WITH METALLOCOMPLEX ANIONS

Several types of metallocomplex anions, essentially of the type metal–bisdichalcogenelene, have been used as counterions in perylene based conductors. In some cases, as for the $M(mnt)_2$ series, different types of metals M with the same ligand have been extensively studied, leading to a large family of charge-transfer solids that are essentially isostructural (see Table 2.4). The magnetic properties of the members of this family of compounds strongly depend on the type of metal M which can lead either to diamagnetic or paramagnetic anions.

## 5.1 Perylene conductors with $M(mnt)_2$ anions

Perylene charge-transfer complexes with $M(mnt)_2$ anions were first studied by Alcácer and Maki, and in 1974–1976 reported the $Per_2M(mnt)_2$ compounds with M = Cu, Ni and Pd [54,55]. The first two were isolated as small single crystals and were characterised as semiconductors, as well as the Pd compound, then obtained only as polycrystalline powder samples [54]. The compounds with M = Pt, Au and Pd were reported a few years later, between 1980 and 1987, as single crystals thanks to the improvement of the crystal growth techniques, which enabled also the study of the Pd compound as single crystals [30,56–61]. These were identified as quasi-one-dimensional metals undergoing metal to insulator (M–I) transitions at low temperatures. More recently new compounds with M = Co and Fe have also been reported [62–64], as well as a reinvestigation of the Ni and Cu compounds [65–68] and more detailed physical studies were made, allowing a more complete picture of this family of compounds [69–71]. Other variants of these counterions have also been studied although not so systematically explored as $M(mnt)_2$ (see Section 5.2 and table 2.8 on p. 141).

### *5.1.1 Sample preparation*

The $Per_nM(mnt)_2$ compounds are prepared by perylene oxidation in solutions containing the $M(mnt)_2^-$ anion. This oxidation can be carried out chemically by the addition of iodine, or electrochemically. The perylene cation once generated, promptly associates with neutral perylene as $Per_2^+$ which reacts with the anions present in the solution [3] to precipitate on the electrodes the low-solubility $Per_nM(mnt)_2$ compounds, usually with $n = 2$. For M = Co compounds with other stoichiometries such as $PerCo(mnt)_2 \cdot 0.5(CH_2Cl_2)$ [72] and $Per_4[Co(mnt)_2]_3$ [73], are usually obtained in the same electrochemical preparation. For M = Pt a 1 : 1 compound was also described by Shibaeva *et al.* [74] as resulting from the iodine oxidation route. However this compound presents a mixed stack arrangement with perylene dimers alternating with dimers of $Pt(mnt)_2$ units and therefore it is a very poor semiconductor with a room temperature conductivity of $10^{-3}$ S/cm. As previously stated, the low solubility of the neutral perylene in organic solvents, where the salts of $M(mnt)_2^-$, usually the TBA salts, (TBA = tetrabutylammonium), are also soluble, is a limiting factor in the crystal growth. Dichloromethane is usually the best choice in which the perylene solubility at room temperature is about $1.5 \times 10^{-2}$ M. Similar results have been obtained also with 1,1,2-trichloroethane or other polar halogenated solvents. Although THF allows a solubility almost ten times larger than dichloromethane, apparently it does not give better results and has not been so extensively used. The low solubility of these compounds and the instability of the perylene cation makes it virtually impossible to recrystallise the compounds.

In the chemical oxidation process, typically a small excess of iodine is added to a solution of perylene and $M(mnt)_2^-$, usually as a TBA salt in stoichiometric proportions, and the crystals are collected after cooling and partial evaporation. The best samples are obtained by a slow diffusion-controlled process lasting a few days.

The electrocrystallisation process, with the exception of the Pd compound in which it does not work, usually gives better quality crystals without the risk of possible iodine contamination. The best results have been obtained using galvanostatic conditions in two-compartment cells with platinum electrodes. The crystals are obtained on the anode and collected after a few days with current densities in the range 5–20 $\mu A/cm^2$. They can be longer than 10 mm but their cross-section is typically $0.05 \times 0.02$ mm$^2$, except for M = Pt and Fe where thicker crystals are obtained. For M = Cu, larger current densities, in the range 20–50 $\mu A/cm^2$ are necessary in order to avoid an insulating decomposition product that covers the electrode, and the crystals, usually very thin ($\sim 5 \times 0.02 \times 0.01$ mm$^3$), are collected after a few hours [65]. As in many other cases of electrocrystallisation, the crystal quality and size are difficult to reproduce but for M = Pt and Fe they are quite larger, although often somewhat fibrous crystals with dimensions of up to $15 \times 1 \times 0.2$ mm$^3$.

**Table 2.4.** Summary of room temperature crystallographic data for $Per_2M(mnt)_2$ compounds

| M | β-Cu | β-Ni | α-Cu | α-Ni | α-Au | α-Pt | α-Pd | α-Co[a] | α-Fe |
|---|---|---|---|---|---|---|---|---|---|
| $a$ (Å) | 15.3(1) | 15.31 | 17.5(1) | 17.44(1) | 16.602(2) | 16.612(4) | 16.469(6) | 17.75(5) | 50.571(6) |
| $b$ (Å) | 4.07(2) | 4.02 | 4.17(5) | 4.176(2) | 4.194(1) | 4.1891(6) | 4.1891(6) | 8.22(5) | 8.212(2) |
| $c$ (Å) | 20.8(1) | 20.33 | 25.5(1) | 25.18(1) | 25.546(3) | 26.583(6) | 26.640(9) | 25.88(5)[a] | 17.726(1) |
| $\alpha$ (°) | ~90 | 89.31 | 90 | 90 | 90 | 90 | 90 | 90 | 90 |
| $\beta$ (°) | 101.5 | 101.53 | 91.4(3) | 91.57(2) | 94.58(1) | 94.54(2) | 95.07(3) | 92.0(3) | 92.43(1) |
| $\gamma$ (°) | ~90 | 93.37 | 90 | 90 | 90 | 90 | 90 | 90 | 90 |
| $V$ (Å$^3$) | ~1200 | 1224 | 1856(10) | 1833(2) | 1841(1) | 1846(2) | 1831(2) | 3778(10) | 7354(3) |
| $Z$ | 1.5 | 1.5 | 2 | 2 | 2 | 2 | 2 | 4 | 8 |
| Space group | | | $P2_1/n$ | $P2_1/n$ | $P2_1/n$ | $P2_1/n$ | $P2_1/n$ | $P2_1/n$[a] | $C2/c$ |
| Ref. | 65 | 65 | 65 | 65 | 61 | 30 | 61 | 63 | 63 |

[a] Most probably the space group is $C2/c$ with the $c$ parameter doubled as in α-Fe.

Several phases can be obtained by these processes. For M = Co different stoichiometries have been referred to above. In the case of the other metals only the stoichiometry $Per_2M(mnt)_2$ was detected, but as discussed below, in many cases (at least for M = Ni, Cu and Au) these crystals can be obtained in two distinct crystallographic forms denoted as α and β [65]. All these crystals are dark, metallic and shining and therefore the α and β phases are difficult to distinguish by eye. In the Co compounds the different stoichiometries sometimes can be distinguished by the crystal morphology. The $Per_2Co(mnt)_2$ crystals, as those with other metals, are always very elongated and needle-shaped, often with a multifibre bundle aspect. $Per_2Co(mnt)_2 \cdot 0.5(CH_2Cl_2)$ crystals have a thicker habit with typical dimensions 3 × 0.5 × 0.5 mm$^3$, which are usually 90–95% of the preparation [72], although occasionally a batch almost entirely of the first stoichiometry can be obtained. $Per_4[Co(mnt)_2]_3$ crystals are always a minority in a preparation and have almost isotropic dimensions and a slightly greenish shine [73].

### 5.1.2 α-$Per_2M(mnt)_2$ phases

The properties of the α-$Per_2M(mnt)_2$ compounds, especially those derived from the coexistence in the same solid of delocalised electron chains (perylene molecules) and chains of localised spins ($M(mnt)_2^-$ units for some M), were recognised early on as a unique and interesting feature of this family of compounds [57], and are the main topic of two short reviews [70,71]. In fact, this type of compound produced the first examples of one-dimensional molecular metals where delocalised electrons were found to clearly interact with localised spins. In this respect they resemble some of the properties of Cu(Pc)I, (Pc = phthalocyanine), a case where the delocalised electrons in stacks of the Pc ligands interact with the paramagnetic $Cu^{2+}$ ions which in this compound are localised in the same chain [75,76]. More recently, other cases of conducting and even superconducting compounds with paramagnetic counterions and even ferromagnetic transitions have been reported and their study is presently a hot topic in the field of molecular conductors. In the present section, the α-$Per_2M(mnt)_2$ compounds will be described and their properties reviewed especially taking into account more recent data enlightening the role of each type of chain in the phase transitions undergone at low temperatures.

#### 5.1.2.1 *Crystalline structures*

All these compounds have a very similar structure [30,61,63,65], with segregated stacks of perylene and $M(mnt)_2$ units along the **b** direction, the main difference being the doubling of the lattice parameter **b** in the M = Fe and Co compounds ($b \approx 8.2$ Å) when compared with the other members of the family ($b \approx 4.18$ Å) [63] (see Table 2.4). The structure of the Pt, Au, Pd, and Ni compounds, space group $P2_1/n$, was solved by refinement of the X-ray diffraction data. The Fe compound was found by synchrotron radiation to have a cell doubled along both the **a**- and **b**-axes, space group $C2/c$. However its crystal structure only could be solved using a conventional X-ray source, as an average structure, neglecting the cell doubling reflections and assuming space group $P2_1/n$. The structure of the Co and Cu compounds was not solved, but their lattice parameters and diffraction patterns indicate that they are isostructural with the Fe and Ni compounds respectively.

In the α-phase each stack of $M(mnt)_2$ is surrounded by six stacks of perylene molecules which are twice in number of the $M(mnt)_2$ units (Figure 2.23). In the $b \approx 4.18$ Å structures these stacks are uniform, the perylene molecules being more tilted with respect to the chain axis **b** than the dithiolate molecules. As a consequence the perylene interplanar distance, ranging from 3.32 Å to 3.36(3) Å (average) in Fe, with essentially the same overlap mode in all compounds (Figure 2.24), is always shorter than that between the $M(mnt)_2$ planes where minor changes are detected in the type of overlap (Figure 2.25). While the Pt and Au compounds present a $M(mnt)_2$ overlap mode with a displacement essentially along the longitudinal axis of the anions, both in the Ni and in the Fe average structure the overlap mode clearly denotes a preferred M over S interaction.

As there is only an average structure for the Fe compound, no detailed description of the lattice doubling in the Fe and Co compounds is known. However $^{57}$Fe Mössbauer spectroscopy of the Fe compound, yielding results virtually identical to those of the tetraalkylammonium salts of $Fe(mnt)_2^-$ [63], provides strong evidence for dimerisation of the $M(mnt)_2^-$ units by M–S interactions, as in the above-mentioned salts, that are known to adopt a standard square-pyramidal coordination of the metal. This is further supported by the magnetic susceptibility data (see below). The transport properties discussed below suggest that any dimerisation effects on the perylene chains should be small.

### 5.1.2.2 *Electrical transport properties*

The α-$Per_2M(mnt)_2$ compounds present at higher temperatures a metallic regime of the electrical conductivity, $\sigma$, measured along the stacking axis **b**, undergoing metal-to-insulator (M–I) transitions at lower temperatures (see Figure 2.26). These transitions are clearly due to a gap opening at the Fermi level, as denoted by maxima in the d ln $\sigma$/d $(1/T)$ plots at temperatures $T_c$ ranging from 8.2 K for M = Pt to 73 K for M = Co (see Table 2.5). Typically at $T_\rho \approx 3T_c$ a broad minimum of resistivity is observed, corresponding to the onset of pretransitional fluctuations. At room temperature the electrical conductivity was found to be of the order of 700 S/cm for the M = Au, Pt, Ni and Cu compounds, 300 S/cm for M = Pd and 200 S/cm for the M = Fe and Co compounds. The lower conductivity of the M = Pd samples when compared with the M = Au, Pd, Ni and Cu ones, is thought to be a consequence of the poorer quality of the M = Pd crystals, that can be obtained only by the iodine oxidation route. In the case of the Fe and Co compounds the lower conductivity reflects the effect of the dimerisation of the counterions which reduces the effective bandwidth. It is also worth noting that in the Fe and Co compounds significantly higher transition temperatures (58 and 73 K respectively) are also observed. In the Pt and Fe compounds, the larger dimensions of some crystals (up to $\sim 15 \times 1 \times 0.2$ mm$^3$) enabled the estimation of the anisotropy $\sigma_{\parallel b}/\sigma_{\perp b} \approx 10^3$, a value that remains almost temperature-independent down to the M–I transition [56,63]. This is one of the highest anisotropy values observed among molecular metals, placing these solids at the extreme end of one-dimensional systems, and it reflects the poor contact and the negligible interactions between perylene molecules in neighbouring chains, as confirmed by the extended Hückel calculations [78]. The anisotropy in the **a**,**c** plane was not measured but in view of the structure it is not expected to be very significant.

In many cases the low temperature gap, $2\Delta$, cannot be correctly estimated from the regime of the electrical conductivity, $\sigma(T)$, well below the M–I transition assuming an intrinsic semiconducting regime and using $\Delta = -\mathrm{d} \ln \sigma / \mathrm{d}\,(1/T)$. Probably due to a larger number of impurities and defects, a well-defined temperature range with constant values of d ln $\sigma$/d $(1/T)$ is not always clearly observed. This is particularly the case of the M = Au compound in which the early studies were unable to detect a clear M–I transition [56]. However, as seen in Table 2.5, the estimated gap values obtained lead to $2\Delta/k_B T_c$ ratios in the range 10–15, values that even considering all the uncertainties are well above the mean field prediction of 3.52, indicating a strong coupling regime.

The thermoelectric power (Figure 2.27) confirms both the metallic regime at high temperatures and the M–I transitions that were observed through resistivity measurements. At room temperature positive thermopower values, in the range 32 to 42 μV/K, are observed, decreasing upon cooling until $T_c$ in a very similar way for all compounds. Particularly in the low $T_c$ members of this series, a plateau in the thermopower is observed below 100 K, whose origin is not fully understood. However, the positive sign and the almost linear temperature regime of thermopower at high temperatures, are indicative of hole transport, as in a 3/4 filled band system and as expected from a full charge-transfer situation leading to regular $Per^{1/2+}$ chains with relatively unimportant Coulomb correla-

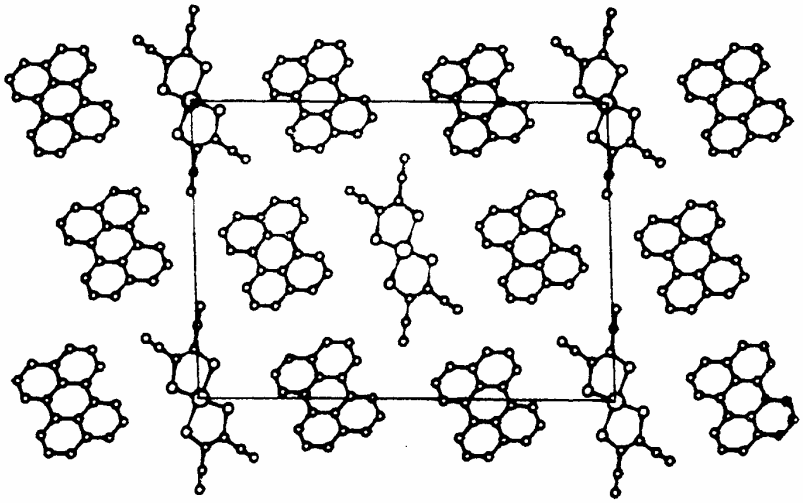

**Figure 2.23.** Projection along the stacking axis **b** of the crystal structure of α-$Per_2M(mnt)_2$ phases (unit cell of the $P2_1/n$ space group). (Reproduced by permission of The American Chemical Society, from ref. 63.)

tions. Applying the tight-binding model to the high temperature thermopower data [42], the bandwidths of these compounds were estimated to be in the range 0.55–0.60 eV depending on the metal M [60,63,68]. The relatively unimportant role of the Coulomb correlations is further confirmed by the magnetic susceptibility measurements as discussed below, as well as by the fact that in the M = Co and Fe compounds with a dimerised lattice along the chain axis **b**, a metallic thermopower, similar to the other members, is also observed. This indicates that the dimerisation potential felt by the conduction electrons in the perylene chains is very small, opening a gap that does not significantly affect the electronic band structure at the Fermi level.

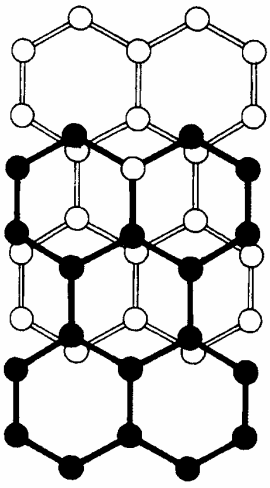

**Figure 2.24.** Perylene overlap mode in $Per_2Au(mnt)_2$. Compounds with other metals show virtually the same mode.

The magnitude of the thermopower (as well as of the Pauli paramagnetism) at high temperature is a measure of the density of states at the Fermi level, and therefore it is expected to be inversely proportional to the bandwidth. In fact, as seen in Table 2.6, a fairly good correlation exists between the observed increase in the perylene intermolecular distances (all with the same type of overlap) and the increase in the high temperature thermopower (and Pauli-like paramagnetism) in this family of compounds.

When comparing compounds of this family with adjacent metals, M(III), from the same line in the periodic table (e.g. Au and Pt or Cu and Ni), one clearly notes that the unpaired electron of the $d^7$ metal complexes (Ni and Pt) does not affect the transport properties and the M–I transition occurs in the same way, irrespective of the paramagnetic or diamagnetic character of the $M(mnt)_2^-$ units. The only systematic

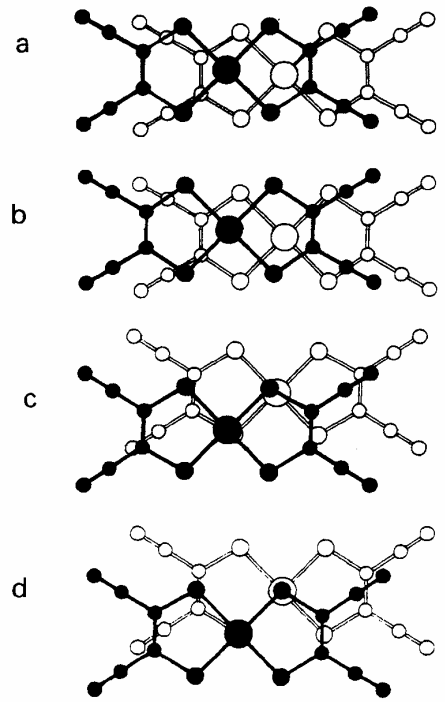


**Figure 2.25.** Overlap mode of the $M(mnt)_2$ units in different $\alpha$-$Per_2M(mnt)_2$ compounds: (a) M = Pt, (b) M = Au, (c) M = Ni, (d) M = Fe (average structure).

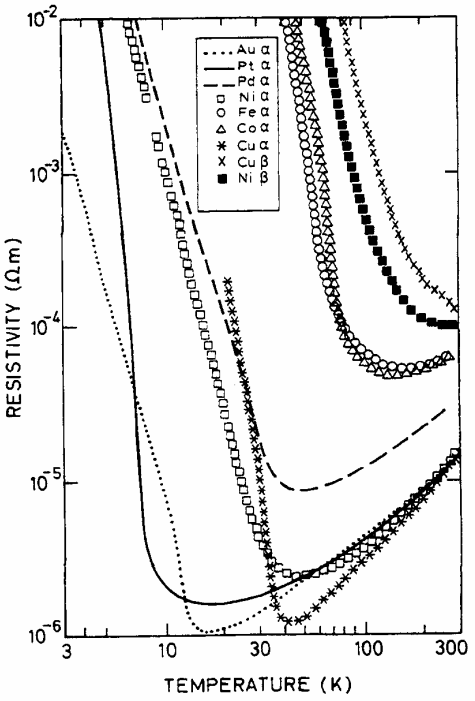


**Figure 2.26.** Electrical resistivity along the chain axis **b** of different $Per_2M(mnt)_2$ compounds as a function of temperature.

**Table 2.5.** Properties of $Per_2M(mnt)_2$ compounds

| M | $S$ | $\sigma$(RT) (S/cm) | $S$(RT) ($\mu$V/K) | $T_\rho$ (K) | $T_c$ (K) | $2\Delta$ (meV) | $10^4\ \chi_p$(RT) (emu/mol) | Dimer | Tetramer | Ref. |
|---|---|---|---|---|---|---|---|---|---|---|
| $\alpha$-Au | 0 | 700 | 32 | 16 | 12.2 | 3.5 | 1.8 | | | 60,70,77 |
| $\alpha$-Cu | 0 | 700 | 38 | 40 | 32 | 20 | 1.8 | | X | 65,68 |
| $\alpha$-Pt | 1/2 | 700 | 32 | 18 | 8.2 | 8.6 | 15.5 | X* | | 30,52,56 |
| $\alpha$-Pd | 1/2 | 300 | 32 | 80 | 28 | | 9.0 | X | | 56,70 |
| $\alpha$-Ni | 1/2 | 700 | 35 | 50 | 25 | 15 | 13.0 | X* | X | 65,67,68 |
| $\alpha$-Co | 0 | 200 | 42 | 160 | 73 | 60 | 2.6 | x | X | 63,64 |
| $\alpha$-Fe | 3/2 | 200 | 42 | 180 | 58 | 50 | 15 | x | X | 63,64 |
| $\beta$-Cu | 0 | 50 | 22 | | – | – | 4.5 | – | – | 65,68 |
| $\beta$-Ni | 1/2 | 50 | 22 | 250 | – | – | 12 | – | – | 65,68 |

$S$ = spin of the $M(mnt)_2^-$ unit; $\sigma$(RT) = room temperature electrical conductivity; $S$(RT) = room temperature thermopower; $T_c$ = metal to insulator transition temperature; $T_\rho$ = minimum electrical resistivity temperature; $2\Delta$ = low temperature gap derived from resistivity; $\chi_p$(RT) = room temperature paramagnetic susceptibility; X = lattice distortion observed below $T_c$; * one-dimensional precursor effects above $T_c$ up to $\sim 3T_c$; x = lattice distortion present over the whole temperature range.

effect is a slight reduction of both $T_c$ and $T_c/T_\rho$ in the $d^7$ metal compounds when compared with the $d^8$ ones. As will also become evident from the discussion of the magnetic properties (see next section) the $M(mnt)_2^-$ chains do not contribute to the conductivity. Extended Hückel-type calculations estimate the HOMO bandwidth of the $M(mnt)_2$ chains as $\sim 50\%$ of the bandwidths of the perylene chains [78]. Therefore the $M(mnt)_2^-$ units, if with an unpaired electron, behave as Mott insulating systems, with only significant contribution to the magnetic properties.

### 5.1.2.3 *Magnetic properties*

At variance with the transport properties, the magnetic behaviour of these compounds is strongly dependent on the type of metal M. For diamagnetic $M(mnt)_2^-$ units, as for M = Au, Cu and Co, the magnetic susceptibility is due only to a small contribution of the perylene conduction electrons, which vanishes at the M–I transition (Figure 2.28a). A much larger magnetic susceptibility, due to an additional contribution of a chain of localised spins in the anions, is observed in cases of paramagnetic $M(mnt)_2^-$ units.

In the compounds with diamagnetic $M(mnt)_2^-$ species, the small paramagnetism vanishes at the M–I transition, clearly indicating that it is due to the conduction electrons. Above the transition there is a noticeable increase of the paramagnetic susceptibility upon increasing temperature in the metallic regime and their values are significantly above the Pauli paramagnetism predicted from the one-dimensional tight-binding model of uncorrelated electrons, considering the bandwidth estimated from thermopower. This difference, as in many other one-dimensional molecular metals, is due to Coulomb correlation enhancement of the paramagnetism, and the ratio between the on-site Coulomb correlation parameter $U$ and the bandwidth $4t$ is estimated as $U/4t \approx 0.5$ [68]. However, in spite of this enhancement, the relative values of the paramagnetic susceptibility, clearly larger in the Co compound than in the Au and Cu ones, follow the same trend of the thermopower, decreasing with the decrease of the intermolecular perylene distances (see Table 2.6).

The larger paramagnetism of the compounds with $S = 1/2$ $M(mnt)_2^-$ units, also vanishes at the M–I transition, indicating that there is a magnetic transition in the localised spin chains of $M(mnt)_2^-$ units that follows the M–I transition in the perylene chains. At temperatures well above the transition, clear antiferromagnetic interactions are already noticed, and the susceptibility of the Pt and Pd compounds can be relatively well described by the Bonner–Fisher model

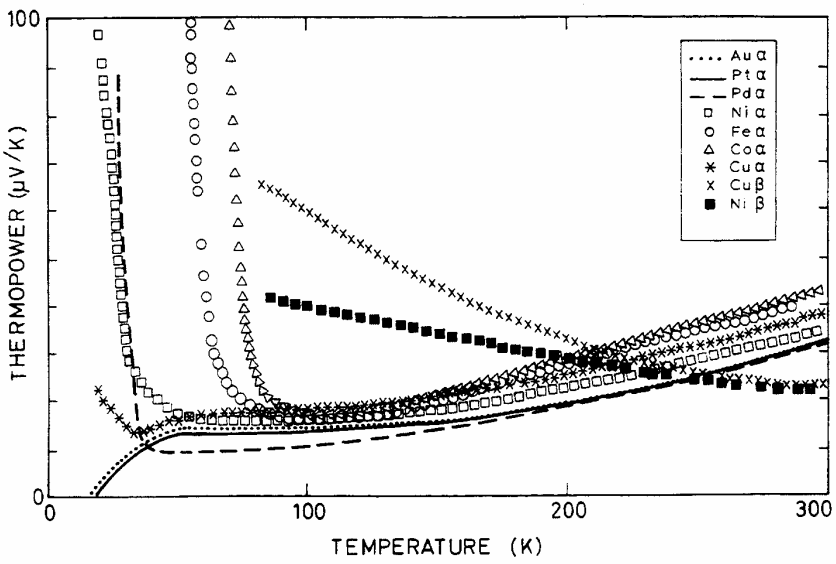


**Figure 2.27.** Thermoelectric power along the chain axis **b** of different $Per_2M(mnt)_2$ compounds as a function of temperature.

**Table 2.6.** Selected structural and physical properties of α-$Per_2M(mnt)_2$ compounds

| M | $d_{p-p}$ (Å) | $S$(RT) (mV/K) | $d_{m-m}$ (Å) | $10^4$ $\chi_P$(RT) (emu/mol) | $J/k_B$ (K) | $\measuredangle_{p,b}$ (°) | $\measuredangle_{m,b}$ (°) | Ref. |
|---|---|---|---|---|---|---|---|---|
| Au | 3.32 | 32 | 3.62 | 1.8 | – | 37 | 30.2 | 61,70 |
| Cu | – | 38 | – | 1.8 | – | – | – | 65,68 |
| Pt | 3.32 | 32 | 3.65 | – | 15 | 37 | 29 | 30,52 |
| Pd | 3.32 | 32 | 3.59 | – | 75 | 37 | 30.9 | 61,70 |
| Ni | 3.34 | 35 | 3.53 | – | ~150 | 36.1 | 32.2 | 65,68 |
| Co | – | 42 | – | 2.7 | – | – | – | 63 |
| Fe[a] | 3.36(3)[a] | 42 | 3.46(3)[a] | – | 300 ($S = 3/2$) | 34.87[a] | 32.4(3)[a] | 63 |

$d_{p-p}$ = interplanar perylene distance; $d_{m-m}$ = interplanar $M(mnt)_2$ distance; $J$ = antiferromagnetic coupling constant between $M(mnt)_2$ units above $T_c$; $\chi_P$(RT) = room temperature paramagnetic susceptibility; $S$(RT) = room temperature thermopower; $\measuredangle e_{p,b}$ = angle between normal of perylene molecule and $b$-axis; $\measuredangle_{m,b}$ = angle between normal of $M(mnt)_2$ unit and $b$-axis. [a] Data from the average structure.

of antiferromagnetically coupled $S = 1/2$ chains with $J/k_B \approx 15$ and 75 K respectively [71]. Stronger antiferromagnetic interactions in the Ni compound ($J/k_B \approx 150$ K), whose susceptibility does not however follow so well the previous model [68].

These magnetic transitions in the compounds with $S = 1/2$ $M(mnt)_2^-$ units contrast with the behaviour of the Fe compound where the $Fe(mnt)_2^-$ contribution to the susceptibility was shown to be well described by a model of antiferromagnetically coupled pairs of $S = 3/2$ spins, with a temperature-independent $J/k_B = 300$ K, as expected for a strongly dimerised chain of $[Fe(mnt)_2]^{2-}$ units and without any noticeable change at the M–I transition [63].

In the larger Pt crystals, magnetic susceptibility measurements, both static or by EPR signal integra-

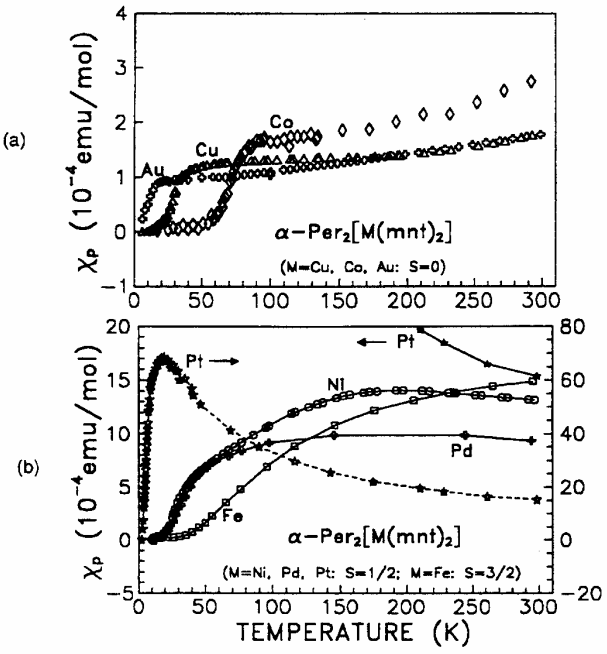


**Figure 2.28.** Paramagnetic susceptibility of different α-$Per_2M(mnt)_2$ compounds as a function of temperature. (a) M = Au, Cu and Co compounds with diamagnetic $M(mnt)_2^-$ anions, (b) M = Ni, Pd, Pt (S = 1/2) and Fe (S = 3/2) compounds with paramagnetic anions. (Reproduced by permission of Gordon & Breach, from ref. 71.)

tion, show an exponential decrease of the susceptibility either with the field parallel or perpendicular the chain axis **b** [52]. This isotropic exponential decrease of the magnetic susceptibility below $T_c$ is typical of a spin–Peierls system and excludes the possibility of an usual antiferromagnetic transition. Further evidence for a spin–Peierls-like transition is provided by the X-ray diffraction studies as described below.

The EPR spectra of the compounds with diamagnetic $M(mnt)_2$ units present a single line that is narrower than in those with paramagnetic counterions. This line has almost isotropic and temperature-independent $g$-values, $\approx 2.0043$, close to those of the perylene cation in solution [79] and its integrated intensity closely follows the static paramagnetic susceptibility data (Figure 2.29). This clearly shows that the Pauli-like susceptibility is due to the delocalised electrons in the perylene chains. The linewidths are relatively small (0.3 G, 0.5 G and 6 G at room temperature for M = Au, Cu and Co respectively) as expected in low-dimensional metals without paramagnetic centres. Upon cooling there is a significant reduction of the width in the Co compound, which becomes comparable to the two others, and all have a small peak just before the M–I transition as in many Peierls systems.

The Fe compound, in spite of the paramagnetic $S = 3/2$ spins in the $Fe(mnt)_2^-$ units, presents a line with $g$-values corresponding to the perylene cation, as in cases of diamagnetic $M(mnt)_2^-$ units, and with an integrated intensity quite different from the static susceptibility but very close to the Pauli contribution expected from the perylene conduction electrons [64] (Figure 2.30). Most probably the expected $Fe(mnt)_2^-$ EPR signal is too broad and remains experimentally undetected. However the linewidth observed (32 G at room temperature, decreasing approximately as the susceptibility of the $Fe(mnt)_2$ chains upon cooling), is much larger than in the compounds with diamagnetic $M(mnt)_2^-$ units and is more comparable to that of the other compounds with paramagnetic $M(mnt)_2^-$ anions.

The EPR spectra of the Pt, Pd and Ni compounds, denote a strong exchange interaction between the itinerant electrons in the perylene chains and the localised spins in the $M(mnt)_2^-$ anions. Not only are the linewidths in these compounds (90 G, $\sim 300$ G at room temperature for M = Pt and Ni respectively) much larger than in those with diamagnetic counterions, but also they occur at temperature-dependent $g$-values very different from the typical values for the perylene cation, $g_P$, or $M(mnt)_2^-$, $g_m$. For M = Pt and Pd, the line is single and occurs at $g$-values that are weight averaged by the relative susceptibility of the two types of chains:

$$g = (g_P\chi_P^+ g_m\chi_m)/(\chi_P^+\chi_m) \qquad (2.3)$$

where $\chi_P$ and $\chi_m$ are the perylene chains and $M(mnt)_2$ chain contributions to susceptibility, in a behaviour typical of fast spin exchange. The linear dependence of the EPR linewidth in the Pt compound above $T_c$ (Figure 2.31) is indicative of a 'bottleneck' regime in which the relaxation and thermal line broadening can be achieved only through the lattice, as the spin flip process between the conducting perylene chain and the localised spin chain ($Pt(mnt)_2$) is very rapid. The linewidth $\Delta H_{pp} = \Delta H_{pp}(0) + cT$, where $c$ is proportional to the reciprocal of spin concentration. At the transition the number of the spins decays exponentially to zero and the linewidth diverges [52].

In the Ni compound, the EPR signal is too broad and as a consequence it was difficult to obtain good data in

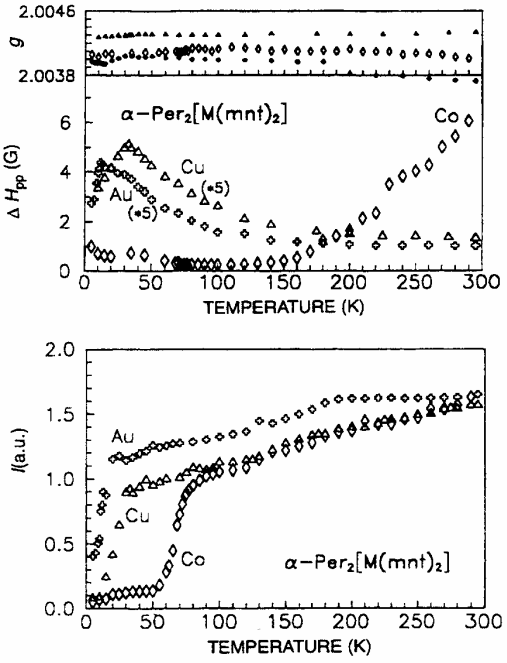


**Figure 2.29.** Temperature dependence of $g$-values, linewidth ($\Delta H_{pp}$) and integrated intensity ($I$) of the EPR signal of different $\alpha Per_2M(mnt)_2$ compounds with diamagnetic anions, in single crystals with $\mathbf{b} \perp \boldsymbol{H}$. Please note $\Delta H_{pp}$ values are multiplied by 5 in the cases of M = Au and Cu.

the very small single crystals. Data obtained in randomly aligned polycrystalline samples (Figure 2.32) showed a very broad line ($\sim$350 G) at room temperature with slightly decreasing $g$-values as the temperature decreased. At 100 K a new, narrower line with $g$-values close to those of perylene starts to become visible and upon further cooling its intensity increases as the broad line starts to slightly shift to values as high as $g \approx 2.8$ at 50 K, well above those for $Ni(mnt)_2^-$ ($g_1 = 2.161$, $g_2 = 2.042$, $g_3 = 1.998$). Finally the narrow lines vanish at the M–I transition, as observed in single crystals.

### *5.1.2.4 Structural aspects of the phase transitions and their nature*

The structural aspects of the phase transitions were studied by X-ray diffuse scattering measurements using the fixed-film fixed-crystal method and monochromatised radiation [56,64,67]. These studies as a function of the temperature in the Pt and Au samples with $T_c = 8.2$ and 12 K respectively, were limited by the lowest temperature achieved by the cryostat used $\sim$12 K, and therefore only limited information could be obtained in these cases. However, as summarised in Table 2.5 two types of structural instabilities have been observed in the family of $\alpha$-$Per_2M(mnt)_2$ compounds.

In the compounds presenting a $S = 1/2$ localised spin in the $M(mnt)_2^-$ units (M = Pt, Pd and Ni), relatively strong one-dimensional precursor effects are clearly observed below $\sim 3T_c$ as diffuse planes at $\mathbf{b}^*/2$. Their intensity increases upon cooling, diverging as the transition temperature is approached in the Pt and Pd compounds. In this last compound with higher transition temperature new Bragg spots corresponding to a lattice doubling along the chain axis **b**, are clearly observed below $T_c$ [56]. Probably due to the poor quality of the samples, this condensation was found rather incomplete in the case of the Ni samples tested [67]. These relatively strong structural effects are ascribed to the dimerisation of the strongly scattering $M(mnt)_2^-$ units.

In the Fe and Co compounds, due to the previously referred too strong chemical dimerisation interaction of the $M(mnt)_2^-$ units, the lattice is already dimerised along the $b$-axis at room temperature, and the M–I transition is associated with the appearance below $T_c$ of new superlattice Bragg spots at $\mathbf{b}^*/2$ [64] (Figure 2.33). Since the lattice in these compounds is already dimerised at room temperature, they correspond to a tetramiserisation ascribed to the perylene chains ($2\mathbf{k}_F$ distortion). In these cases only very small three-dimensional pretransitional effects, just five degrees above $T_c$, could be detected, but the experimental conditions used were not appropriate for their more careful study [64]. Similarly in the Ni and Cu compounds, weak $2\mathbf{k}_F$ satellites became visible below $T_c$, without visible pretransitional precursor effects [67].

The comparison of the behaviour of all the compounds in this family makes clear that, in spite of the absence of direct experimental evidence for the tetramerisation in the Pt, Au and Pd compounds, attributed to unfavourable experimental conditions, the M–I transition is associated with a tetramerisation ($2\mathbf{k}_F$ transition) of the perylene chains. In compounds with $S = 1/2$ $M(mnt)_2^-$ units (M = Pt, Pd and Ni), at the same critical temperature, a dimerisation of the $M(mnt)_2^-$ chains also takes place. This last distortion is more easily detected and clearly presents one-dimensional precursor effects visible up to $\sim 3T_c$, while the precursor effects of the tetramerisation, weaker in the X-ray region, have not been studied in detail or detected at all.

The two types of chains existing in the $\alpha$-phases, the conducting perylene chains and the $M(mnt)_2^-$ chains that for some metal can have localised spins, make the discussion on the nature of the low temperature transitions more complicated than in other simpler molecular conductors. In fact each of these chains is *a priori* prone to Peierls or spin–Peierls instabilities of the one-dimensional conducting and magnetic systems respectively and these *a priori* could be either coupled or uncoupled in a complex and interesting situation for which at present there are no detailed theoretical models.

In the systems with diamagnetic $M(mnt)_2^-$ units, only a tetramerisation of the perylene chains, corresponding to the $2\mathbf{k}_F$ Peierls transition, is observed. In the other cases, except for M = Fe, where the dimerisation is of stronger chemical nature, a dimerisation of the $M(mnt)_2^-$ units takes place simultaneously with the distortion in the perylene chains. This distortion in the $M(mnt)_2^-$ chains with $S = 1/2$ can be associated with a spin–Peierls-like transition, and this association is especially tempting in view of the typical spin–Peierls exponential decrease of the susceptibility below $T_c$ for directions parallel and perpendicular to the chain axis. However for this transition to be spin–phonon driven, it lacks the usual criteria for a spin–Peierls transition requiring an antiferromagnetic interaction $J \gg k_B T_{sp}^{\circ}$, where $T_{sp}^{\circ}$ is the mean field transition temperature [80]; for instance in the case of M = Pt with a $T_c = 8.2$ K, $J/k_B$ was estimated as 15 K while $T_{sp}^{\circ}$ should be $\sim$25 K, the temperature at which one-dimensional

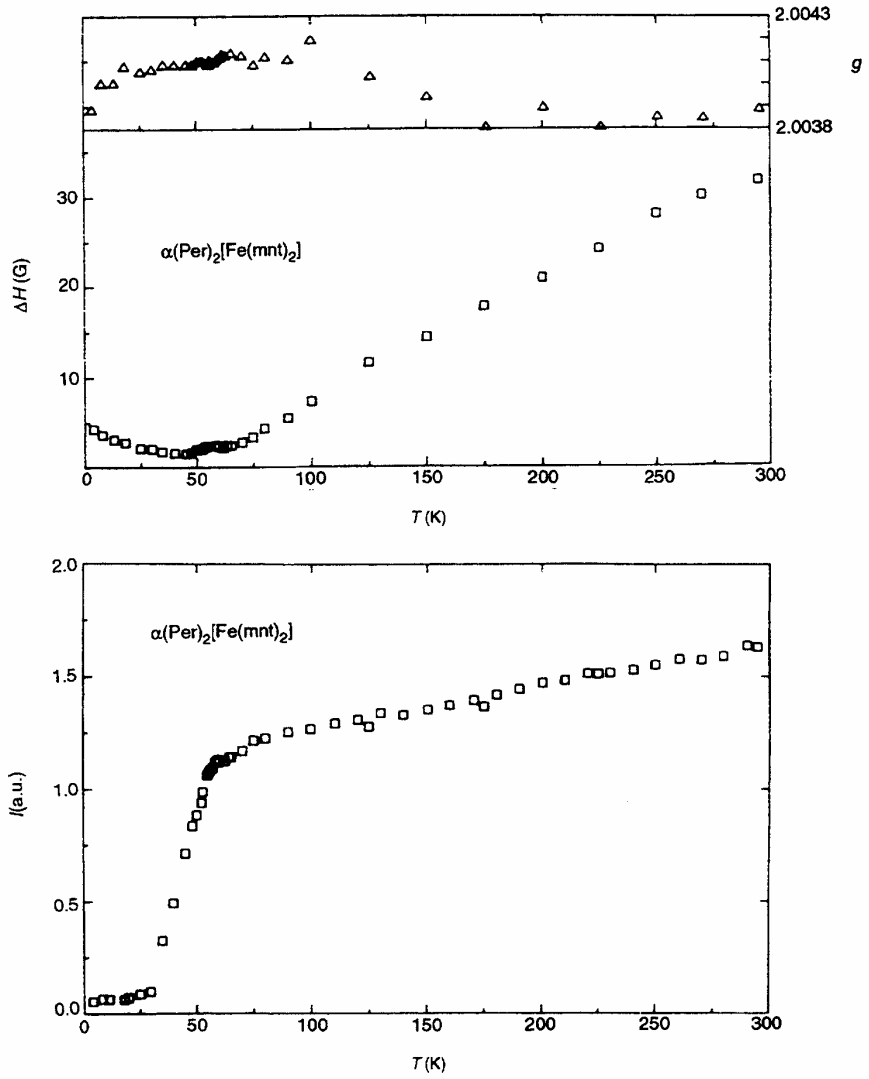


**Figure 2.30.** Temperature dependence of $g$-values, linewidth ($\Delta H_{pp}$) and integrated intensity ($I$) of the EPR signal of a $Per_2Fe(mnt)_2$ single crystal ($\mathbf{b} \perp \boldsymbol{H}$). (Reproduced by permission of Editions de Physique, from ref. 64.)

precursor effects are visible in the X-rays region. Therefore this transition will be referred to as spin–Peierls-like.

The fact that in the compounds with diamagnetic $M(mnt)_2^-$ units a similar M–I transition also occurs, indicates that the Peierls instability in the perylene chain is the dominant one and that the spin–Peierls-like transition in the dithiolate chains is triggered by the perylene chains distortion. This picture is entirely corroborated by studies of the alloys $Per_2[Pt_xAu_{1-x}(mnt)_2]$, indicating that apart from the special $x = 0.5$ composition, there is a smooth change

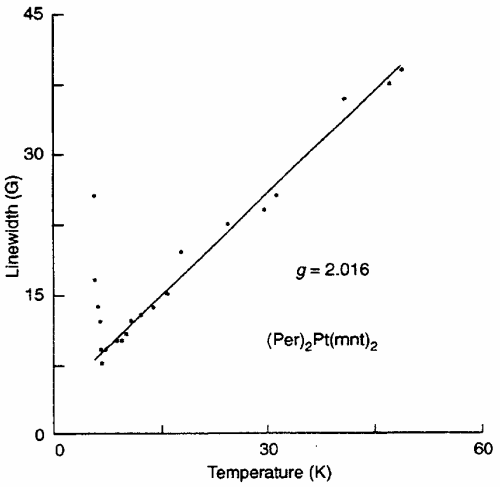


**Figure 2.31.** EPR signal linewidth as a function of temperature for $Per_2Pt(mnt)_2$. (Reproduced by permission of Gordon & Breach, from ref. 58.)

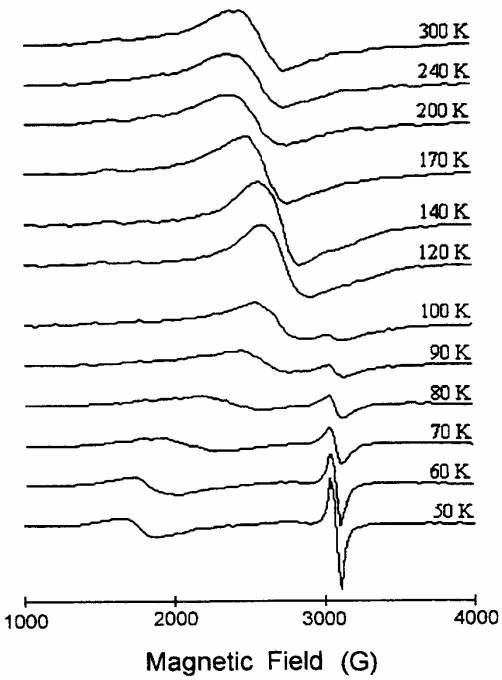


**Figure 2.32.** EPR spectra of a polycrystalline sample of $\alpha$-$Per_2Ni(mnt)_2$ at different temperatures. (Reproduced by permission of American Chemical Society, from ref. 68.)

of $T_c$ with $x$ with no other changes in the transport properties, while the magnetic properties of the $M(mnt)_2$ chains are drastically affected by the alloying [81]. The $x = 0.5$ composition with a different thermopower regime and a lower conductivity seems to be a special case of ordered alloying, but its characterisation requires further studies. The dominant role of the Peierls instability in the transition is consistent with the previous observation that spin–phonon coupling is too small in these compounds.

### *5.1.2.5 Other physical measurements*

The detailed mechanism of the coupling between the magnetic and conducting chains, and the triggering of the spin–Peierls-like transition in the $M(mnt)_2^-$ chains by the Peierls transition in the perylene chains are not yet clear. Additional insights into this interesting problem are provided by more detailed physical measurements, like proton NMR spin–lattice relaxation time, specific heat and magnetoresistance in the Au and Pt compounds, whose comparison clearly illustrates the role of the magnetic chains in these systems.

$^1H$ nuclear spin–lattice relaxation rate, $T_1^{-1}$, measurements in the Au and Pt compounds (Figure 2.34) [52,82] denote a quite different behaviour due to the coupling of the proton spins of the perylene molecules to the localised $M(mnt)_2^-$ spins in the Pt compound. In $Per_2Pt(mnt)_2$, $T_1^{-1}$, is $\approx 20\ s^{-1}$ and temperature-independent above 40 K, while below this temperature it decreases almost linearly with the absolute temperature. This behaviour contrasts with the much smaller relaxation rates of the gold compound, with upwards deviations to the Korringa law, especially at high temperatures, as is typical in many one-dimensional metals [83,84].

These results can be understood considering the sum of all contributions to the relaxation time $T_1^{-1}$; either of dipolar nature ($_d$) or of contact ($_c$) and both intra perylene chains and interchain, i.e. between the perylene and $Pt(mnt)_2$ chains ($_\perp$) [52]:

$$T_1^{-1} = T_{1,d}^{-1} + T_{1,c}^{-1} + T_{1,d\perp}^{-1} + T_{1,c\perp}^{-1} \qquad (2.4)$$

The $T_{1,d\perp}^{-1}$ contribution can be estimated as proportional to $T\chi_m$. As for $T > 40$ K the susceptibility in the Pt compound follows the Curie–Weiss law, a temperature-independent relaxation rate is obtained if this term is dominant. This seems to be the case even for $T < 40$ K where the susceptibility, due to the lattice fluctuations already visible by X-rays, starts to deviate from the Curie–Weiss law.

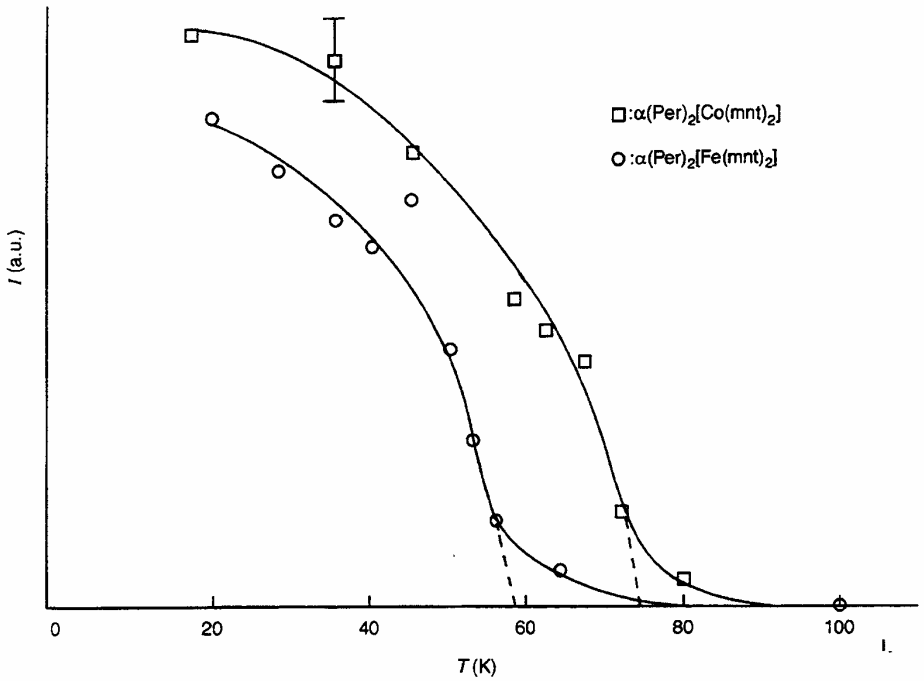


**Figure 2.33.** Temperature dependence of the integrated intensity ($I$) of the $\mathbf{b}^*/2$ superlattice spots in $Per_2Fe(mnt)_2$ and $Per_2Co(mnt)_2$. (Reproduced by permission of Les Editions de Physique, from ref. 64.)

The relaxation in the Au compound with no chains of localised spins is dominated by the $T_{1,d}^{-1}$ term, the dipolar contribution of the itinerant electrons that in the diffusive regime can be estimated as proportional to $T\chi^{3/2}$. The observed deviations to the strictly linear behaviour predicted by the Korringa law, $T_1^{-1} \propto T$, is accounted for by the temperature dependence of the susceptibility which, as referred to previously, is enhanced by Coulomb correlations. This enhancement is however smaller than in other low-dimensional systems, such as the Bechgaard salts [84], confirming that they are indeed relatively small.

The specific heat, $C_p$, of the Au and Pt compounds was measured in the temperature range 1.5–20 K [85] (Figure 2.35). While no $C_p$ anomaly is observed in the Au compound, as expected since the specific heat contribution expected from a Peierls transition is too small to be detected, a large anomaly is visible around 8 K in the Pt sample. This anomaly is clearly due to the magnetic specific heat of the transition. By comparison of the $C_p$ results in the two compounds and taking the lattice contribution in the Pt compound as equal to the $C_p$ values measured in the Au compound (just with a small correction factor to account for possible mass errors), this magnetic contribution, as well as the associated spin entropy, could be accurately estimated without any particular hypothesis on the behaviour of the lattice contribution. The magnetic specific heat obtained in this way (Figure 2.36) clearly shows a transition at 8.25 K. Below this temperature it decreases exponentially as in other spin–Peierls systems like MEM $TCNQ_2$ (MEM = N-methyl-N-ethyl-morpholinium [86]. However the values above $T_c$ are not in agreement with the Bonner–Fisher calculations for a uniform antiferromagnetic chain [87] with $J/k_B =$ 15 K, which could fit well the magnetic sus-ceptibility in this range. This is especially visible in the entropy derived from $C_p$ data, which is almost double that predicted in this model, and approaches much better an Ising model [85].

The low transition temperatures of the Au and Pt compounds makes them ideal candidates for the study

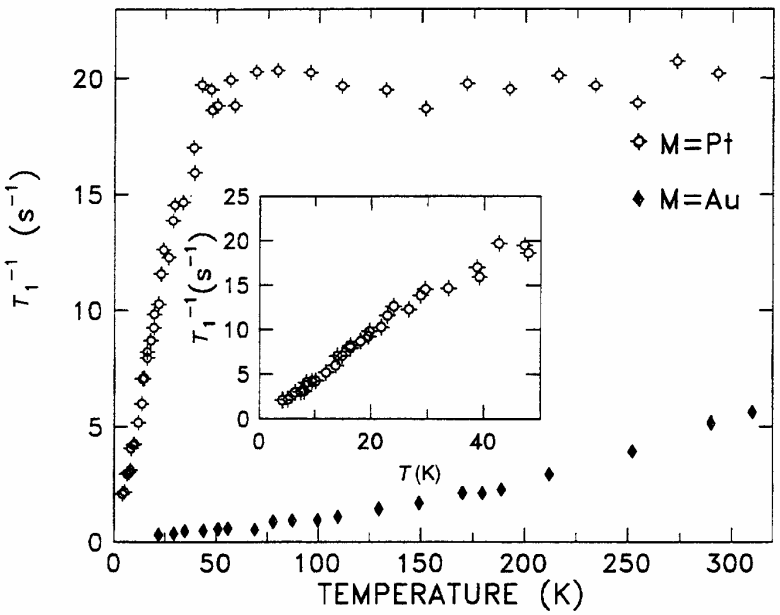


**Figure 2.34.** Proton spin–lattice relaxation rates for $Per_2Pt(mnt)_2$ and $Per_2Au(mnt)_2$ as a function of temperature. (Reproduced by permission of Gordon & Breach, from ref. 58.)

of the magnetic field dependence of these transitions. In fact the Au compound has the lowest Peierls transition among molecular conductors and the Pt compound has a transition temperature that is comparable to or lower than other spin–Peierls systems. In both compounds the magnetic field effect on the transitions can be studied by accurate measurements of the temperature-dependent electrical resistivity, $\rho(T, B)$, under different magnetic fields, $B$ [77,88]. A significant decrease of the transition temperature $T_c$, taken as the maximum in the derivative d log $\rho$/d(1/$T$), was observed with increasing field (Figure 2.37). The first results under fields up to 8 T [77] indicated a similar field dependence of the transition temperature in both compounds, closely following a shift of the transition temperature, $\delta T_c = T_c(B) - T_c(0)$, given by

$$\delta T_c/T_c = (\gamma/4)[\mu_B B/k_B T_c(0)]^2 \qquad (2.5)$$

with $\gamma$ between 0.8 and 1. This type of field dependence with $\gamma \approx 1$ is theoretically predicted for a Peierls transition [89], while for a spin–Peierls transition a faster dependence with $\gamma = 2$ has been experimentally observed [90]. The fact that both compounds follow the same field dependence indicates that the leading transition mechanism is the same in both compounds and it is due to the Peierls instability in the perylene chains. More recent measurements under larger fields (up to 18 T) enabling more precise determinations, indicate slightly smaller $\gamma$ values in the Au compound, which are independent of the magnetic field orientation, and parallel or perpendicular to the chain axis $b$ (Figure 2.38). Similar measurements in the Pt compound indicate that $\gamma$ is dependent on the field orientation [91]. for $\boldsymbol{B} \parallel \mathbf{b}$ a $\gamma$ value comparable to the Au compound is obtained, while for $\boldsymbol{B} \perp \mathbf{b}$ a slightly faster field dependence (but still far from the spin–Peierls cases) with deviations from the $B^2$ law above 14 T are observed [91]. Although denoting a slight influence of the magnetic chains in the transition of the $Per_2Pt(mnt)_2$ compound, these results clearly support the idea that the main driving force for the transition is the Peierls instability and that the spin-Peierls-like transition in the $Pt(mnt)_2^-$ chains could not take place without the coupling to the Peierls transition in the perylene chains.

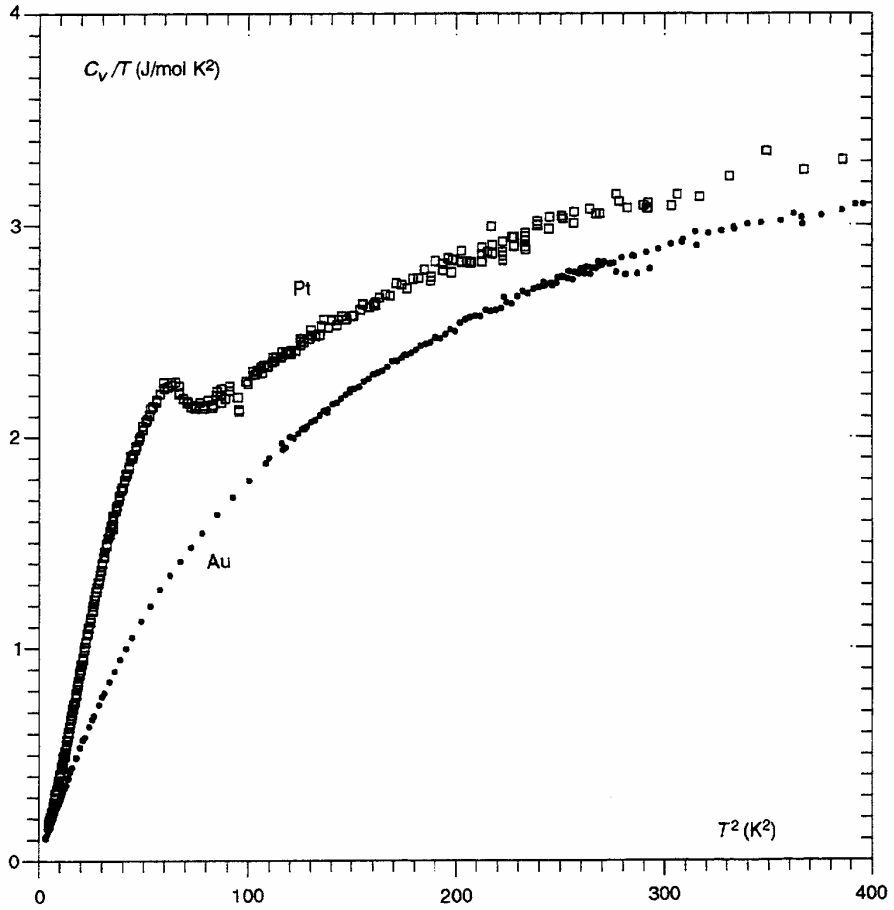


**Figure 2.35.** Specific heat of $Per_2Pt(mnt)_2$ and $Per_2Au(mnt)_2$ as a function of temperature. (Reproduced by permission of Les Editions de Physique, from ref. 85.)

### *5.1.2.6 Non-linear transport*

As expected for a charge density wave (CDW) system, below the M–I transition, and for electrical fields high enough to depin the CDW, non-linear transport phenomena are observed in many α-phase compounds, namely those with M = Au and Pt [92–94]. In spite of the non-linear transport being a recent aspect of the research in this family of compounds, the experimental data already existing provides by far the strongest and more complete evidence for non-linear transport as due to a CDW motion in molecular conductors. The Au and Pt compounds with low transition temperatures at 8.2 and 12.2 K, have been more studied because their emersion in liquid helium easily allows detailed studies at 4.2 K, without the risk of heating effects [92,94]. Probably these phenomena are a general feature of the α-phase compounds but its study has not yet been extended to all other compounds.

Clear non-linear current–voltage characteristics are observed both by d.c. and pulsed measurements at 4.2 K in the Pt and Au compounds. The first non-linear threshold field $E_{t1}$ observed at 4.2 K is of the order of 0.4–0.5 V/cm in the Au [92] (Figure 2.39) and 5 V/cm in the Pt compound [94]. A second threshold field $E_{t2} \approx 30$ V/cm at 4.2 K, is also observed in the Pt compound, probably not associated with CDW depinning and whose origin remains unclear. These

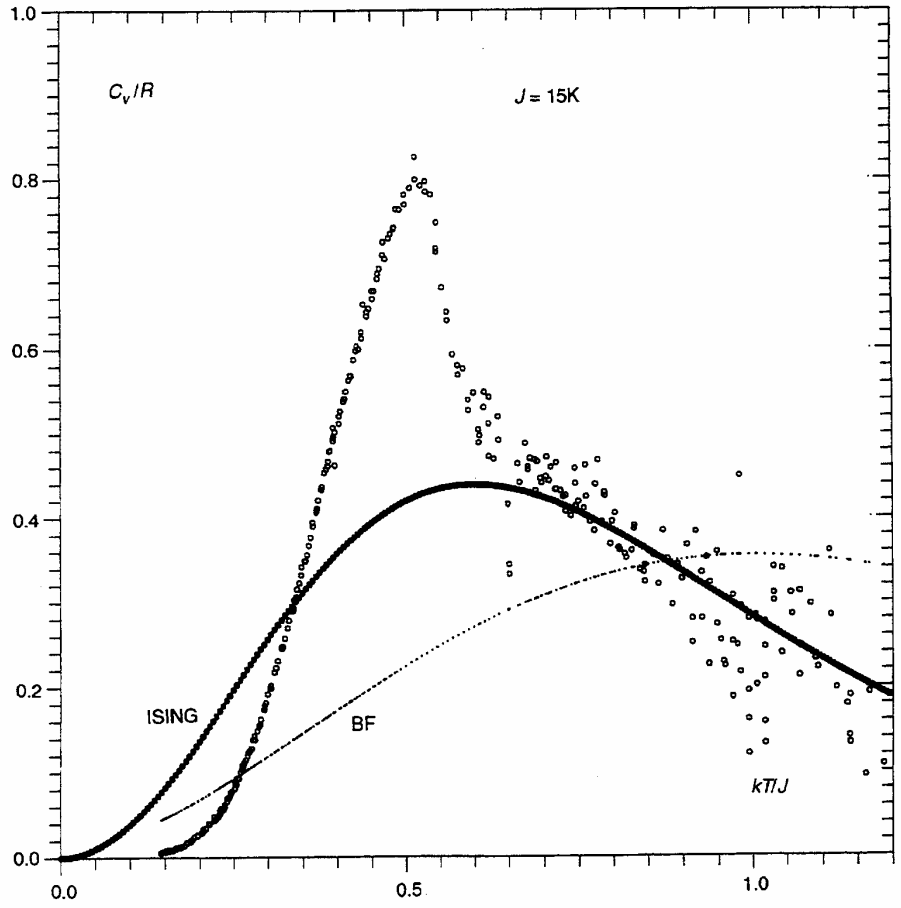


**Figure 2.36.** Magnetic specific heat of $Per_2Pt(mnt)_2$ as a function of temperature. The Ising and Bonner–Fisher (BF) calculations corresponding to $J/k_B = 15$ K are also shown. (Reproduced by permission of Les Editions de Physique, from ref. 85.)

non-linear current–voltage characteristics in the low field range are similar to those observed in $Per_2(PF_6)_{1.1}\cdot 0.8CH_2Cl_2$ and $Per_2PF_6\cdot 0.66THF$ well below their CDW transition (see Section 4.2) where threshold fields of the order of 0.08 V/cm and 1 V/cm respectively have been observed [40]. However, in the $Per_2M(mnt)_2$ compounds, much more clear evidence for this non-linear effect as due to the CDW motion is provided by the response pulse shape analysis and the noise measurements. The onset of the non-linearity is associated with the appearance of broad band noise as well as narrow band noise. The narrow band noise, usually taken as an unequivocal signature of the CDW and demonstrating the coherent nature of its motion as the origin of the non-linearities, has been very difficult to observe in other CDW molecular systems. Narrow band noise associated with the non-linear current was observed both in the Au and Pt samples and it was particularly clear in a Pt sample (Figure 2.40) where the relation between the excess non-linear current due to the charge density wave motion, $J_{CDW}$, and the fundamental frequency of the narrow band noise, $\nu_o$,

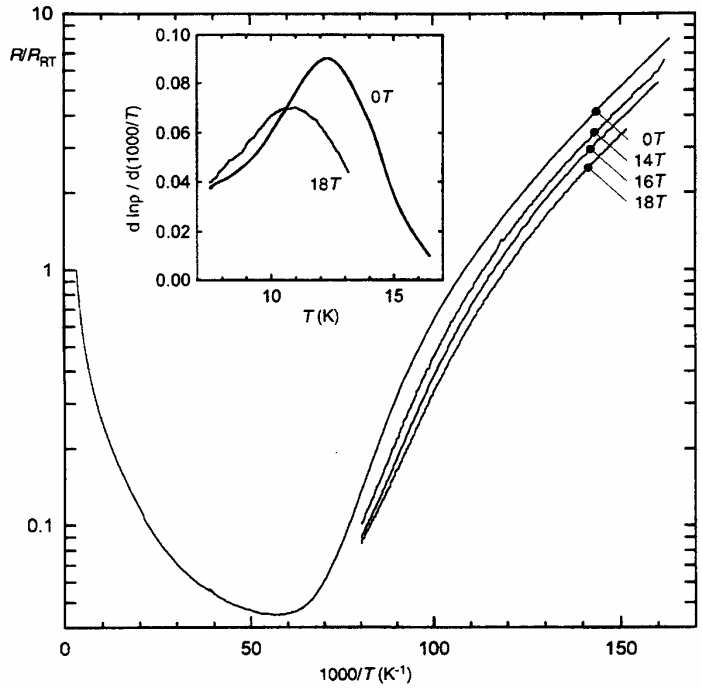


**Figure 2.37.** Normalized electrical resistivity, $R/R_{RT}$, of a $Per_2Au(mnt)_2$ single crystal under different magnetic fields perpendicular to the **b**-axis. The inset shows the shift of the maximum of d log $R$/d $(1/T)$ used to define $T_c$. (Reproduced by permission of Elsevier Science B.V., from ref. 88.)

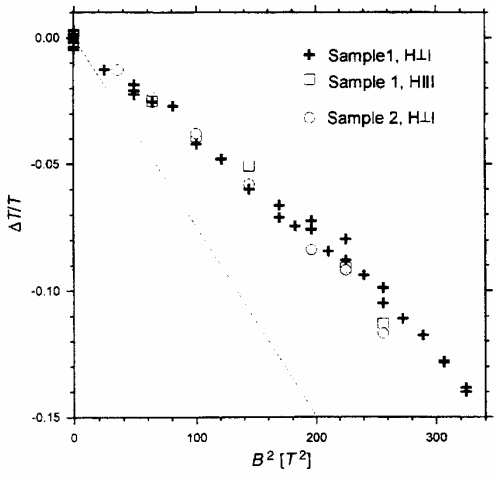


**Figure 2.38.** Relative shift of the transition temperature $\Delta T/T$ of $Per_2Au(mnt)_2$ as a function of the square of the magnetic field $\boldsymbol{B}$. (Reproduced by permission of Elsevier Science B.V., from ref. 88.)

closely follows the relation

$$v_o = J_{CDW}/ne\lambda \tag{2.6}$$

$\lambda$ being the wavelength corresponding to the tetramerisation, $\lambda \approx 16.5$ Å, and $n$ being the condensed CDW electron concentration (Figure 2.41) [94]. This result demonstrates that the CDW is coherently depinned in almost all the sample.

Pulsed measurements also show a response pulse shape modification above $E_{t1}$, characteristic of a CDW system, with an overshooting at the leading edge of the pulses, as shown for a Au sample in Figure 2.42. This transient dynamics of the depinning is due to the non-rigidity of the CDW and the competition between the depinning energy and the elastic energy of the CDW deformation as described for many well-studied CDW inorganic systems [95,96]. The decay time of this overshoot decreases when the voltage above $E_{t1}$ increases. Probably reflecting the higher resistivity at 4.2 K of the Pt samples and the reduced screening of

the CDW by the normal carriers, the timescale of this relaxation phenomenon is longer in the Pt compound than in the Au one. In the Pt samples above $E_{t1}$ real-time voltage oscillations are seen as sharp asymmetric peaks (Figure 2.43), whose frequency, analysed by wavelet techniques, also increases roughly proportionally to the excess current [97]. These oscillations have been interpreted as the direct observation of CDW motion by the slip of phase dislocations.

### 5.1.3 *β-Per$_2$M(mnt)$_2$ phases*

The β-Per$_2$M(mnt)$_2$ phases are well characterised by X-ray diffraction, electrical transport and magnetic measurements in the case of M = Cu and Ni [65]. Although not confirmed by X-ray diffraction they probably exist also in other cases, such as M = Au, where transport and magnetic studies provide similar evidence for the existence of a β-phase.

A full structural refinement of the β-phases does not exist. However their lattice parameters determined by X-ray diffraction, with a cell volume $\approx$ 1220 Å$^3$, are clearly distinct from the α-phases which have a cell volume $\approx$ 1840 Å$^3$ (see Table 2.4). This volume is too small to accommodate all the units expected for $Z = 2$ as in the α-phases, and it rather corresponds to $Z \approx 1.5$, clearly indicating a disordered structure. The disordered nature of the structure is also indicated by the

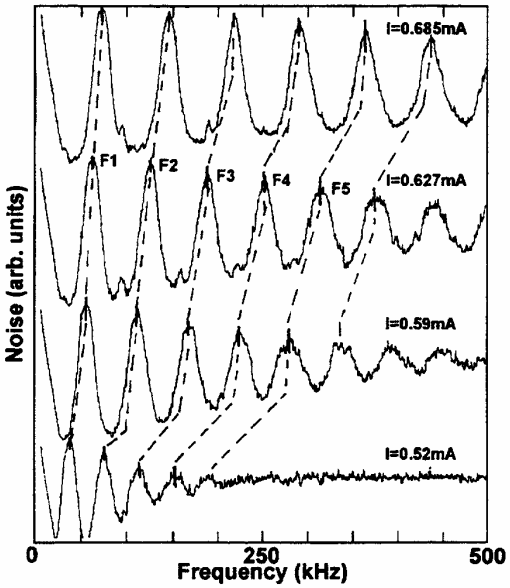


**Figure 2.40.** Voltage noise amplitude as a function of the frequency in Per$_2$Pt(mnt)$_2$ at 4.2 K under different values of the applied d.c. bias current indicated. (Reproduced by permission of American Physical Society, from ref. 94.)

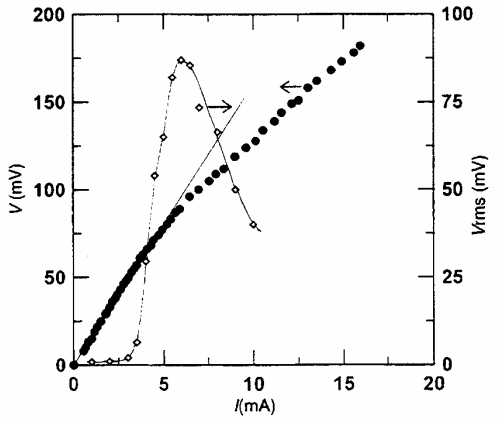


**Figure 2.39.** Current–voltage characteristics (left axis) and low-field broad band noise as a function of the d.c. bias current (right axis) of a Per$_2$Au(mnt)$_2$ single crystal at 4.2 K. (Reproduced by permission of Les Éditions de Physique, from ref. 92.)

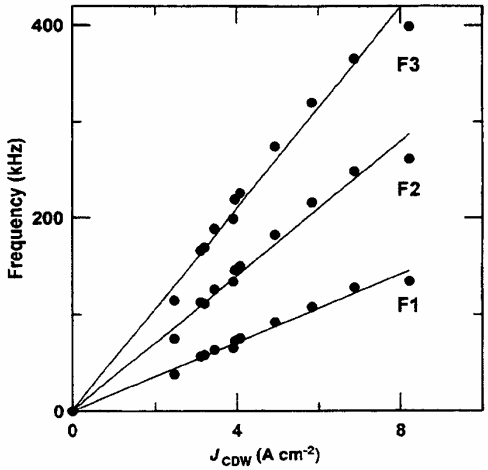


**Figure 2.41.** Narrow band noise frequency as a function of the excess current density in Per$_2$Pt(mnt)$_2$. (Reproduced by permission of American Physical Society, from ref. 94.)

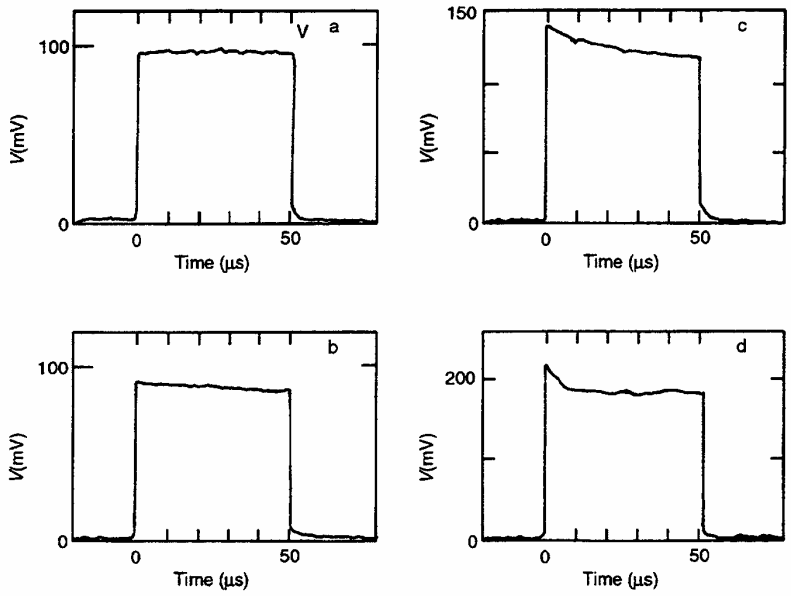


**Figure 2.42.** Voltage waveform response of a $Per_2Au(mnt)_2$ sample with the characteristics shown in Figure 2.39, for different current pulse amplitudes $I = V_p/R_s$ near the non-linear threshold $E_t \approx$;70 mV at 4.2 K: (a) $V_p = 50$ mV, (b) $V_p = 90$ mV, (c) $V_p = 120$ mV and (d) $V_p = 180$ mV. (Reproduced by permission of Les Editions de Physique, from ref. 92.)

presence of strong temperature-independent X-ray diffuse scattering planes at $n\mathbf{b}^*/6$, with $n = 1$, 2, and 3. The temperature dependence of the physical properties, as discussed below, also denotes this disordered nature of the structure.

The transport properties of the $\beta$-phases, displaying a semiconducting behaviour clearly distinct from the high temperature metallic regime of the $\alpha$-phases (see Figure 2.26 and 2.27), provided the first experimental evidence for the existence of the two phases in these compounds. At clear variance from the highly conducting and metallic properties of the $\alpha$-phases, the $\beta$-phases present a poorer conductivity ($\sigma \approx$ 50–80 S/cm at room temperature) which are thermally activated. The energy of activation of the electrical conductivity, which is very small at room temperature for the Ni compound, smoothly increases upon cooling without any maximum down to 100 K in both compounds. The thermopower of the $\beta$-phases, $S \approx 22$ $\mu$V/K at room temperature, is almost one-half of that found for the $\alpha$-phases and therefore it has been used as a way of identifying the phase of the crystals. In agreement with the semiconducting behaviour of the

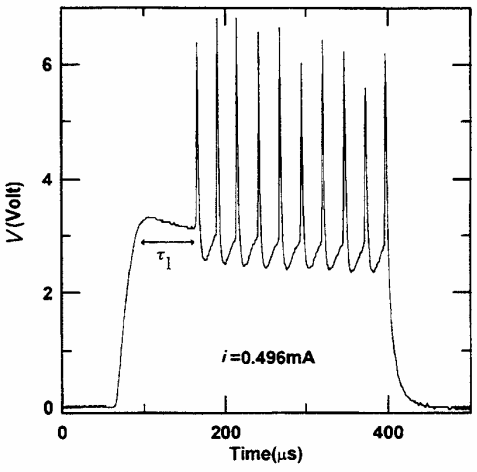


**Figure 2.43.** Voltage waveform response of some $Per_2Pt(mnt)_2$ samples above the threshold also showing large asymmetric voltage spikes. (Reproduced by permission of American Physical Society, from ref. 94.)

electrical resistivity, thermopower increases continuously upon cooling, reaching $\approx 100$ $\mu$V/K at 100 K. These transport properties, with an electrical conductivity that is relatively high for a semiconductor and the absence of a linear regime in both the plots of log $\sigma$ and $S$ versus $1/T$, exclude a simple standard semiconducting model and have been interpreted as indicative of transport by hopping or a tunnelling mechanism of the carriers that have been localised by disorder [65].

The study of the magnetic properties of these $\beta$-phases has been done, both by EPR in single crystals previously identified as $\beta$-phase by thermopower measurements, or by static susceptibility measurements by the Faraday method in polycrystalline samples containing essentially the $\beta$-phase [68]. The $\beta$-phase has a significantly larger susceptibility than the $\alpha$-phases and therefore its absolute value could be more easily determined than that of the $\alpha$-phases. Both types of measurement in spite of the different absolute values of the two compounds ($12 \times 10^{-4}$ emu/mol for M = Ni and $4.5 \times 10^{-4}$ emu/mol for M = Cu) show an increase of the susceptibility upon cooling following $T^{-\alpha}$ with $\alpha = 0.8$ and 0.75 for M = Cu and Ni respectively (Figure 2.44). This type of behaviour with $\alpha < 1$ as in many other one-dimensional systems with random exchange antiferromagnetic interactions, denotes the disorder of the system [46,98–100]. The larger values of the susceptibility in the Ni compound are due to the $Ni(mnt)_2^-$ spins and the comparison with the Cu compound suggests that the disorder is essentially associated with the perylene cations.

The $\beta$-phase crystals present an EPR line wider than the corresponding $\alpha$-phase crystals. As in the $\alpha$-phases the linewidth of the Ni compound (300 G at room temperature decreasing to 15 G at 4 K) is significantly larger than the Cu one ($\approx 4$ G in the range 4–300 K). As in the $\alpha$-phases the $g$-values of the Cu compound are temperature-independent and those of the Ni are temperature-dependent, also denoting possible spin exchange between spins in the perylene cations and $Ni(mnt)_2$ anions (Figure 2.45) [68].

### 5.1.4 *PerCo(mnt)$_2$·0.5CH$_2$Cl$_2$*

$PerCo(mnt)_2 \cdot 0.5CH_2Cl_2$ presents a rare and interesting structural type in which stacks of perylene coexist with a true polymeric arrangement of $Co(mnt)_2$ units [72]. Its crystal structure at room temperature, i.e. well above the phase transitions undergone at lower temperatures, presents already an incommensurate modulation with wave vector $\mathbf{q} = (0.22\mathbf{a}^*, -0.13\mathbf{b}^*, -0.36\mathbf{c}^*)$ as denoted by first- and second-order X-ray satellite reflections. The modulated structure was recently solved [101] but for sake of clarity we will refer first to the average structure that is triclinic space group $P\bar{1}$ $a = 6.551(2)$ Å, $b = 11.732(2)$ Å, $c = 16.481(2)$ Å, $\alpha = 92.08(1)°$, $\beta = 95.30(1)°$, $\gamma = 94.62(1)°$, $Z = 2$ and $V = 1248.6(3)$ Å$^3$ [72]. The crystal structure

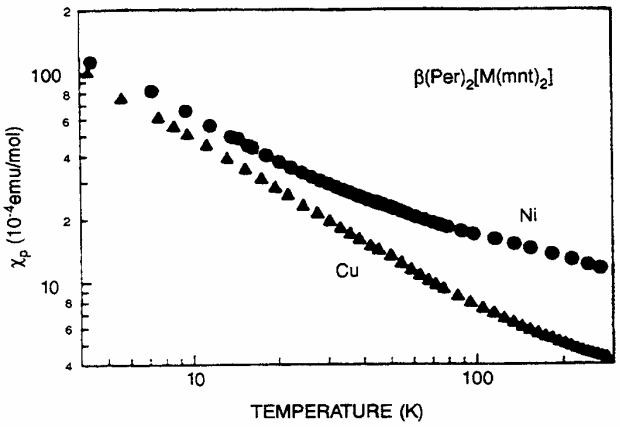


**Figure 2.44.** Paramagnetic susceptibility of $\beta$-$Per_2Cu(mnt)_2$ and $\beta$-$Per_2Ni(mnt)_2$ as a function of temperature. (Reproduced by permission of American Chemical Society, from ref. 68.)

consists of almost regular stacks of perylene and dimerised chains of $Co(mnt)_2$ units along **a** axis, with dichloromethane solvent molecules disordered in the free spaces between the two types of chains (Figure 2.46).

The perylene molecules are almost perpendicular to the chain axis **a** and overlap with a mode that, as shown in the Figure 2.46, is essentially equal to that observed in the $\alpha$-$Per_2(mnt)_2$ phases. However in this compound the molecules are stacked in almost regular zig-zag chains with intermolecular distances of 3.27 and 3.28 Å. This difference in interplanar distances is probably not significant in view of the experimental error (0.005 Å) and therefore the chains can be considered as regular. The $Co(mnt)_2$ units are arranged in dimerised polymeric chains with two Co–S bonds between each $Co(mnt)_2$ unit (Figure 2.47). The apical and equatorial Co–S distances observed in this compound are listed in Table 2.7 where they are also compared with the corresponding distances in other $Co(mnt)_2$ complexes.

The modulated structure was solved more recently by Lam *et al.* [101] and the results show that the structure modulation is essentially associated with the Co–S apical coordination, denoting possible fluctuations in the Co oxidation state. This picture is also consistent with the band structure calculation performed in the framework of the extended Hückel approximation, indicating as most favourable a partial charge transfer of slightly less than one electron per perylene unit, as $Per^{+\rho}$ $Co(mnt)_2^{-\rho}\cdot 0.5CH_2Cl_2$, with $\rho \leqslant 1$ [78]. As will become evident from the transport properties, this will imply that the electrical conductivity is provided essentially by the perylene stacks.

The compound is a relatively poor metal with a room temperature electrical conductivity of $60 \mp 20$ S/cm and a broad maximum of conductivity at ~340 K. Upon cooling a metal-to-semiconductor transition with thermal hysteresis is evident at ~270 K, as well as a second semiconductor–semiconductor phase transition at ~170 K, also with hysteresis (Figure 2.48). These transitions are also seen in thermopower (Figure 2.49) which at room temperature approaches a metallic regime with a small negative and nearly temperature-independent value of $-8$ $\mu$V/K. At lower temperatures the thermopower becomes more negative denoting an electron-dominated semiconducting regime. The actual temperature of the transitions and the magnitude of their thermal hysteresis depend on the heating or cooling rates. The 170 K transition has been attributed to the freezing of the dichloromethane molecules in the structure, while the upper transition, in spite of its unusual hysteresis is probably Peierls driven.

At room temperature the paramagnetic susceptibility of this compound is small ($3.4 \times 10^{-4}$ emu/mol), only slightly larger than the Pauli-like contributions in many molecular conductors. The two-phase transitions are seen in static magnetic susceptibility measurements as two decreasing steps of the susceptibility upon cooling with similar hysteresis (Figure 2.50). The first

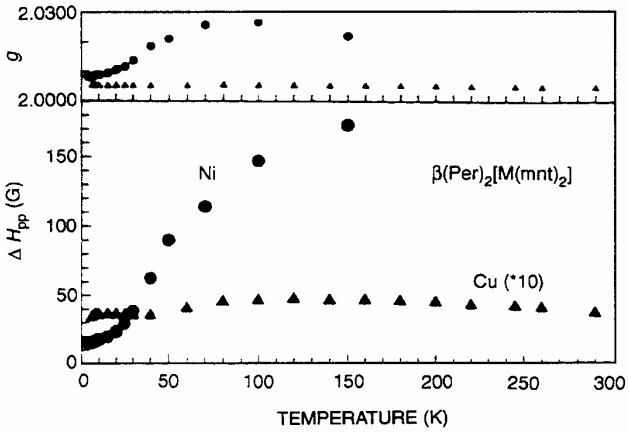


**Figure 2.45.** EPR linewidth ($\Delta H_{pp}$) and $g$-values of $\beta$-$Per_2Cu(mnt)_2$ and $\beta$-$Per_2Ni(mnt)_2$ single crystals ($H_\perp b$) as a function of temperature. Please note that the linewidth of the Cu compound is multiplied by 10. (Reproduced by permission of American Chemical Society, from ref. 68.)

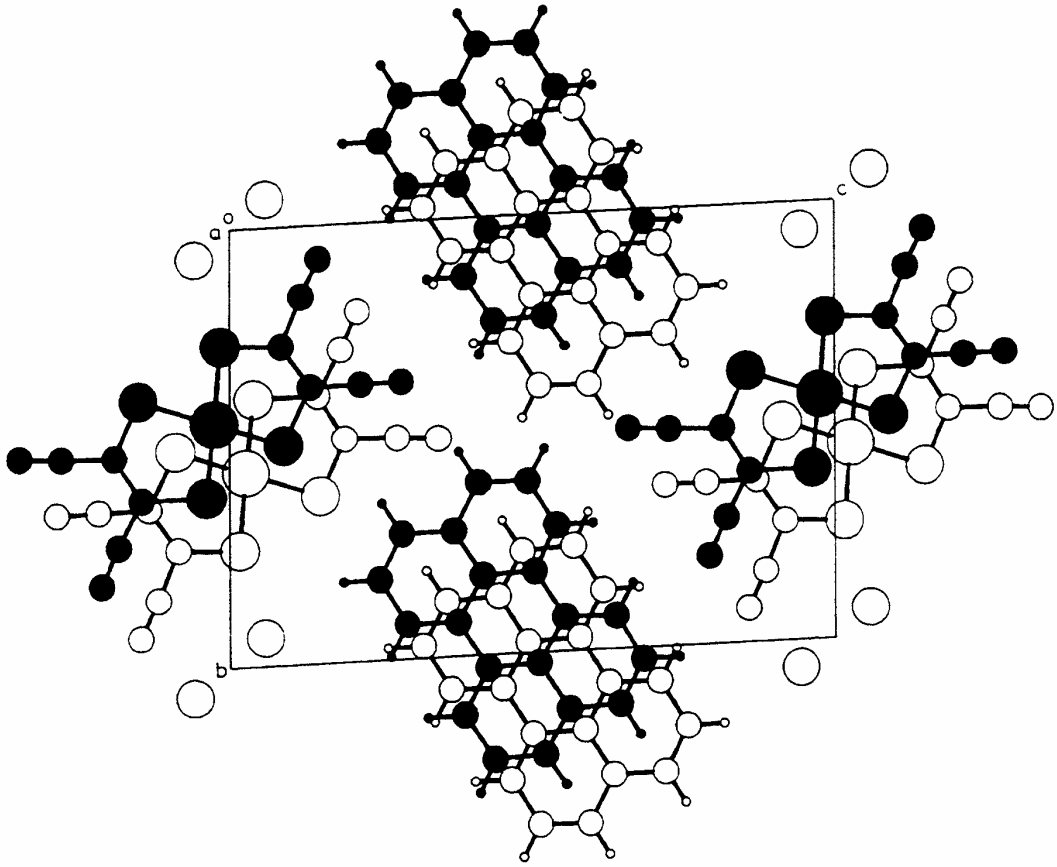


**Figure 2.46.** Projection along the *a*-axis of the $PerCo(mnt)_2 \cdot 0.5CH_2Cl_2$ crystal structure. (Reproduced by permission of American Chemical Society, from ref. 72.)

step can be a decrease of the Pauli-like contribution of the conduction electrons, but the second one is more probably associated with a reduction of temperature-independent paramagnetism of the inorganic polymeric chains. Just below the second transition a residual value of $1.8 \times 10^{-4}$ emu/mol is observed, probably indicative of a temperature-independent paramagnetism, and upon further cooling an increase of the susceptibility due to a Curie tail is observed. This tail shows an increase as $T^{-\alpha}$ with $\alpha = 0.6$, an exponent that is indicative of disorder [98–100], most probably associated with the solvent. Since this compound is EPR silent no further indications on the origin of the observed susceptibility can be taken from these data alone.

### 5.1.5 *$Per_4[Co(mnt)_2]_3$*

The structure of $Per_4[Co(mnt)_2]_3$ is monoclinic, space group $P1_1/n$ with cell parameters, $a = 12.093(1)$ Å, $b = 20.912(1)$ Å, $c = 16.633(1)$ Å, $\beta = 94.290(6)°$, $Z = 2$ and $V = 4194.5(5)$ Å$^3$, and consists of $[Co(mnt)_2]_3$ units, alternating with trimers of perylene units and an extra perylene molecule almost perpendicular to the trimers (Figure 2.51) [73]. Along the **a**-axis there are segregated stacks of perylene and $[Co(mnt)_2]_3$ units. However, the trinuclear inorganic anions are separated from each other by distances well above van der Waals contacts and the perylene trimers and the perylene isolated units are stacked alternating almost perpendicular to each other. Electrical con-

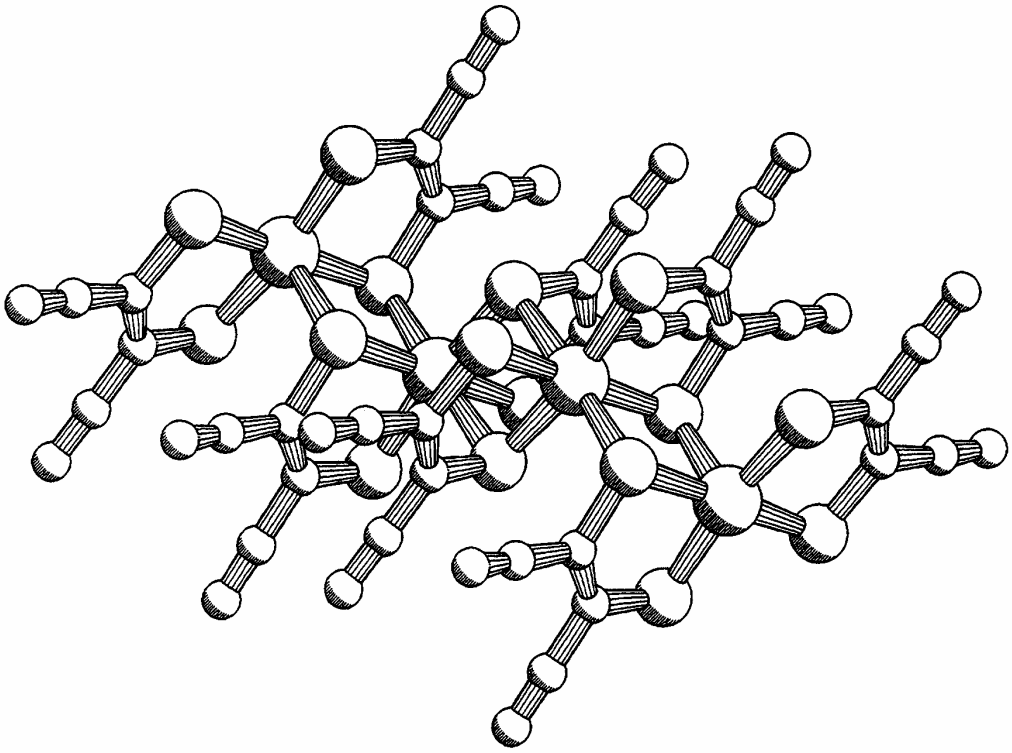

**Figure 2.47.** View of four $Co(mnt)_2$ units in the polymeric arrangement of $PerCo(mnt)_2 \cdot 0.5CH_2Cl_2$. (Reproduced by permission of American Chemical Society, from ref. 72.)

**Table 2.7.** Co–S bond lengths (Å) in different Co–bis(dithiolene) complexes

| | Equatorial | Apical | Ref. |
|---|---|---|---|
| $Co(mnt)_2^{2-}$ | 2.16 | – | 105 |
| $Co(S_2C_2(CF_3)_2)_4^0$ | 2.16(2) | 2.38(4) | 104 |
| $Co(S_2C_6Cl_4)_4^{2-}$ | 2.185(7) | 2.404(7) | 103 |
| $[Co(mnt)_2]_2^{2-}$ | 2.188(3) | 2.429(1) | 102 |
| $\{[Co(mnt)_2]_2\}_n$ | 2.237(7) | 2.443(9) | 75 |
| | 2.224(7) | | |
| | 2.232(7) | 2.62(1) | |
| | 2.225(7) | | |
| $[Co(mnt)_2]_3^-$ | 2.2116(17) | 2.5502(19) | 76 |
| central | | | |
| | 2.2202(17) | | |
| outer | 2.200(2) | | |
| | 2.175(2) | 2.312(2) | |
| | 2.167(2) | | |
| | 2.168(2) | | |

ductivity measurements were not reported in this compound because single crystals obtained were too small, but in view of the absence of an extended pathway for electronic interaction and delocalisation in this solid, it is expected to be an insulator and therefore it will be only briefly mentioned. The main interest of this compound is its structure, especially interesting due to the unusual trinuclear Co anion (Figure 2.52). Their Co–S bond lengths are listed in Table 2.7 together with the corresponding distances in other Co–bisdithiolenes. The analysis of the anion geometry and the extended Hückel-type calculations [73] support the description of the compound as $Per_3^+Per^0[Co(mnt)_2]_3^-$.

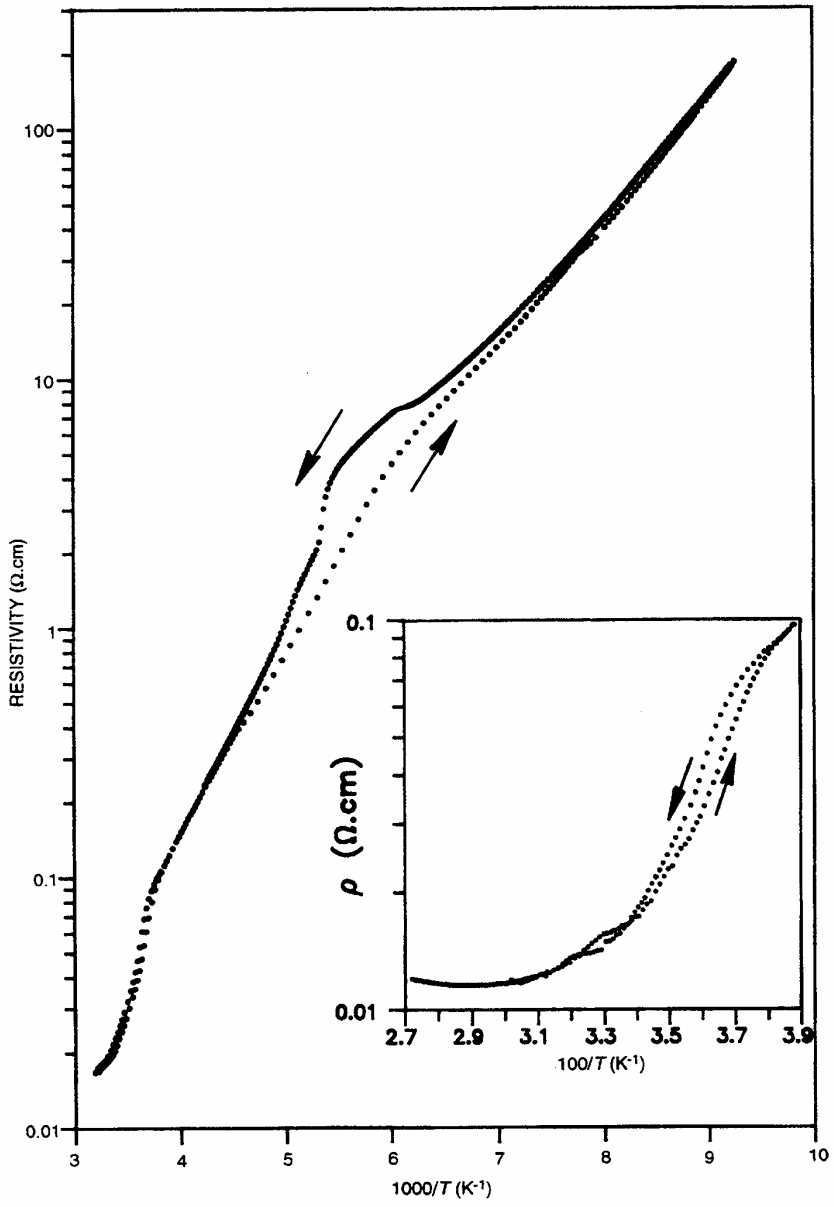


**Figure 2.48.** Electrical resistivity measured along the chain axis a of PerCo(mnt)$_2$·0.5$CH_2Cl_2$ as function of the reciprocal temperature. (Reproduced by permission of American Chemical Society, from ref. 72.)

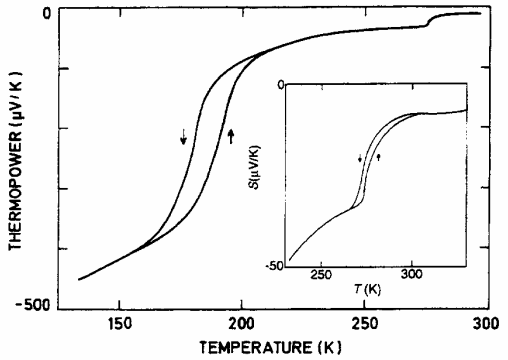


**Figure 2.49.** Absolute thermoelectric power measured along the chain axis **a** of $PerCo(mnt)_2 \cdot CH_2Cl_2$ as function of temperature. (Reproduced by permission of American Chemical Society, from ref. 72.)

## 5.2 Perylene based conductors with other metallocomplexes

Perylene complexes with other types M–dithio or M–diseleno complexes as anions, such as $Au(i\text{-}mnt)_2$ [106,107], $Au(i\text{-}mns)_2$ [108], $Au(cdc)_2$ [109], Ni–thiete [110] and $Ni(tcdt)_2$ [111], have also been reported (see Tables 2.8 and 2.9). Many of these anions can be taken as ligand variants of the corresponding $M(mnt)_2$ complexes. However these compounds have been obtained only with one type of metal M, lacking the extensive and systematic exploration of the metal effect previously described for the $Per_2M(mnt)_2$ family.

The compounds $Per_2Au(i\text{-}mnt)_2$ and $Per_2Au(i\text{-}mns)_2$ have been reported as very thin needle crystals obtained by electrocrystallisation procedures similar to those used to obtain the $Per_2M(mnt)_2$ compounds (see Section 5.1.1). For these ligands, monoanionic complexes with other metals such as Pt or Pd are not stable. Their structure was not solved but the physical

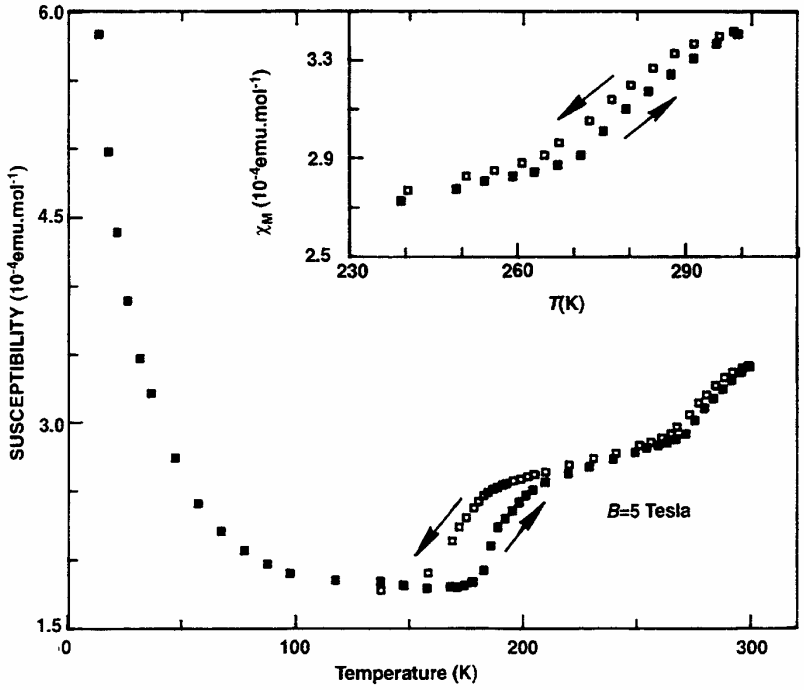


**Figure 2.50.** Paramagnetic susceptibility of $PerCo(mnt)_2 \cdot 0.5CH_2Cl_2$ as function of temperature. (Reproduced by permission of American Chemical Society, from ref. 72.)

properties are very similar to those of the $Per_2Au(mnt)_2$ compound, suggesting an identical structure [106–108].

Their room temperature electrical conductivities are in the range 150–500 S/cm with metallic behaviour at high temperature. Probably as a consequence of a not so high crystal quality and as found in the early α-$Per_2Au(mnt)_2$ and $Per_2Au(i\text{-}mnt)_2$ studies [56,106], no clear M–I transition is observed in $Per_2Au(i\text{-}mns)_2$ and there is just a broad resistivity minimum at temperatures that, depending on the sample quality, can be in the range 43–53 K. Independently of this sample quality, the thermopower in the high temperature range is virtually identical to the $Per_2M(mnt)_2$ compounds, indicating also that electrical transport takes place in a similar 3/4 filled band of stacked perylene molecules.

Also as in $Per_2Au(mnt)_2$, the EPR lines of these compounds are relatively narrow (0.5 G in i-mnt and 1 G in i-mns compounds) and have $g$-values corresponding to the perylene molecule [79]. The static magnetic susceptibility of the $Per_2Au(i\text{-}mns)_2$ compound shows a small Pauli-like temperature-independent paramagnetism, $\sim 1.6 \times 10^{-4}$ emu/mol [108], comparable to that of $Per_2Au(mnt)_2$.

In the perylene complex with the gold–bisdicyanodithiocarbimate anion, $Per_2Au(cdc)_2$, differences from the previously mentioned Au complexes, due to the

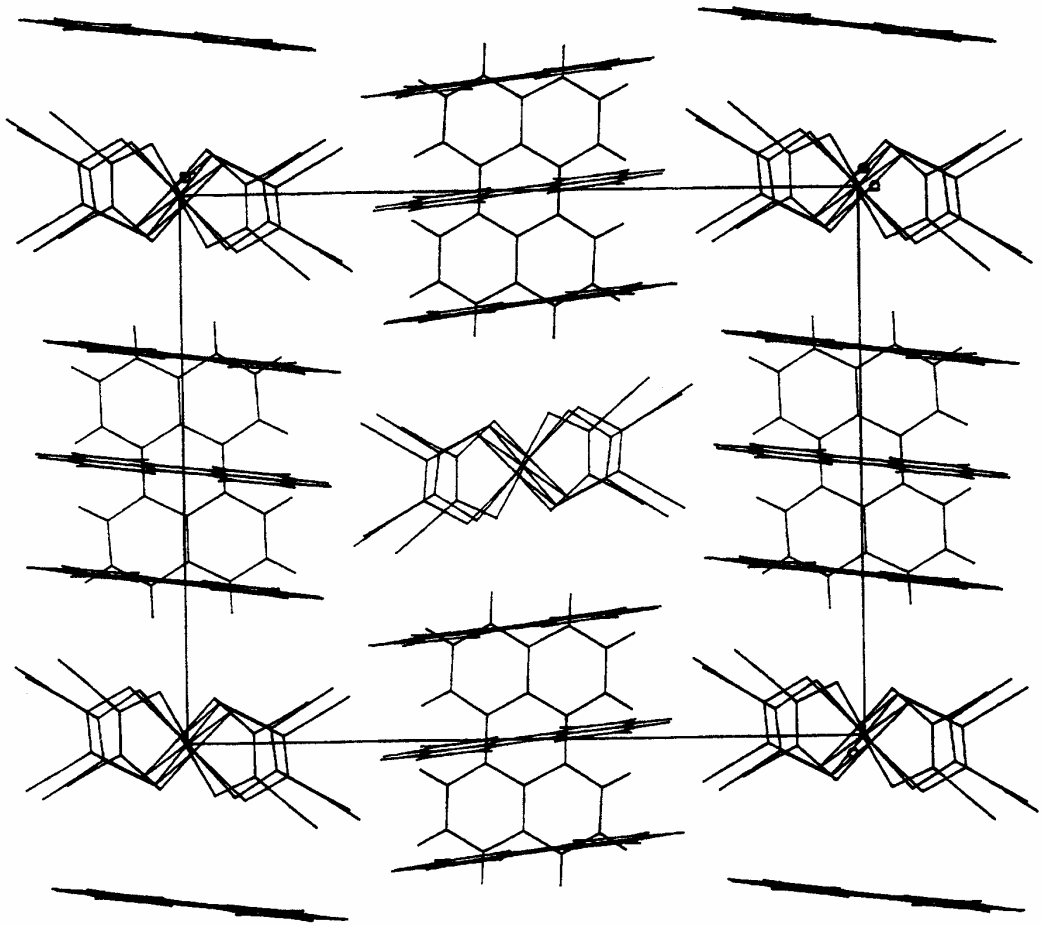

**Figure 2.51.** Projection of the $Per_4[Co(mnt)_2]_3$ crystal structure along the **a** axis. (Reproduced by permission of American Chemical Society, from ref. 73.)

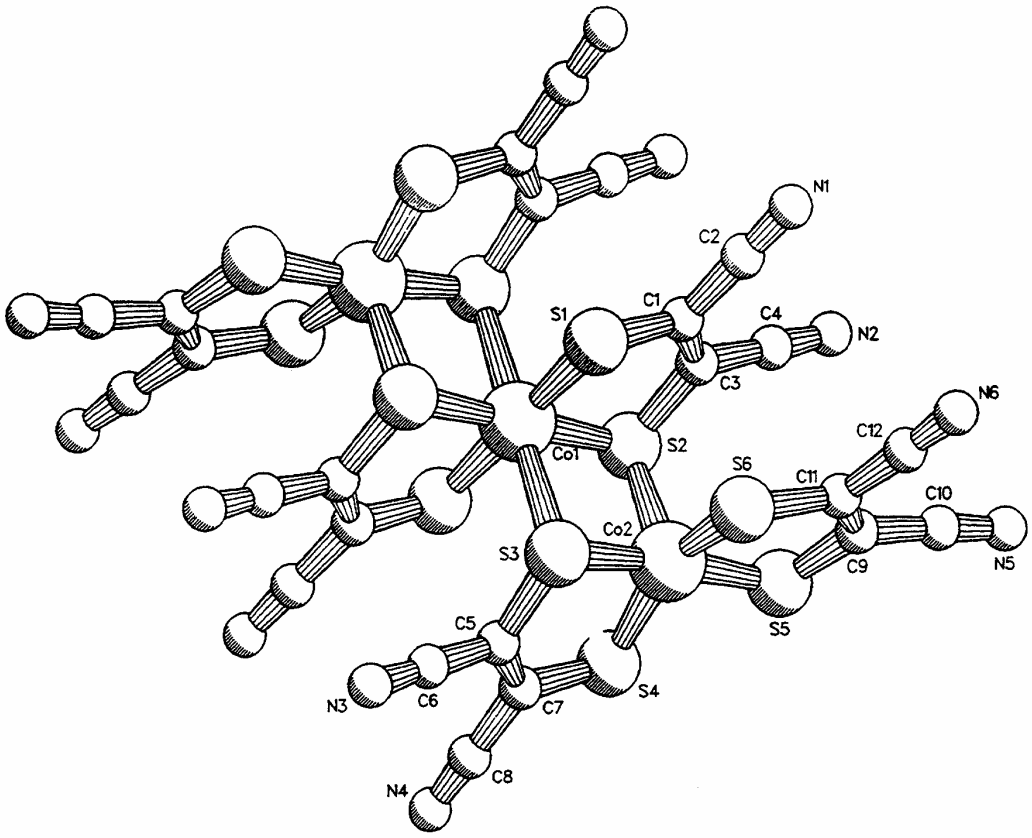


**Figure 2.52.** The trinuclear $[Co(mnt)_2]_3^-$ anion in $Per_4[Co(mnt)_2]_3$.

lower symmetry of this anion, are noticeable [109]. Although the crystal structure is not solved, the lattice parameters ($a = 12.6$ Å, $b = 8.34$ Å, $c = 17.9$ Å, $\alpha = 100.7°$, $\beta = 105.8°$, $\gamma = 74.7°$ and $V = 1739$ Å$^3$ [109]), particularly the $b$ parameter, which is approximately double that found in $\alpha$-$Per_2Au(mnt)_2$, suggests an alternating packing of the inorganic anions. The electrical conductivity is of the order of 150 S/cm at room temperature, presents a broad minimum at 145 K and becomes clearly activated at lower temperatures, with values indicating a gap of 260 K (Figure 2.53). The transition to the semiconducting regime is not very sharp, although indicative of a possible gap opening at $\sim 50$ K, smeared by disorder. The thermopower, 35 $\mu$V/K at room temperature, has a behaviour at high temperatures comparable to the other perylene complexes with gold anions (Figure 2.54). However below 50 K it starts decreasing and becomes negative. The magnetic susceptibility that at high temperatures has a Pauli-like behaviour, comparable to the other Au compounds but with more enhanced values ($5 \times 10^{-4}$ emu/mol at 300 K), also vanishes at $\sim 50$ K (Figure 2.55).

The complex obtained by electrochemical oxidation of perylene in the presence of $Ni(tcdt)_2$ has a 1 : 1 stoichiometry, $PerNi(tcdt)_2$, and it is a semiconductor with a room temperature conductivity of $4 \pm 2$ S/cm [111]. This different stoichiometry is not unexpected in view of the smaller electron accepting ability of the complex in which the oxidation potential of $Ni(tcdt)_2^-$ (0.73 V versus SCE) is lower than that of perylene (0.91 V versus SCE) under the same conditions. This

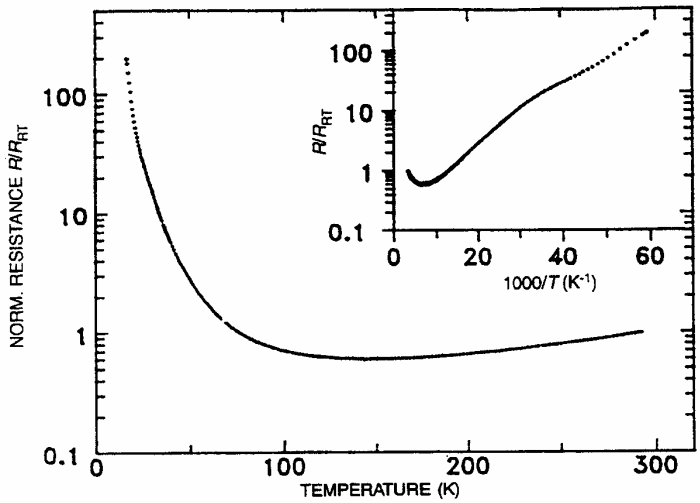


**Figure 2.53.** Normalised electrical resistivity, $R/R_{RT}$, of $Per_2Au(cdc)_2$ as a function of temperature. (Reproduced by permission of Elsevier Science S.A., from ref. 109.)

suggests that in this solid there is a partial charge transfer, probably as $Per^{\delta+}Ni(tcdt)_2^{\delta-}$ with $\delta \approx 1/2$, since otherwise for a full charge transfer with $Per^+$ and $Ni(tcdt)_2^-$ it would lead to half-filled bands, where a Mott insulator situation would be the most likely situation. The discussion of the properties of this compound is limited by the lack of a crystal structure determination but thermopower, with high temperature positive values, also supports the partial charge-transfer situation. Both the electrical conductivity (Figure 2.56) and the thermopower (Figure 2.57) measurements show anomalies at $\sim 195$ K. At this temperature the apparent activation energy, which is of the order of 0.12 eV below 150 K, shows a maximum

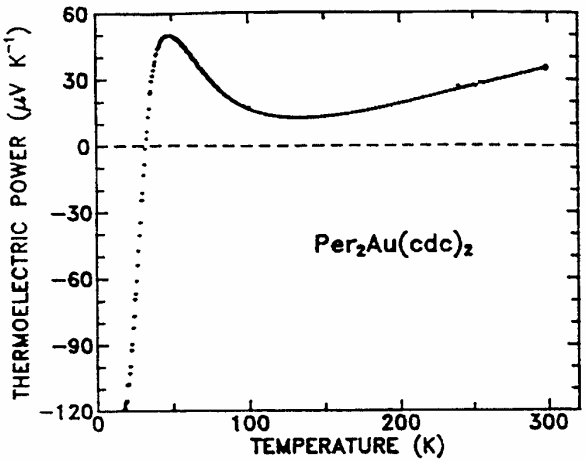


**Figure 2.54.** Thermopower of $Per_2au(cdc)_2$ as a function of temperature. (Reproduced by permission of Elsevier Science S.A., from ref. 109.)

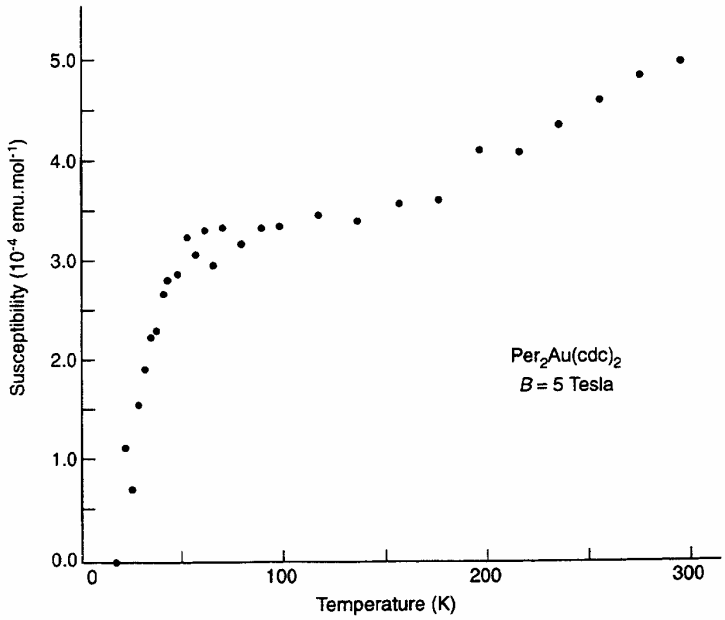


**Figure 2.55.** Paramagnetic susceptibility of $Per_2Au(cdc)_2$ as a function of temperature. (Reproduced by permission of Elsevier Science S.A., from ref. 109.)

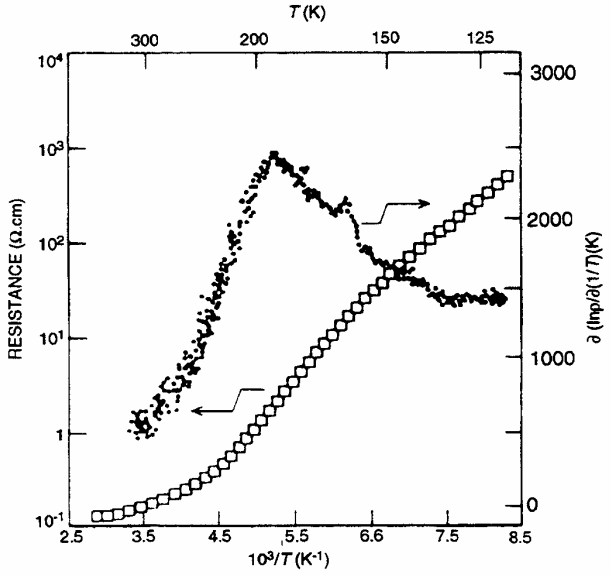


**Figure 2.56.** Electrical resistivity of $PerNi(tcdt)_2$ and its logarithmic derivative exhibiting an anomaly at 195 K. (Reproduced by permission of Elsevier Science S.A., from ref. 111.)

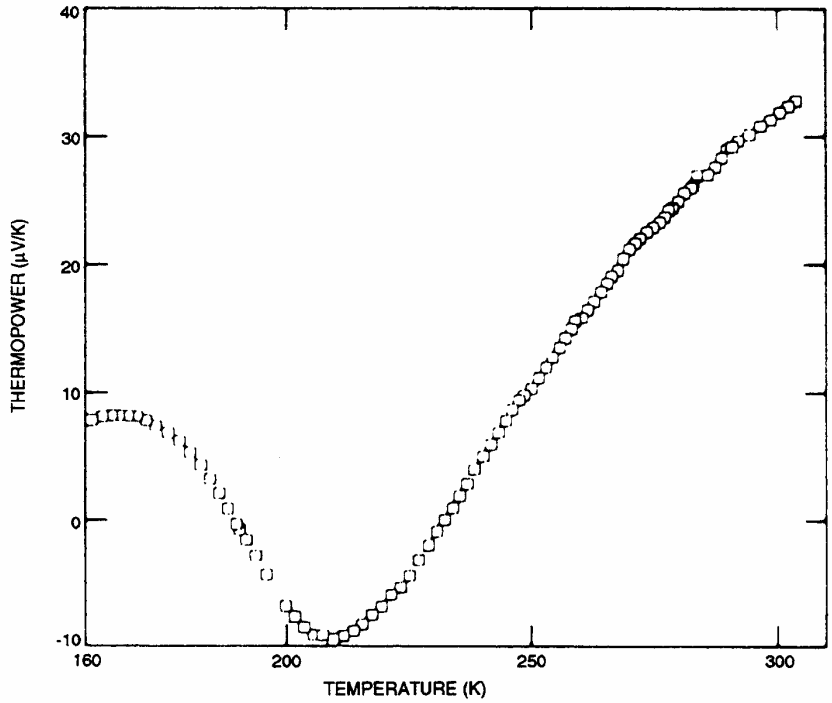


**Figure 2.57.** Thermopower of PerNi(tcdt) as a function of temperature. (Reproduced by permission of Elsevier Science S.A., from ref. 111.)

and the thermopower reaches negative values, both anomalies suggesting that the gap undergoes a fast decrease at around 200 K.

The Ni–thiete complex when reacted in solution with perylene gives a 1 : 1 charge-transfer solid reported in 1969 by Schmitt *et al.* [110]. Reasonably large single crystals of PerNi–thiete were obtained by diffusion controlled reactions lasting a few days. Its structure is triclinic, space group $P\bar{1}$, with $a = 12.71$, $b = 6.89$, $c = 8.41$ Å, $\alpha = 87.4$, $\beta = 110.3$, $\gamma = 103.4°$ and $Z = 2$, and it consists of an alternated packing of perylene and Ni–thiete units regularly stacked along the **c** direction. The analysis of bond lengths, electronic absorption spectra and EPR spectra supports the description of the complex as essentially covalent. The conductivity, as expected for a mixed stack solid, is relatively small, $\sim 2 \times 10^{-3}$ S/cm at room temperature, following a semiconducting regime with an activation energy of 0.23 eV. Thermopower with temperature-independent values of $-1.4$ mV/K in the range $-10$ to 30°C, is indicative of electron-dominated conduction.

## 6 CONDUCTORS BASED ON PERYLENE DERIVATIVES

The perylene derivatives 1,2,7,8-tetrahydrodicyclopenta[*cd* : *lm*]perylene, (CPP), 3,4,9,10-tetramethylperylene, (TMP), 3,4,9,10-tetrathioperylene (TTP), 3,4,9,10-tetraselenoperylene (TSeP) and perylothiophene (PeT), indicated below, have also been used as variants of perylene to prepare molecular conductors.

In the perylene derivatives CPP and TMP, the outer substituent $CH_2$–$CH_2$ or $CH_3$ groups leave the perylene $\pi$-electron system essentially unchanged, and apart from stereo effects and a small reduction of the oxidation potential, no other significant changes in the basic solid state properties of the solids based on this

donor, when compared with those based on perylene, are expected.

CPP was first combined with $PF_6$ by Lapuyade *et al.* [112] to give the conductor $CPP_2PF_6{\cdot}CH_2Cl_2$. This compound has an electrical conductivity of $\sigma \approx 30$–70 S/cm at room temperature, which presents a broad maximum just above room temperature, and a broad transition detected as a maximum of the logarithmic derivative of the conductivity versus the reciprocal temperature, at around 150 K.

Its structure is monoclinic, space group $C2/m$ with $a = 16.941$ Å, $b = 12.650$ Å, $c = 8.867$ Å, $\beta = 109.68°$, $V = 1789.3$ Å$^3$ and $Z = 2$, and consists of very slightly dimerised stacks of CPP molecules with 3.456 and 3.457 Å spacings and making an angle of 38.8° between their normal and the stacking axis **c** [112] (Figure 2.58). The overlap mode is similar to the one found in the $\alpha$-$Per_2M(mnt)_2$ compounds, with a continuous longitudinal displacement of 2.65 Å per CPP molecule. The anions as well as the non-centrosymmetric solvent molecules are at inversion centres located in channels between the donor molecules. This implies the random occupation of two symmetrically equivalent positions for $CH_2Cl_2$. As a consequence of this type of disorder, strong diffuse planes of X-ray scattering, with a weak modulation, are observed at odd $l$ layers [112–114]. These were interpreted as the positional disorder of the long-range ordered alternating solvent and anion molecules in the channels. In addition to the structural diffusive scattering, weak diffuse lines are also visible in the middle between two successive $l$ layers [113,114]. Upon cooling these scattering planes condense at 158 K in Bragg satellites, at the reduced wave vector (0,1/2,1/2), clearly indicating that they are due to a $2\mathbf{k}_F$ (tetramerisation) Peierls distortion of the CPP molecules.

The room temperature electrical conductivity of this compound increases under pressure from 50 to 220 S/cm at 12 kbar, while the transition temperature has a slight increase, ascribed to an increase of the transverse coupling between the chains [113].

The TMP analogue, $TMP_2PF_6{\cdot}CH_2Cl_2$, was also obtained under similar conditions by Michel *et al.* [115], and, as expected, presents very similar properties but with a smaller electrical conductivity that at room temperature is of the order of 5 S/cm. Closely related CPP and TMP compounds with other centrosymmetric anions such as $AsF_6^-$ and $SbF_6^-$ or with other related halomethane solvents such as $CH_2ClBr$, $CH_2Br_2$ and $CHCl_3$ have been also obtained, but their study was limited to the analysis of the temperature-independent diffuse scattering by Ilakovac *et al.* [114]. In these CPP and TMP compounds it was observed that an increase of the solvent size leads to the change in the location of the diffusive lines without affecting the same basic donor lattice. In CPP compounds with $PF_6$ and $CH_2Br_2$ or $CHCl_3$ with $AsF_6$ and $CH_2ClBr$ they appear at $c^*/3$ suggesting a change to the stoichiometry of 3 : 1, while in the TMP compound with $SbF_6$ and $CH_2Cl_2$ they indicate a 5 : 4 stoichiometry [114].

The complex $CPP_2(I_3)_{1-\delta}$ can be obtained by electrochemical oxidation of CPP in the presence of tetrabutylammonium triodide and under conditions similar to those used for the preparation of the $Per_2M(mnt)_2$ compounds [116,117]. No CPP compounds with $M(mnt)_2$ anions are known and in fact $CPP_2(I_3)_{1-\delta}$ crystals were first obtained while trying to prepare $CPP_2M(mnt)_2$ from iodine-contaminated TBA $M(mnt)_2$ salts. Two types of crystal morphologies are

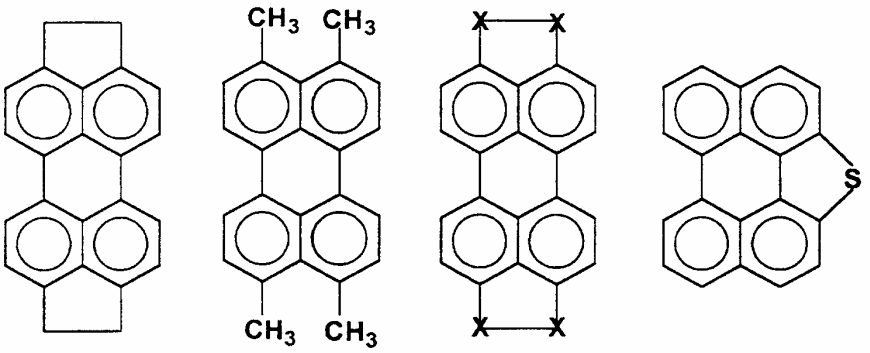


CPP TMP X=S, TTP. X=Se, TSeP PeT

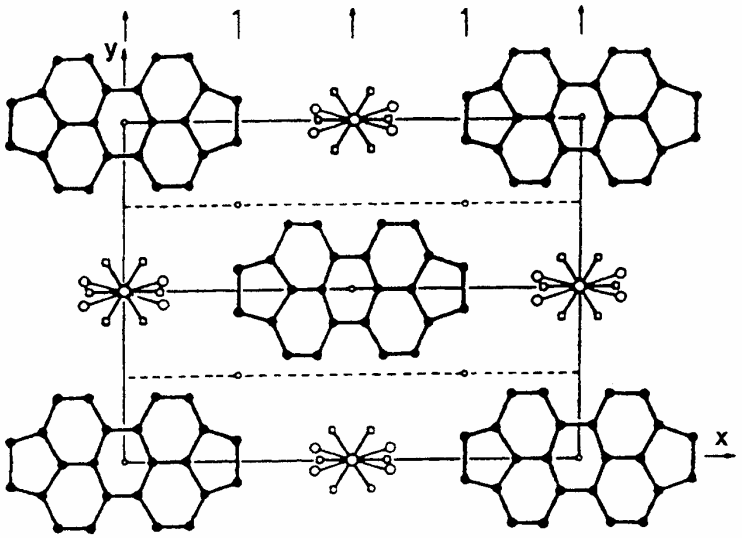


(a)

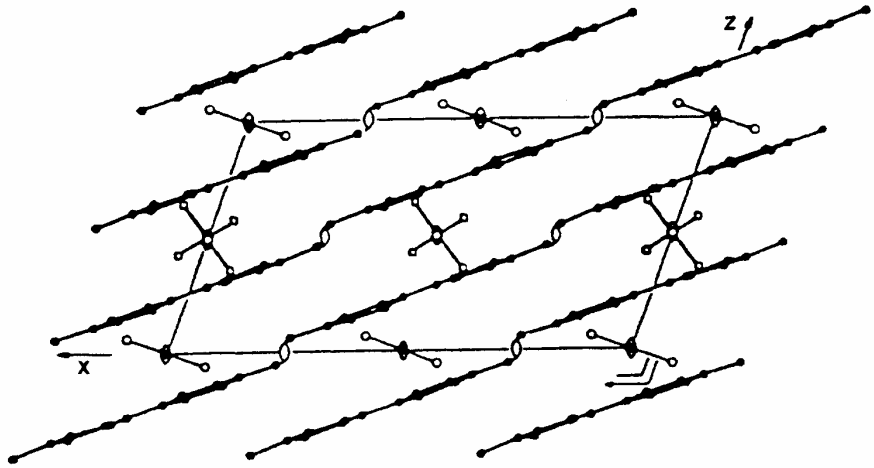


(b)

**Figure 2.58.** Crystal structure of $CPP_2PF_6 \cdot CH_2Cl_2$ projected along the stacking axis **a** (a) and along the temperature **b** axis (b). (Reproduced by permission of Les Editions de Physique, from ref. 112.)

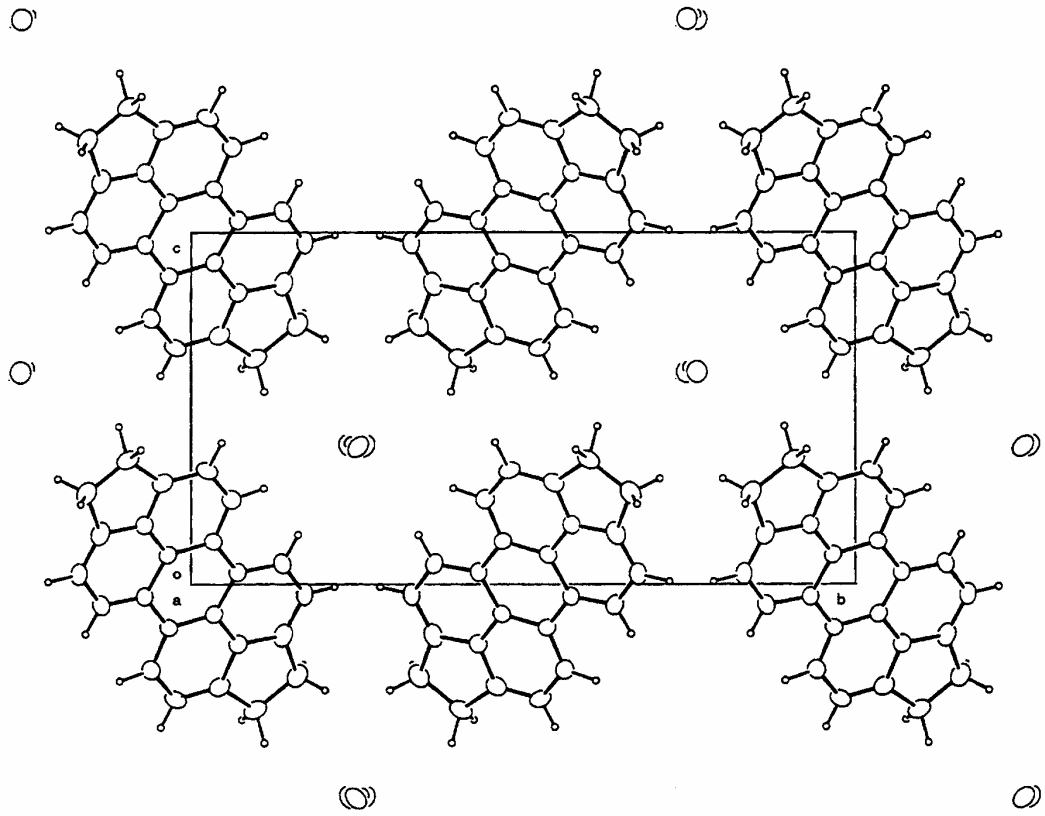


**Figure 2.59.** Projection of the $CPP_2(I_3)_{1-\delta}$ crystal structure along the stacking axis **a**. (Reproduced by permission of American Chemical Society, from ref. 117.)

**Table 2.8.** Summary of crystallographic data for miscellaneous complexes of perylene (Per) and perylene derivatives complexes

| Complex | Space group | *a* (Å) | *b* (Å) | *c* (Å) | α (°) | β(°) | γ (°) | *Z* | *V*(Å$^3$) | Ref. |
|---|---|---|---|---|---|---|---|---|---|---|
| $Per_4[Co(mnt)_2]_3$ | $P2_1/n$ | 12.093(1) | 20.912(1) | 16.633(1) | 90 | 94.290(6) | 90 | 2 | 4194.5(5) | 73 |
| $PerCo(mnt)_2(CH_2Cl_2)_{0.5}$ | $P\bar{1}$ | 6.551(2) | 11.732(2) | 16.481(2) | 92.08(1) | 95.30(1) | 94.62(1) | 2 | 1248.6(3) | 72 |
| $Per_2Au(cdc)_2$ | | 12.6 | 8.34 | 17.9 | 100.7 | 105.8 | 74.7 | 2 | 17.39 | 109 |
| $PerPt(mnt)_2$ | $P\bar{1}$ | 11.296 | 11.502 | 11362 | 104.01 | 120.11 | 80.83 | 2 | 1223 | 74 |
| PerNi–thiete | $P\bar{1}$ | 12.71(1) | 6.89(1) | 8.41(1) | 87.4(5) | 110.35(5) | 103.4(5) | 1 | 671 | 110 |
| $CPP_2PF_6{\cdot}CH_2Cl_2$ | $C2/m$ | 16.941 | 12.650 | 8.867 | 90 | 109.68 | 90 | 2 | 1789.3 | 112 |
| $TMP_2PF_6{\cdot}CH_2Cl_2$ | $C2/m$ | 15.814(2) | 13.684(3) | 8.926(8) | 90 | 101.30(2) | 90 | 2 | 1896.8 | 115 |
| $CPP_2(I_3)_{0.89}$ | $P2_1/a$ | 4.357(9) | 19.3681(11) | 10.0860(11) | 90 | 98.050(8) | 90 | 4 | 846.4(2) | 117 |
| $TTP–I_{1.28}$[a] | $C2/m$ | 15.973 | 12.475 | 4.208 | 90 | 98.45 | 90 | 2 | 829 | 120 |
| $PeT_3[Ni(mnt)_2]_2$ | $P\bar{1}$ | 10.2972(9) | 11.5037(12) | 13.3297(10) | 78.320(8) | 87.096(7) | 87.785(8) | 2 | 1543.1(2) | 119 |

[a] Data for the TTP lattice. The iodine lattice is incommensurate, having the same parameters except $c = 3.28$ Å and $\beta = 96.7°$
CPP = 1,2,7,8-tetrahydrodicyclopenta[*cd*,*lm*]perylene, TMP = 3,4,9,10-tetramethylperylene, PeT = perylothiophene.

**Table 2.9.** Physical properties of different perylene (Per) based conductors and related derivatives

| | $\sigma$(RT) (S/cm) | $T_c$ (K) | $T_\rho$ (K) | $E_a$ (meV) | $S$(RT) ($\mu$V/K) | $10^4\chi_P$(RT) (emu/mol) | Ref. |
|---|---|---|---|---|---|---|---|
| $PerBr_4$ | $0.1–10^{-3}$ | | | 65 | | | 4 |
| $Per_2(I_2)_3$ | $1.2 \times 10^{-1}$ | | | 19[a], 30[b] | | 0.62 | 6,7,9 |
| $Per(I_2)_3$ | | | | 30 | > 0 | | 7 |
| $Per(I_2)_4$ | 33–52 | | 235 | 50 | | | 10 |
| Per–fluoranil | $10^{-14}$ | | | 730 | | | 16 |
| $PerClO_4$ | 0.1–0.8 | | | | | 0.14 | 3,27 |
| $Per_2ClO_4$ | $5 \times 10^{-5}$ | | | | | | 3 |
| $Per_3ClO_4$ | 0.5–2 | | | | | | 37 |
| $Per_6ClO_4$ | $10^{-2}$ | | | | | | 37 |
| $Per_2BF_4$ | $4 \times 10^{-4}$ | | | | | | 33 |
| $Per_6PF_6$ | $10^{-4}$ | | | | | 12 | 39 |
| $Per_2(PF_6)_{1.1}$·0.8DCM | $10^2–1.4 \times 10^3$ | ~100 | 200–150 | 45,38 | | | 31,37,40 |
| $Per_2(AsF_6)_{1.1}$·0.8DCM | $10^2–1.4 \times 10^3$ | ~100 | 200–150 | 35,27 | | | 31,37,40 |
| $Per_2(AsF_6)_{0.75}(PF_6)_{0.35}$·0.85DCM | 200–1200 | | | | 20 | 0.92 | 37,38,46 |
| $Per_2(AsF_6)_{1.5}$·0.5THF | 70–700 | | 200 | 20 | 10 | | 31,37 |
| $Per_2(PF_6)_{1.5}$·0.5THF | 70–700 | | 200 | 20 | | | 31 |
| $Per_2PF_6$·0.66THF | 60 | 110 | | | | | 37 |
| $Per_2PF_6$·0.66THF | 10–100 | 120 | | 35 | | | 40 |
| $Per_2(AsF_6)_{0.45}(PF_6)_{0.55}$·0.66THF | 95 | 120 | | | −7 | | 37 |
| $Per_3FeCl_4$ | 0.17 | | | 120 | 275 | 160 | 35 |
| $Per_3FeBr_4$ | | | | | | 150 | 35 |
| $Per_2Au(mnt)_2$ | 700 | 12.2 | 16 | 1.75 | 32 | 1.8 | 60,70,77 |
| $Per_2Co(mnt)_2$ | 200 | 73 | 95 | 30 | 42 | 2.7 | 63 |
| $\alpha$-$Per_2Cu(mnt)_2$ | 700 | 32 | 40 | 10 | 38 | 1.8 | 65,68 |
| $\beta$-$Per_2Cu(mnt)_2$ | 50 | | | 90 | 22 | 4.5 | 65,68 |
| $Per_2Fe(mnt)_2$ | 200 | 58 | 105 | 25 | 42 | 15 | 63 |
| $\alpha$-$Per_2Ni(mnt)_2$ | 700 | 25 | 50 | 7.5 | 35 | 13 | 65,68 |
| $\beta$-$Per_2Ni(mnt)_2$ | 50 | | 250 | 90 | 23 | 12 | 65,68 |
| $Per_2Pd(mnt)_2$ | 300 | 28 | 80 | | 32 | 9 | 56,60,71 |
| $Per_2Pt(mnt)_2$ | 700 | 8.2 | 18 | 4.3 | 32 | 15.5 | 30,56,60 |
| $Per_1Co(mnt)_2$·0.5DCM | 60 | 272–277 | 340 | 150[c],100[d] | −8 | 3.4 | 72 |
| $PerPt(mnt)_2$ | $\sim 10^{-3}$ | | | | | | 74 |
| $Per_2Au(cdc)_2$ | ~150 | ~50 | ~140 | | 35 | 5.0 | 109 |
| $Per_2Au(i\text{-}mnt)_2$ | ~1000 | ~9 | ~30 | | 42 | | 107 |
| $Per_2Au(i\text{-}mns)_2$ | ~300 | 25 | 50 | | 36 | | 108 |
| PerNi–thiete | $3 \times 10^{-3}$ | | | 0.23 | −1400 | | 110 |
| $PerNi(tcdt)_2$ | 4 | | | | 32 | | 111 |
| $TTP–I_{1.23}$ | 800 | | | | | | 120 |
| $CPP_2(I_3)_{1-\delta}$ 'diamonds' | 2 | 64 | 170 | | −8 | | 117 |
| $CPP_2(I_3)_{1-\delta}$ 'needles' | 200 | 62 | 130 | | 30 | 1.2 | 117 |
| $CPP_2PF_6$·$CH_2Cl_2$ | 50 | ~150 | ~310 | | | | 112 |
| $TMP_2PF_6$·$CH_2Cl_2$ | 5 | | | | | | 115 |
| $PeT_3[Ni(mnt)_2]_2$ | 4 | | | | | 18 | 118 |

$\sigma$(RT) = room temperature electrical conductivity, $T_c$ = metal to insulator transition temperature, $T_\rho$ = minimum electrical resistivity temperature, $S$(RT) = room temperature thermopower, $\chi_P$(RT) = room temperature paramagnetic susceptibility, $E_a$ = activation energy of the electrical conductivity in the semiconducting regime. [a] From ref 6. [b] From ref 7. [c] In the range 190–270 K. [d] Below 165 K.

apparent in the crystals obtained by these preparations; thin needles and larger elongated diamond shaped crystals. Alternatively the direct reaction of CPP with iodine, best carried out in H-shaped diffusion cells, can also be used but it affords only the small needle-shaped crystals. At variance with the perylene–iodine complexes these compounds are very stable and no iodine loss is noticed even after an extended period of several weeks at open atmosphere or after vacuum exposure. In spite of this compositional stability, elemental analysis indicates for the $\delta$ values a variability from batch to batch in the range 0.0–0.13. Both types of crystals present the same CPP lattice parameters, as in the case of the diamond-shaped crystal $CPP_2(I_3)_{0.892}$, whose structure was solved by X-ray diffraction. The difference between the two forms is most certainly due to changes in the iodine content and

possible different types of disorder associated with iodine species in the same CPP lattice. The two types of morphologies also have distinct transport properties as discussed below.

$CPP_2(I_3)_{1-\delta}$ crystallises with a monoclinic cell, space group $P2_1/a$, with $a = 4.3757(9)$ Å, $b = 19.3681(11)$ Å, $c = 10.0860(11)$ Å and $\beta = 98.050(8)°$, $V = 846.4(2)$ Å$^3$ and $Z = 4$ [117]. Its structure (Figure 2.59) consists of regular stacks of CPP molecules along **a** with a 3.41 Å spacing and with an overlap mode similar to the $\alpha$-$Per_2M(mnt)_2$ phases. Iodine atoms are located in channels of free space along **a** between the CPP molecules. Their exact position could not be located in the structural refinement of the diamond-shaped crystals, but X-ray photographic work clearly indicates one-dimensional order along axis *a* with a repeat of 10.2 Å, as denoted by strong diffuse planes perpendicular to **a***, consistent with $I_3^-$ [15]. The presence of $I_3^-$ species is further confirmed by the strong intensity of the third-order diffuse layers. In the thinner needle-shaped crystal no detailed X-ray studies have been reported and therefore the type of iodine species and arrangement in this case cannot be characterised.

The iodine atoms are tightly located in the channels with close contacts with the CPP molecules, explaining the relatively good stability of the iodine content. Band structure calculations indicate that this compound is as rigidly one-dimensional as the $\alpha$-$Per_2M(mnt)_2$ phases and with a similar bandwidth.

The transport properties of the crystals of these two forms are quite different. The electrical resistivity, $\rho$ (Figure 2.60), although with a similar temperature dependence (in both cases reaching a broad maximum at $\sim 150$ K, followed by a rapid decrease with a maximum of d ln $\rho$/d $(1/T)$ at $\sim 62$ K), have quite different absolute values. At room temperature (RT) the thin crystals present $\sigma(RT) = 200$ S/cm while the diamond-shaped crystals present values about two orders of magnitude smaller. Thermopower, $S$ (Figure 2.61), although confirming the metallic behaviour at high temperature, with $S$ roughly proportional to $T$, presents distinct room temperature values and signs. For the thin needles, positive values of 30 $\mu$V/K are observed, while the diamond-shaped crystals have negative values, $-8$ $\mu$V/K.

The two types of crystal have similar EPR signals, as expected if due to the CPP molecules in the same arrangement. This is confirmed by the almost isotropic *g*-values of 2.0044 in the *b,c* plane, almost identical to that of $CPP_2PF_6{\cdot}CH_2Cl_2$, with a 6 G wide signal in the range 300–80 K. At around 60 K, where the transition

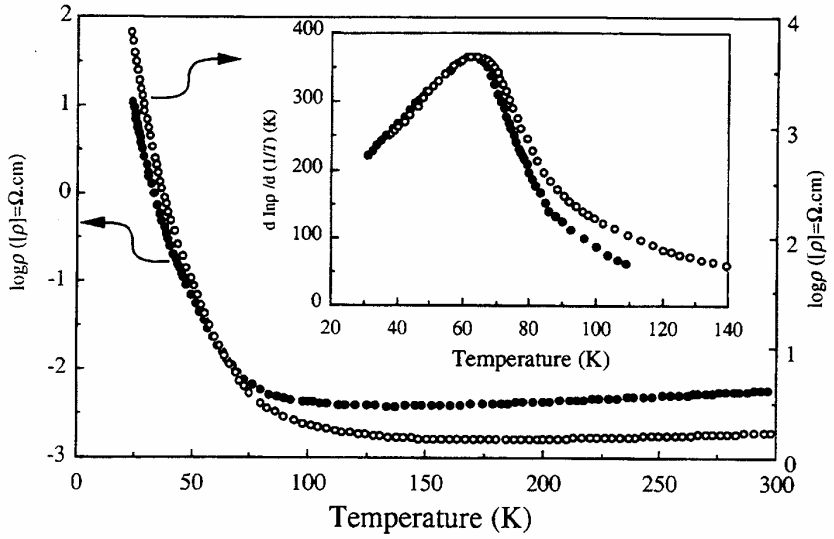


**Figure 2.60.** Electrical resistivity, $\rho$, of $CPP_2(I_3)_{1-\delta}$ thin needles (solid circles) and diamond-shaped crystals (open circles), as a function of temperature. The inset shows the derivative d ln $\rho$/d $(1/T)$ at low temperatures. (Reproduced by permission of American Chemical Society, from ref. 117.)

occurs, there is a fast linewidth decrease upon cooling. The integrated intensity of the EPR line of both types of crystal has the same temperature dependence as the static magnetic susceptibility, measured in the needle-shaped crystals (Figure 2.62). These measurements show a small paramagnetic contribution ($1.2 \pm 0.2 \times 10^{-4}$ emu/mol at room temperature) with a small decrease upon cooling until the transition temperature where it has a faster decrease followed by a Curie tail that dominates at lower temperatures.

In spite of the poor characterisation of the iodine in the thin needles, probably also more disordered $I_3^-$ species than in the diamond-shaped crystals, giving rise to significant differences in the thermopower, the physical properties indicate in both compounds metallic properties at higher temperatures and M–I transitions at lower temperatures comparable to many other perylene conductors.

The only conductor based on PeT (perylothiophene) so far reported is $PeT_3[Ni(mnt)_2]_2$ [118]. This compound has a stoichiometry quite different from the perylene based conductors previously mentioned, in spite of being obtained under similar conditions by electrocrystallisation from dichloromethane solutions with PeT and $TBANi(mnt)_2$ in a 2 : 1 molar ratio. This compound is a semiconductor with $\sigma(RT) = 7$ S/cm. The semiconducting properties of this compound are explained by the structure (triclinic, space group $P\bar{1}$ with $a = 10.297$ Å, $b = 11.503$ Å, $c = 13.329$ Å, $\alpha = 78.32°$, $\beta = 87.09°$, $\gamma = 87.78°$ and $Z = 2$ [119]) with trimerised stacks of PeT molecules in an average oxidation state of $PeT_3^{2+}$. In these stacks the sulphur atom of one molecule is oriented towards the opposite side of the other two molecules. In spite of the relatively short interplanar distances, comparable to the other perylene conductors, the trimerisation with this degree of charge transfer implies a gap at the Fermi level.

The $Ni(mnt)_2$ anions in this compound are arranged as dimers, $[Ni(mnt)_2]_2^{2-}$, and the formal oxidation of Ni(III) is in good agreement with the temperature-dependent paramagnetic susceptibility that can be well described by a singlet–triplet model of pairs of antiferromagnetically coupled $S = 1/2$ spins, with $J/k_B = -226$ K (Figure 2.63) [118].

The use of the tetrachalcogenoperylene molecules such as TTP to obtain molecular conductors has been greatly limited by the low solubility of these compounds, which is much smaller than perylene in the usual solvents. Hilti *et al.* [120] obtained, by co-sublimation of this donor and iodine, a highly conducting compound, $TTP\text{–}I_{1.28}$. In this case, as opposed to the perylene–iodine complexes, the iodine composition was found to be much more stable in a

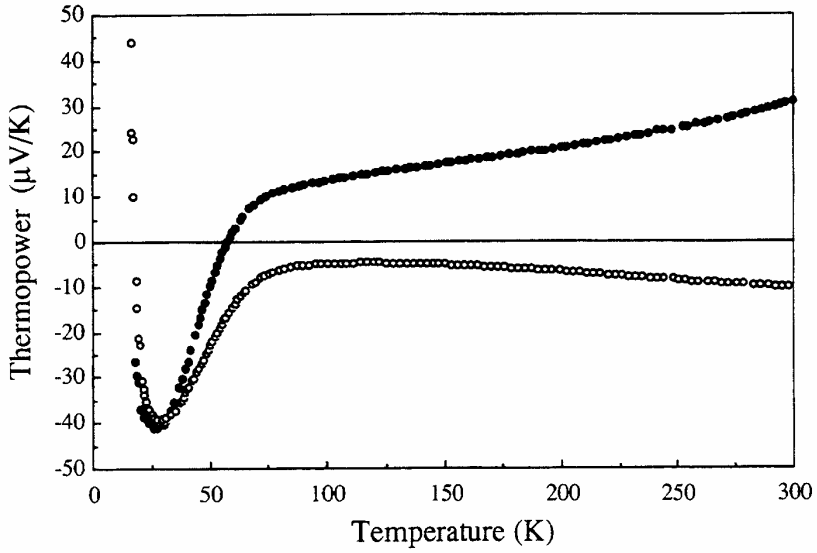


**Figure 2.61.** Thermopower of $CPP_2(I_3)_{1-\delta}$ thin needles (solid circles) and diamond-shaped crystals (open circles), as a function of temperature. (Reproduced by permission of American Chemical Society, from ref. 117.)

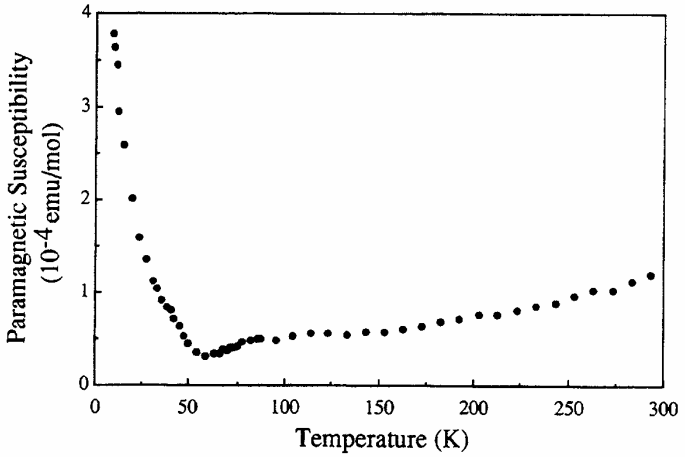


**Figure 2.62.** Paramagnetic susceptibility of $CPP_2(I_3)_{1-\delta}$ as a function of temperature. (Reproduced by permission of American Chemical Society, from ref. 117.)

situation comparable to CPP–iodine, but, as judged by the scattering of the electrical properties and the difficulties in locating the iodine positions in the lattice, the iodine is believed to be more disordered. The crystal structure consists of two incommensurate sublattices of the TTP molecules and iodine atoms. The TTP lattice (Figure 2.64) is monoclinic ($a = 15.973$ Å, $b = 12.475$ Å, $c = 4.208$ Å, $\beta = 98.45°$ and $V = 829$ Å$^3$) with regular stacks of TTP molecules tilted 45° towards the chain axis $c$ and closely spaced at 3.25 Å with an overlap similar to the perylene

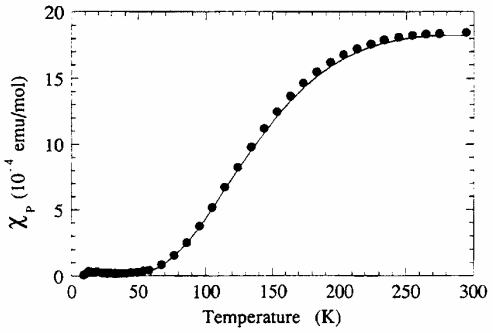


**Figure 2.63.** Paramagnetic susceptibility of $PeT_3[Ni(mnt)_2]_2$ as a function of temperature. (Reproduced by permission of Elsevier Science S.A., from ref. 118.)

molecules in the α-$Per_2M(mnt)_2$ compounds. There are close (4.36 Å) contacts between sulphur atoms of TTP molecules in neighbouring chains. The iodine atoms are disordered in between the TTP molecules, with a lattice with the same $a$, $b$ and $\beta$ parameters, but with $c = 3.28$ Å. In this case, as opposed to the other perylene derivatives, the sulphur atoms have a large contribution to the HOMO, and therefore both an increased bandwidth and dimensionality, compared with similar perylene compounds, are expected to occur. The bandwidth, although not experimentally estimated, is certainly larger than in the α-$Per_2M(mnt)_2$ compounds in view of the reduced intermolecular spacing (3.25 Å in this compound compared with 3.32 Å for $Per_2Au(mnt)_2$) with the additional sulphur atoms in TTP.

Probably as a consequence of variable degrees of iodine content or disorder in the crystals, their electrical conductivity shows a remarkable sample dependence: values as high as 800 S/cm at room temperature, with a broad maximum at ~200 K, were reported for the best crystals.

## 7 ACKNOWLEDGEMENTS

The continued collaboration with the coauthors listed in the references is greatly acknowledged.

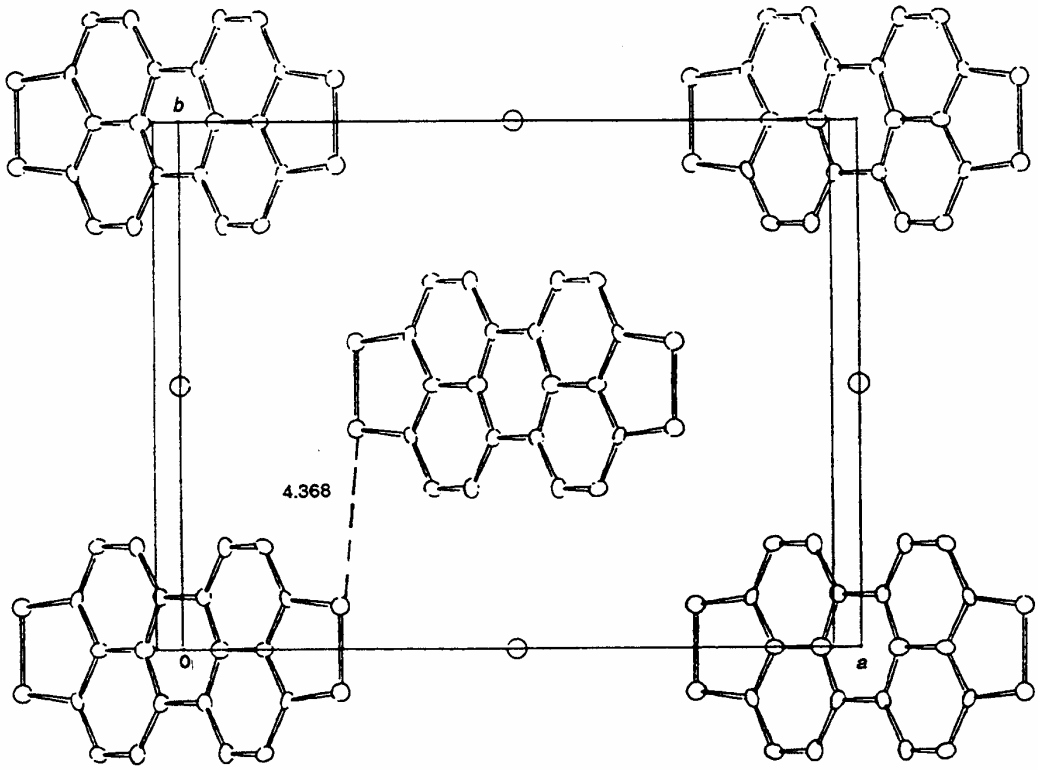


**Figure 2.64.** Projection of the TTP–$I_{1.28}$ lattice along the *a,b* plane. (Reproduced by permission of Pergamon Press, from ref. 120.)

## 8 REFERENCES


1. H. Akamatu, H. Inokuchi and Y. Matsunaga, *Nature* **173**, 168 (1954).
2. R.S Nicholson and I. Shain, *Anal. Chem.* **36**, 706 (1974).
3. D.S. Rosseinsky and P. Kathirgamanathan, *J. Chem. Soc., Perkin Trans.* **2** 135 (1985).
4. H. Akamatu, H. Inokuchi and Y. Matsunaga, *Bull. Chem. Soc. Jpn.* **29**, 213 (1956).
5. E. Clar and K. Brass, *Berichte* **65**, 1660 (1932).
6. J. Kommandeur and F.R. Hall, *J. Chem. Phys.* **34**, 129 (1961).
7. T. Uchida and H. Akamatu, *Bull. Chem. Soc. Jpn.* **34**, 1015 (1961).
8. L.S. Singer and J. Kommandeur, *J. Chem. Phys.* **34**, 133 (1961).
9. M. Kinoshita, H. Kanda and H. Akamatu, *Bull. Chem. Soc. Jpn.* **49**, 1407 (1976).
10. H.C.I. Kao, M. Jones and M.M. Labes, *J. Chem. Soc., Chem. Commun.* 329 (1979).
11. C.M. Cobb and E.B. Wallis, *J. Phys. Chem.* **72**, 2986 (1968).
12. S. Aronson, G. Sinensky, Y. Langsam and M. Binder, *J. Inorg. Nucl. Chem.* **38**, 407 (1976).
13. R.C. Teitelbaum, S.L. Ruby and T.J. Marks, *J. Am. Chem. Soc.* **101**, 7568 (1979).
14. T. Uchida and H. Akamatu, *Bull. Chem. Soc. Jpn.* **35**, 981 (1962).
15. P. Coppens, in *Extended Linear Chain Compounds*, J.S. Miller (Ed.), Vol. 1, Plenum Press, New York, 1982, p. 341.
16. H. Hokado, K. Hasegawa and W.G. Schneider, *Can. J. Chem.* **42**, 1084 (1964).

17. K.D. Truong and A.D. Bandrauk, *Chem. Phys. Lett.* **44**, 232 (1976).
18. I.J. Tickle and C.K. Prout, *J. Chem. Soc., Perkin Trans.* **2** 720 (1973).
19. A.W. Hanson, *Acta Crystallogr., Sect. B* **34**, 2339 (1978).
20. M. Michaud, C. Carlone, N.K. Hota and J. Zauhar, *Chem. Phys.* **36**, 79 (1979).
21. P.J. Munoch and J.D. Wright, *J. Chem. Soc., Faraday Trans. 1* **72**, 1981 (1976).
22. H. Kuroda, T. Sakurai and H. Akamatu, *Bull. Chem. Soc. Jpn.* **39**, 1893 (1966).
23. A.W. Hanson, *Acta Crystallogr.* **16**, 1147 (1963).
24. J.C.A. Boeyens and F.H. Herbstein, *J. Phys. Chem.* **69**, 2160 (1965).
25. I. Ikemoto, K. Yakushi and H. Kuroda, *Acta Crystallogr., Sect. B,* **26**, 800 (1970).
26. H. Yamochi, G. Saito, T. Sugano, M. Kinoshito, *Synth. Met.* **19**, 533 (1987).
27. Y. Sato, M. Kinoshita, M. Sano and H. Akamatu, *Bull. Chem. Soc. Jpn.* **42**, 3051 (1969).
28. T.C. Chiang, A.H. Reddoch and D.F. Williams, *J. Chem. Phys.* **54**, 2051 (1971).
29. K. Bechgaard, C.S. Jacobsen, K. Mortensen, H.J. Pedersen and N. Thorup, *Solid State Commun.* **33**, 1119 (1980).
30. L. Alcácer, H. Novais, F. Pedroso, S. Flandrois, C. Coulon, D. Chasseau and J. Gaultier, *Solid State Commun.* **35**, 945 (1980).
31. H.J. Keller, D. Nöthe, H. Pritzkov, D. Wehe, M. Werner, P. Koch and D. Schweitzer, *Mol. Cryst. Liq. Cryst.* **62**, 181 (1980).
32. H.J. Keller, D. Nöthe, H. Pritzkov, D. Dewe, R.M. Harms, P. Koch and D. Schweitzer, *Chem. Scr.* **17**, 101 (1981).
33. C. Kröhnke, V. Enkelmann and G. Wegner, *Angew. Chem.* **92**, 941, 1980.
34. H. Endres, H.J. Keller, B. Muller and D. Schweitzer, *Acta Crystallogr., Sect. C,* **41**, 607 (1985).
35. J.A. Ayllón, I.C. Santos, R.T. Henriques, M. Almeida, E.B. Lopes, J. Morgado, L. Alcácer, L.F. Veiros and M.T. Duarte, *J. Chem. Soc., Dalton Trans.*, 3543 (1995).
36. C.V. Ristagno and H.J. Shine, *J. Org. Chem.*, **36**, 4050 (1971).
37. D. Schweitzer, I. Hennig, K. Bender, H. Endres and H.J. Keller, *Mol. Cryst. Liq. Cryst.* **120**, 213 (1985).
38. P. Koch, D. Schweitzer, R.H. Harms, H.J. Keller, H. Schäfer, H.W. Helberg, R. Wilckens, H.P. Geserich and W. Ruppel, *Mol. Cryst. Liq. Cryst.* **86**, 87 (1982).
39. W.F. Kuhs, G. Mattern, W. Brütting, H. Dragan, M. Burggraf, B. Pilawa and E. Dormann, *Acta Crystallogr., Sect. B,* **50**, 741 (1994).
40. W. Brütting and W. Riess, *Acta Phys. Pol. A* **87**, 785 (1995).
41. K. Bender, D. Schweitzer and H.J. Keller, *J. Phys. Colloq.* **44** (C3), 1433 (1983).
42. J.F. Kwak, G. Beni and P.M. Chaikin, *Phys. Rev. B* **13**, 641 (1976).
43. R. Wilckens, H.P. Geserich, W. Ruppel, P. Koch, D. Schweitzer and H.J. Keller, *Solid State Commun.* **41**, 615 (1982).
44. H.P. Geserich, R. Wilckens, W. Ruppel, V. Enkelmann, G. Wegner, G. Wieners, D. Schweitzer and H.J. Keller, *Mol. Cryst. Liq. Cryst.* **93**, 385 (1983).
45. H.P. Geserich, B. Kock, W. Ruppel, R. Wilkens, D. Schweitzer, V. Enkelmann, G. Wegner, G. Wieners and H.J. Keller, *J. Phys. Colloq.* **44** (C3), 1461 (1983).
46. I. Moritz, S.A. Shaheen, U. Hardebusch, J.S. Schilling, M. Weger, K. Bender, D. Schweitzer and H.J. Keller, *Solid State Commun.* **48**, 281, 1983.
47. H. Brunner, K.H. Hausser, H.J. Keller and D. Schweitzer, *Solid State Commun.* **51**, 107 (1984).
48. D. Meenenga, K.P. Dinse, D. Schweitzer and H.J. Keller, *Mol. Cryst. Liq. Cryst.* **120**, 243 (1985).
49. G.G. Maresch, M. Mehring, J.U. von Schütz and H.C. Wolf, *Chem. Phys.* **85**, 333 (1984).
50. O. Dobbert, T. Prisner, K.P. Dinse, D. Schweitzer and H.J. Keller, *Solid State Commun.* **61**, 499 (1987).
51. J. Wieland, U. Haeberlen, D. Schweitzer and H.J. Keller, *Synth. Met.* **19**, 393 (1987).
52. C. Bourbonnais, R.T. Henriques, P. Wzietek, D. Kongeter, J. Voiron and D. Jérôme, *Phys. Rev. B* **44**, 641 (1991).
53. A.P. Ginsberg and M.B. Robin, *Inorg. Chem.* **2**, 817 (1963).
54. L. Alcácer and A.H. Maki, *J. Phys. Chem.* **78**, 215 (1974).
55. L. Alcácer and A.H. Maki, *J. Phys. Chem.* **80**, 1912 (1976).
56. R.T. Henriques, L. Alcácer, J.P. Pouget and D. Jérome, *J. Phys. C* **17**, 5197 (1984).
57. L. Alcácer, *Mol. Cryst. Liq. Cryst.* **120**, 221 (1985).
58. R.T. Henriques, L. Alcácer, M. Almeida and S. Tomic, *Mol. Cryst. Liq. Cryst.* **120**, 237 (1985).
59. R.T. Henriques, L. Alcácer, D. Jérôme, C. Bourbonnais and C. Weyl, *J. Phys. C* **19**, 4663 (1986).
60. R.T. Henriques, M. Almeida, M.J. Matos, L. Alcácer and C. Bourbonnais, *Synth. Met.* **19**, 379 (1987).
61. A. Domingos, R.T. Henriques, V. Gama, M. Almeida, A. Lopes Vieira and L. Alcácer, *Synth. Met.* **27**, B411 (1988).
62. V. Gama, R.T. Henriques, M. Almeida and L. Alcácer, *Synth. Met.* **42**, 2553 (1991).
63. V. Gama, I.C. Santos, G. Bonfait, R.T. Henriques, M.T. Duarte, J.C. Waerenborgh, L. Pereira, J.M.P. Cabral and M. Almeida, *Inorg. Chem.* **31**, 2598 (1992).
64. V. Gama, R.T. Henriques, M. Almeida, C. Bourbonnais, J.P. Pouget, D. Jérôme, P. Auban-Senzier and B. Gotschy, *J. Phys. I***3**, 1235 (1993).
65. V. Gama, M. Almeida, R.T. Henriques, I.C. Santos, A. Domingos, S. Ravy and J.P. Pouget, *J. Phys. Chem.* **95**, 4263 (1991).

66. V. Gama, R.T. Henriques and M. Almeida, in *Lower Dimensional Solids and Molecular Electronics*, R.M. Metzger, P. Day and G. Papavassiliou (Eds.), Plenum Press, New York, 1991, p. 205.
67. V. Gama, R.T. Henriques, M. Almeida and J.P. Pouget, *Synth. Met.* **56**, 1677 (1993).
68. V. Gama, R.T. Henriques, M. Almeida and L. Alcácer, *J. Phys. Chem.* **98**, 997 (1994).
69. M. Almeida, V. Gama, R.T. Henriques and L. Alcácer, in *Inorganic and Organometallic Polymers with Special Properties*, R.M. Laine (Ed.), Kluwer Academic, Dordrecht, 1992, p. 163–177.
70. R.T. Henriques, V. Gama, G. Bonfait, I.C. Santos, M.J. Matos, M. Almeida, M.T. Duarte and L. Alcácer, *Synth. Met.* **56**, 1846 (1993).
71. V. Gama, R.T. Henriques, G. Bonfait, M. Almeida, S. Ravy, J.P. Pouget and L. Alcácer, *Mol. Cryst. Liq. Cryst.*, **234**, 171 (1993).
72. V. Gama, R.T. Henriques, G. Bonfait, M. Almeida, A. Meetsma, S. van Smaalen and J.L. de Boer, *J. Am. Chem. Soc.* **114**, 1986 (1992).
73. V. Gama, R.T. Henriques, M. Almeida, L. Veiros, M.J. Calhorda, A. Meetsma and J.L. de Boer, *Inorg. Chem.* **32**, 3705 (1993).
74. R.P. Shibaeva, V.F. Kaminskii, M.A. Simonov, E.B. Yagubskii and E.E. Katioshenko, *Kristallografiya* **30**, 488 (1985).
75. M.Y. Ogawa, B.M. Hoffman, S. Lee, M. Yudkowsky and N.M. Halperin, *Phys. Rev. Lett.* **37**, 1177 (1986).
76. G. Quirion, M. Poirier, K.K. Liou, M.Y. Ogawa and B.M. Hoffman, *Phys. Rev. B* **37**, 4272 (1988).
77. G. Bonfait, E.B. Lopes, M.J. Matos, R.T. Henriques and M. Almeida, *Solid State Commun.* **80**, 391 (1991).
78. L.F. Veiros, M.J. Calhorda and E. Canadell, *Inorg. Chem.* **33**, 4290 (1994).
79. G. Vincow and P.M. Johnson, *J. Chem. Phys.*, **39**, 1143 (1963).
80. M.C. Cross and D.S. Fisher, *Phys. Rev. B* **19**, 402 (1979).
81. M.J. Matos, V. Gama, G. Bonfait and R.T. Henriques, *Synth. Met.* **56**, 1858 (1993).
82. R.T. Henriques, C. Bourbonnais, P. Wzietek, D. Köngeter, D. Jérôme and J. Voiron, *Synth. Met.* **42**, 2339 (1991).
83. C. Bourbonnais, P. Wzieteck, D. Jérôme, F. Creuzet, L. Valade and P. Cassoux, *Europhys. Lett.* **6**, 177 (1988).
84. C. Bourbonnais, P. Wzieteck, F. Creuzet, D. Jérôme, P. Batail and K. Bechgaard, *Phys. Rev. Lett.* **62**, 1532 (1989).
85. G. Bonfait, M.J. Matos, R.T. Henriques and M. Almeida, *J. Phys. IV, Colloq. C2*3, 251 (1993).
86. S. Huizngа, J. Kommandeur, G.A. Sawatzky, B.T. Thole, K. Kopinga, W.J. de Jonge and J. Roos, *Phys. Rev. B* **19**, 4723 (1979).
87. J. C. Bonner and D. S. Fisher, *Phys. Rev.* **135**, A640 (1964).
88. G. Bonfait, M.J. Matos, R.T. Henriques and M. Almeida, *Physica B* **211**, 297 (1995).
89. T. Tiedje, J.F. Carolan, A.J. Berlinski and L. Weiler, *Can. J. Phys.* **53**, 1593 (1975).
90. J.W. Bray, L.V. Interrante, I.S. Jacobs and J.C. Bonner; in *Extended Linear Chain Compounds*, J.S. Miller (Ed.), Vol. 3, Plenum Press, New York, 1983.
91. M. Matos, G. Bonfait, R.T. Henriques and M. Almeida, *Phys. Rev. B.*, In Press.
92. E.B. Lopes, M.J. Matos, R.T. Henriques, M. Almeida and J. Dumas, *Europhys. Lett.* **27**, 241 (1994).
93. E.B. Lopes, M.J. Matos, R.T. Henriques, M. Almeida and J. Dumas, *Synth. Met.* **70**, 1267 (1995).
94. E.B. Lopes, M.J. Matos, R.T. Henriques, M. Almeida and J. Dumas, *Phys. Rev. B* **52**, R2237 (1995).
95. P. Monceau, in *Electronic Properties of Inorganic Quasi One Dimensional Metals*, P. Monceau (Ed.), Reidel, Dordrecht, 1985, p. 139.
96. G. Grüner, *Density Waves in Solids*, Addison Wesley, London, 1994.
97. J. Dumas, N. Thirion, E.B. Lopes, M.J. Matos, R.T. Henriques and M. Almeida, *J. Phys. I* **5**, 539 (1995).
98. W.G. Clark and L.C. Tippie, *Phys. Rev. B* **20**, 2914 (1979).
99. W. Duffy Jr., F.M. Weinhaus, D.L. Stanburg and J.F. Dec, *Phys. Rev. B* **20**, 1164 (1979).
100. L.N. Bulaevskii, A.V. Zvarykina, Y.S. Karimov, R. Lyubovskii and I.F. Schegolev, *Sov. Phys. JETP* **35**, 284 (1972).
101. E.J.W. Lam, P.T. Beurs Kens, J.M.M. Smits, S. van Smaalen, J.L. de Boer and H.-F. Fan, *Acta Crystallogr., Sect. B*, **51**, 779 (1995).
102. J.V. Rodrigues, I.C. Santos, V. Gama, R.T. Henriques, J.C. Waerenborgh, M.T. Duarte and M. Almeida, *J. Chem. Soc., Dalton Trans.* 2655 (1994).
103. M.J. Backer-Hawkes, Z. Dori, R. Heisenberg and H.B. Gray, *J. Am. Chem. Soc.* **90**, 4253 (1968).
104. J.H. Hanemark and W.H. Lipscomb, *Inorg. Chem.* **4**, 1729 (1965).
105. J.D. Forrester, A. Zalkin and D.H. Templeton, *Inorg. Chem.* **3**, 1500 (1964).
106. M.J. Matos, R.T. Henriques and L.J. Alcácer, *Synth. Met.* **19**, 389 (1987).
107. M.J. Matos, R.T. Henriques and L. Alcácer, in *Lower-Dimensional Systems and Molecular Electronics*, R.M. Metzger, P. Day and G. Papavassiliou (Eds.), Plenum Press, New York, 1991, p. 211.
108. J. Morgado, L. Alcácer, R.T. Henriques and M. Almeida, *Synth. Met.* **71**, 1945 (1995).
109. C.B. Dias, I.C. Santos, V. Gama, R.T. Henriques, M. Almeida and J.P. Pouget, *Synth. Met.* **56**, 1688 (1993).
110. R.D. Schmitt, R.M. Wing and A.H. Maki, *J. Am. Chem. Soc.* **91**, 4394 (1969).
111. L.L. Gonçalves, V. Gama, R.T. Henriques and M. Almeida, *Synth. Met.* **40**, 397 (1991).
112. R. Lapuyade, J.P. Morand, D. Chasseau, C. Hauw and P. Delhaes, *J. Phys. Colloq.* **44** (C3), 1235 (1983).

113. P. Penven, D. Jérôme, S. Ravy, P.A. Albouy and P. Batail, *Synth. Met.* **27**, B405 (1988).

114. V. Ilakovac, S. Ravy, A. Moradpour, L. Firlej and P. Bernier, *Phys. Rev. B* **52**, 4108 (1995).

115. P. Michel, A. Moradpour, P. Penven, L. Firlej, P. Bernier, B. Levy, S. Ravy and A. Zahab, *J. Am. Chem. Soc.* **112**, 8285 (1990).

116. J. Morgado, L. Alcácer, R.T. Henriques, E.B. Lopes, M. Almeida and M. Fourmigué, *Synth. Met.* **56**, 1735 (1993).

117. J. Morgado, I.C. Santos, R. T. Henriques, M. Fourmigué, P. Matias, L.F. Veiros, M.J. Calhorda, M.T. Duarte, L. Alcácer and M. Almeida, *Chem. Mater.* **6**, 2309 (1994).

118. L. Alcácer, J. Morgado, R.T. Henriques and M. Almeida, *Synth. Met.* **70**, 1093 (1995).

119. J. Morgado, I.C. Santos, L.F. Veiros, R.T. Henriques, M.T. Duarte, M. Almeida and L. Alcácer, submitted for publication.

120. B. Hilti, C.W. Mayer and G. Rihs, *Solid State Commun.* **38**, 1129 (1981).